MODELING OF ASYMMETRIC MEMBRANE FORMATION BY DRY CASTING METHOD

By

Bülent ÖZBAŞ

A Dissertation Submitted to the
Graduate School in Partial Fulfillment of the
Requirements for the Degree of

MASTER OF SCIENCE

Department: Materials Science and Engineering
Major: Materials Science and Engineering

İzmir Institute of Technology
İzmir, Turkey

June, 2001

We approve the thesis of Bülent ÖZBAŞ

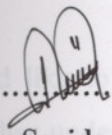

..... 29.06.2001

Assist. Prof. Dr. Sacide ALSOY ALTINKAYA

Supervisor

Deparment of Chemical Engineering

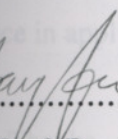

..... 29.06.2001

Assoc. Prof. Dr. Gökmen TAYFUR

Co-Advisor

Department of Civil Engineering

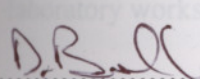

..... 29.06.2001

Prof. Dr. Devrim BALKÖSE

Department of Chemical Engineering

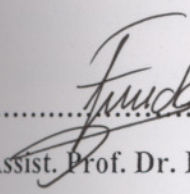

..... 29.06.2001

Assist. Prof. Dr. Funda TIHMINLIOĞLU

Department of Chemical Engineering

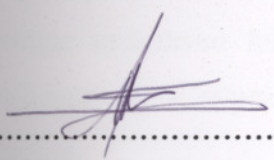

..... 29.06.2001

Assist. Prof. Dr. Metin TANOĞLU

Department of Mechanical Engineering

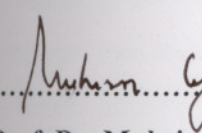

..... 29.06.2001

Prof. Dr. Muhsin ÇİFTÇİOĞLU

Head of Interdisciplinary Materials Science and Engineering Program

ACKNOWLEDGEMENTS

I would like to thank and express my deepest gratitude to Dr. Sacide Alsoy Altınkaya for her understanding, help, guidance and encouragement during this study and in the preparation of this thesis.

I also would like to thank to Dr. Muhsin Çiftçioğlu, for his encouragement and guidance in applying to Materials Science and Engineering Department for MS degree.

Thanks are also to Dr. Devrim Balköse and Dr. Sevgi Ulutan for their contributions on the permeability studies.

I also would like to express my thanks to Hacer Yenal for her efforts in the laboratory works.

Finally, I would like to thank to my family for their help, support and patience during the course of this work.

ABSTRACT

Many polymeric membranes are produced by phase inversion technique invented by Loeb and Sourirajan in 1962. One of the most challenging problems in membrane industry is to produce membranes with desirable structural characteristics which cause best performance for a specific application. The solution of this problem is facilitated by the development of mathematical models.

The polymeric membrane formation process is a complicated process due to phase separation, simultaneous heat and mass transfer mechanisms controlled by complex thermodynamic and transport properties of polymer solutions. In this work, a fully predictive mathematical model developed by Alsoy (1998) was used to describe the mechanisms of membrane formation by dry casting method. Model equations consist of coupled unsteady state heat and mass transfer equations, film shrinkage as well as complex boundary conditions especially at polymer gas interface. A key component of the model is incorporation of multicomponent diffusion coefficients that consist of thermodynamic factors and self-diffusivities. The predictions from the model provide composition paths, temperature and thickness of the membrane. The beginning of phase transition was determined when compositions paths were plotted on the phase diagram. The model was applied to cellulose acetate/acetone/water system which is commonly used for asymmetric membrane formation. The model was used as a tool to optimize membrane formation process by investigating the effect of gas phase conditions, initial thickness and composition of the cast solution on the final membrane structure.

The predictive ability of the model was evaluated by comparison with the data obtained from gravimetric measurements. Structural studies were conducted using scanning electron microscopy. Also, the permeability of prepared membranes to water vapor was measured using steady state technique. Both experimental and predicted results indicated that morphologies ranging from dense nonporous to asymmetric ones, in which a dense skin layer is supported by a porous layer, can be obtained with dry cast technique.

ÖZ

Polimerik membranların çoğu Loeb ve Sourirajan tarafından 1962' de bulunan "faz ayrımı" yöntemiyle üretilmektedir. Membran endüstrisindeki hedef, özel işlemlerde kullanıma uygun yapıda yüksek performanslı membranların üretilmesidir. Bu amaca ulaşılması için matematik modeller geliştirilmektedir.

Membran oluşumu; faz dönüşümü, ve polimer çözeltilerinin karmaşık termodinamik-taşınım özellikleri tarafından kontrol edilen eş zamanlı ısı ve kütle iletim mekanizmaları nedeniyle zor bir işlemdir. Bu projede, kuru döküm metodu ile membran oluşum mekanizmasını tanımlamak amacıyla Alsoy (1998) tarafından geliştirilen bir matematik model kullanılmıştır. Model, yatışkın olmayan durum için yazılmış tek boyutlu ısı ve kütle iletimini, film büzülmesini ve polimer-hava ara yüzeyindeki sınır koşullarını tanımlayan denklemlerden oluşmaktadır. Modelin en önemli kısmını termodinamik çarpanlardan ve öz yayınımdan oluşan çok bileşenli yayınım katsayıları oluşturmaktadır. Model , membran içerisindeki derişim dağılımlarını, membran kalınlığını ve sıcaklığını öngörebilmektedir. Derişim değişimlerinin faz diyagramı üzerinde gösterilmesiyle faz dönüşümünün başlangıcı da belirlenebilir. Modelin uygulanması için, membran oluşumunda tipik olarak kullanılan selüloz asetat/aseton/su üçlüsü örnek sistem olarak seçilmiştir. Gaz fazı koşullarının, döküm çözeltisinin ilk kalınlığının ve derişimlerinin, membran yapısı üzerindeki etkileri incelenerek, model membran oluşumun optimize edilmesi amacıyla kullanılmıştır.

Modelin öngörüm yeteneğinin değerlendirilmesinde gravimetrik ölçümlerden elde edilen veriler kullanılmıştır. Membran yapıları taramalı elektron mikroskobu ile incelenmiştir. Bunların yanında, hazırlanan membranların su buharı geçirgenlikleri yatışkın koşullar altında ölçülmüştür. Model ve deneysel sonuçları, gözenekli bir yapının destek sağladığı yoğun yüzey tabakası içeren asimetrik, ve aynı zamanda gözeneksiz ve yoğun morfolojik özelliklere sahip membranların, kuru döküm yöntemiyle üretilebileceğini göstermektedir.

TABLE OF CONTENTS

LIST OF FIGURES

LIST OF TABLES

NOTATION

A_i	Constant pre-exponential factor for component i (g/cm.s)
a_i	Activity of component i
C_i	Dimensionless concentration of component i in the polymer cast solution
C_p^J	Heat Capacity of phase J (J/g.K)
C_{11}^{WLF}	Solvent WLF parameter
C_{21}^{WLF}	Solvent WLF parameter (K)
C_{12}^{WLF}	Polymer WLF parameter
C_{22}^{WLF}	Polymer WLF parameter (K)
CA	Cellulose acetate
D	Mutual diffusion coefficient (binary solution) (cm^2/g)
D_{ij}	Mutual diffusion coefficient (cm^2/s)
D_0	Constant pre-exponential factor (cm^2/s)
D_{0i}	Constant pre-exponential factor (when E=0) (cm^2/s)
D_i	Self diffusion coefficient of component i (cm^2/g)
$D_{i,G}$	Diffusion coefficient of component i in the gas phase (cm^2/s)
E	Energy required to overcome attractive forces from neighboring molecules (J/mol)
G^M	Gibbs free energy of mixing.
g	Gravity constant (cm/s^2)
Gr	Grashof number
H	Thickness of substrate (cm)
$\hat{H}$	Specific enthalpy (J/g)
$\Delta\hat{H}_{vi}$	Heat of vaporization
h	Heat transfer coefficient ($W/cm^2.K$)
h_i	The size of the grid corresponding to grid point i
J_i^*	Mass diffusive flux of component i with respect to volume average velocity ($g/cm^2.s$)
K_{11}	Solvent free volume parameter ($cm^3/g.K$)

K_{21}	Solvent free volume parameter (K)
K_{12}	Polymer free volume parameter ($cm^3/g.K$)
K_{22}	Polymer free volume parameter (K)
K_{11}	Nonsolvent free volume parameter for ternary solution ($cm^3/g.K$)
K_{12}	Solvent free volume parameter for ternary solution ($cm^3/g.K$)
K_{13}	Polymer free volume parameter for ternary solution ($cm^3/g.K$)
K_{21}	Nonsolvent free volume parameter for ternary solution (K)
K_{22}	Solvent free volume parameter for ternary solution (K)
K_{23}	Polymer free volume parameter for ternary solution (K)
k_i	Mass transfer coefficient of component i (s/cm)
k^J	Thermal conductivity of phase J (J/s.cm.K)
L	Initial thickness of cast polymer solution (cm)
L_c	Characteristic length of the substrate (cm)
M_i	Molecular weight of component i (g/mol)
$M_{i.j}$	Molecular weight of jumping unit of component i (g/mol)
N	Number of components in the solution
$\mathbf{n}^*$	Unit normal vector
n_i	Number of moles of component i
$n_{i.x}$	Mass flux of component i with respect to stationary coordinates ($g/cm^2.s$)
P	Permeability coefficient
P_{ii}	Partial pressure of component i at the interface ($g/cm.s^2$)
P_{ib}	Partial pressure of component i in the gas phase ($g/cm.s^2$)
P_i^{sat}	Saturated pressure of component i ($g/cm.s^2$)
Pr	Prandtl number
$\mathbf{q}^J$	Conductive heat flux vector in phase J ($J/s.cm^2$)
R	Gas Constant
R_i	Rate of reaction of component i ($g/cm^3.s$)
Re	Reynolds number
S	Solubility coefficient
Sc	Schmit number

T	Temperature (K)
T^*	Dimensionless temperature
T_{gi}	Glass transition temperature of component i (K)
$\mathbf{T}^J$	Stress tensor in phase J.
t	Time (s)
$\hat{U}$	Specific internal energy (J/g)
$\mathbf{U}^*$	Velocity vector of the phase interface
$\tilde{V}_i^*$	Critical molar volume of component i (cm^3/mol)
$\tilde{V}_i$	Molar volume of component i (cm^3/mol)
$\tilde{V}_{FH}$	Free volume per mole of all individual jumping units (cm^3/mol)
$\hat{V}_{FH}$	Specific free volume of all individual jumping units (cm^3/g)
$\hat{V}_i^0(0)$	Specific volume of pure component i at 0 K.
$\hat{V}_{i,G}$	Partial specific volume of component i in the gas phase (cm^3/g)
$\hat{V}_i$	Specific volume of component i (cm^3/g)
$\mathbf{v}_i$	Velocity vector of component i (cm/s)
v_i	Molar volume of component i (cm^3/mol)
X^*	Dimensionless thickness of polymer
$X(t)$	Time dependent film thickness (cm)
x	Vertical position coordinate relative to casting surface (cm)
$y_{i,i}$	Mole fraction of component i at the interface
$y_{i,G}$	Mole fraction of component i in the gas phase

Greek letters

β	Polymer specific proportionality constant
β	Expansion coefficient (K^{-1})
χ_{ij}	Interaction parameter between components i and j
ϕ_i	Volume fraction of component i
γ	Overlap factor which accounts for shared free volume
η	Dimensionless length variable

μ_G	Viscosity of gas phase (g/cm.s)
μ_i	Chemical potential of component i (J/mol)
ρ_i	Mass density of component i (g/cm^3)
ρ_G	Density of gas phase (g/cm^3)
ρ_i^0	Pure component density of i (g/cm^3)
υ_G	Velocity of bulk gas phase (cm/s)
η_i	Viscosity of component i (g/cm.s)
υ_i	Velocity of the component i with respect to stationary coordinates (cm/s)
υ^*	Volume average velocity (cm/s)
ω_i	Mass fraction of component i
ξ_{ij}	Ratio of critical molar volume of component i jumping unit to that of component j jumping unit
ζ_{ij}	Friction coefficient between components i and j

Subscripts

b	Bulk
i	Component i
i	Interface
l	Polymer lean phase
r	Polymer rich phase
x	Vertical position coordinate relative to casting surface (cm)
1	Nonsolvent
2	Solvent
3	Polymer

Superscripts

G	Gas phase adjacent to polymer solution
g	Gas phase adjacent to substrate.
p	Polymer solution phase
s	Substrate phase

CHAPTER 1

INTRODUCTION

After the development of asymmetric membranes by Loeb and Sourirajan in 1962, polymeric membranes have achieved commercial importance in many separation applications in the chemical, food, pharmaceutical and biotechnology industries.

Asymmetric membranes consist of a thin selective surface skin layer supported by a highly permeable non selective layer which provides mechanical strength. The majority of asymmetric membranes are produced by phase inversion process. The phase inversion process can be achieved through four principle methods: the dry cast, wet cast, thermal cast and vapor induced processes. The major challenge in all these processes is to form defect free, high permeability and high selectivity membrane structures.

The functional behavior of polymeric membranes is closely related to the membrane formation mechanism. Slight changes in the membrane production process can greatly influence the final membrane morphology. Therefore, mathematical models are needed to predict the formation of membranes and to choose the best membrane fabrication recipes giving optimum, desired membrane structures. In this way, extensive and time consuming trial and error experimentation is avoided.

Most of the models in the literature have been developed for the wet cast and thermal cast processes. In this study, membrane formation by dry casting method was modeled. The dry cast process is characterized by evaporation of solvent and/or nonsolvent from an initially homogeneous polymer solution. As a result of the evaporation, the polymer solution becomes unstable and it is phase separated into polymer lean and polymer rich phases. The final membrane thickness is usually a fraction of the initial cast film thickness.

There have been several modeling studies in the literature which, most of them are related to the evaporation and immersion steps of the immersion precipitation technique. However, there are limited studies on the dry casting technique.

In this study, a model originally derived for multicomponent drying of polymer solutions (Alsoy 1998) was used to predict the membrane formation by dry casting

method. The model consists of coupled heat and mass transfer equations, film shrinkage and boundary conditions. The complexity of the model equations is decreased by using a volume averaged reference frame in mass transfer equations and assuming that temperature gradients in the solution and substrate are negligible. The latter assumption is based on the fact that resistance to heat transfer in the gas phase is much greater than that in the solution and the substrate. The model can predict temperature and thickness of the membrane as well as the compositions of each component in the casting solution. The onset of phase separation and the morphology of the final membrane structure is predicted when the composition paths are plotted on the phase diagrams. The ternary phase diagrams were predicted using the Flory-Huggins thermodynamic theory with constant interaction parameters. The key component of the model is incorporation of multicomponent diffusion theory which predicts multicomponent diffusivities from available self diffusion and thermodynamic data.

The model was applied to the well characterized cellulose acetate/acetone/water system and solved numerically using finite difference technique. To facilitate numerical solution, moving boundary was immobilized using an appropriate coordinate transformation and nonuniform grid size distribution was applied to estimate sharp concentration gradients accurately.

The model was used to investigate the effect of initial composition and thickness of the casting solution, evaporation conditions (free or forced convection) and relative humidity on the final membrane structure.

The experimental aspect of the thesis consists of three parts. First, the validity of the model was confirmed using the measurement of total evaporation rate by monitoring the overall mass change as a function of time. Second, the morphology of the prepared membranes was investigated using scanning electron microscope pictures. Finally, the water vapor permeability and density of membranes were measured.

CHAPTER 2

BASIC CONCEPTS OF MEMBRANES

Membranes are the materials used in separation processes as a selective barrier between two phases. In principle, the aim is to permeate the selected components (permeate) of a phase and reject the undesired ones (retentate). The separation may occur under a variety of driving forces (pressure, concentration, electrical, etc.), and a variety of continuos flows as shown in Figure 2.1.

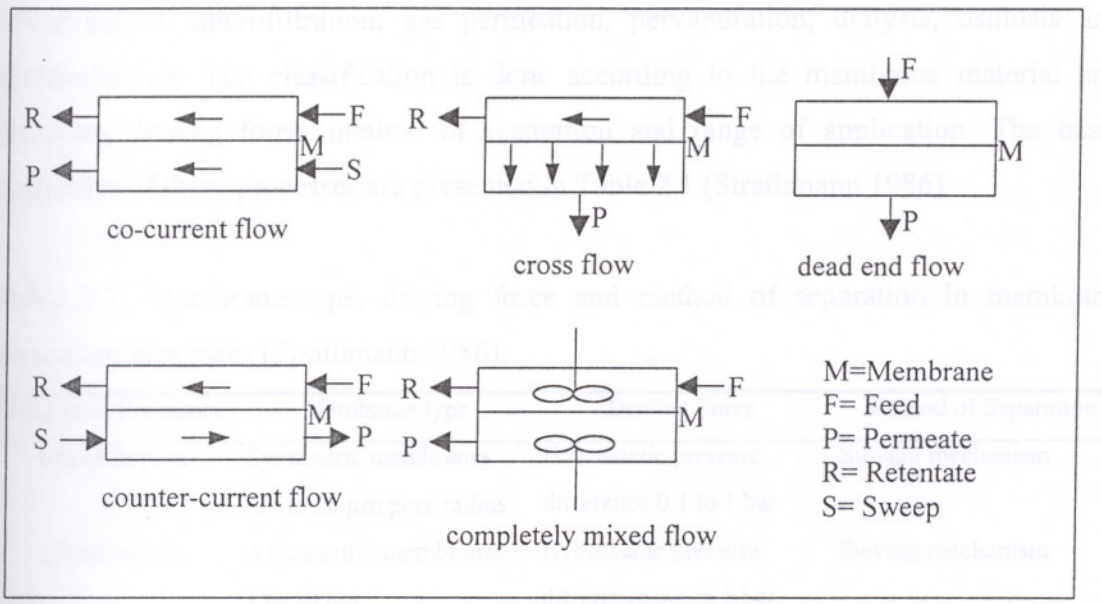

Figure 2.1. Types of ideal continuos flows used in membranes operations.

The thickness of a membrane may vary in the order of nanometers to centimeters (Strathmann 1986). Therefore, instead of a single membrane layer, membrane modules such as; hollow fiber, plate-and-frame and spiral wound, are preferred for separation processes.

The separation characteristics of membranes are determined by the structure, i.e., dimension distribution, network of pores, thickness of dense skin layer and the interaction of membrane with the components separated. Desirable properties of a membrane typically include (Strathmann 1999); high selectivity, high permeability, mechanical and thermal stability, chemical resistance, low fouling rate and low cost. Permeability can be defined as the flux of permeating substance per unit of driving force and membrane thickness. Whereas, the selectivity can be defined as the ratios of

the components in the upstream to those in the downstream. The permeability of a membrane can be increased by increasing the surface area of a membrane. However, the selectivity can only be increased for a specific membrane by multi stage processes which lead to an increase in the operating costs (Rautenbach and Albrecht 1989).

2.1. Membrane processes

The use of membranes in separation processes are very broad. Applications range from gas separation process in a refinery to a hemodialysis operations in hospital. In general, membrane based separation processes are classified as: reverse osmosis, ultrafiltration, microfiltration, gas permeation, pervaporation, dialysis, osmosis and electrodialysis. The classification is done according to the membrane material and structure, driving force, method of separation and range of application. The basic properties of these processes are presented in Table 2.1 (Strathmann 1986).

Table 2.1. Membrane type, driving force and method of separation in membrane separation processes (Strathmann 1986).

Separation Processes	Membrane type	Driving Force	Method of Separation
Microfiltration	Symmetric membranes 0.1 to 10 μm pore radius.	Hydrostatic pressure difference 0.1 to 1 bar	Sieving mechanism
Ultrafiltration	Asymmetric membranes 1 to 10 nm	Hydrostatic pressure difference 0.5 to 5 bar	Sieving mechanism
Reverse Osmosis	Asymmetric membranes	Hydrostatic pressure 20 to 100 bar	Solution-diffusion mechanism
Dialysis	Symmetric membranes 0.1 to 10 nm	Concentration gradient	Diffusion in convection free layer
Electrodialysis	Cation and anion exchange membranes	Electrical potential gradient	Electrical charge and size of particle

2.2 Membrane materials

Polymers and ceramics are widely used as membrane materials. Commercial separations are usually dominated by polymeric membranes due to their cost efficiency and performance. However, ceramic membranes are preferred for high temperature applications due to their thermal stability at higher temperatures. Typical polymers and

ceramics used in membrane fabrication are shown in Table 2.2. Among these materials, cellulose acetate and triacetate are the most popular ones used in reverse osmosis, ultra filtration and gas permeation processes (Rautenbach and Albrecht 1989).

Table 2.2. Polymers and ceramics used as membranes materials.

Polymers	Modified natural	cellulose acetate, cellulose 2-acetate, cellulose 3-acetate, cellulose nitrate
	Synthetic	Polyamide, polysulphone, polycarbonate, polyetheylene,
Inorganic and ceramics		Porous glass, graphite oxide, ZrO_2, Al_2O_3

2.3. Membrane structures

The structure of a membrane is characterized by fraction of dense and porous layers, the shape and size of the pores as well as the pore size distribution. Cross sections of different membrane morphologies are shown in Figure 2.2 (Kools 1998).

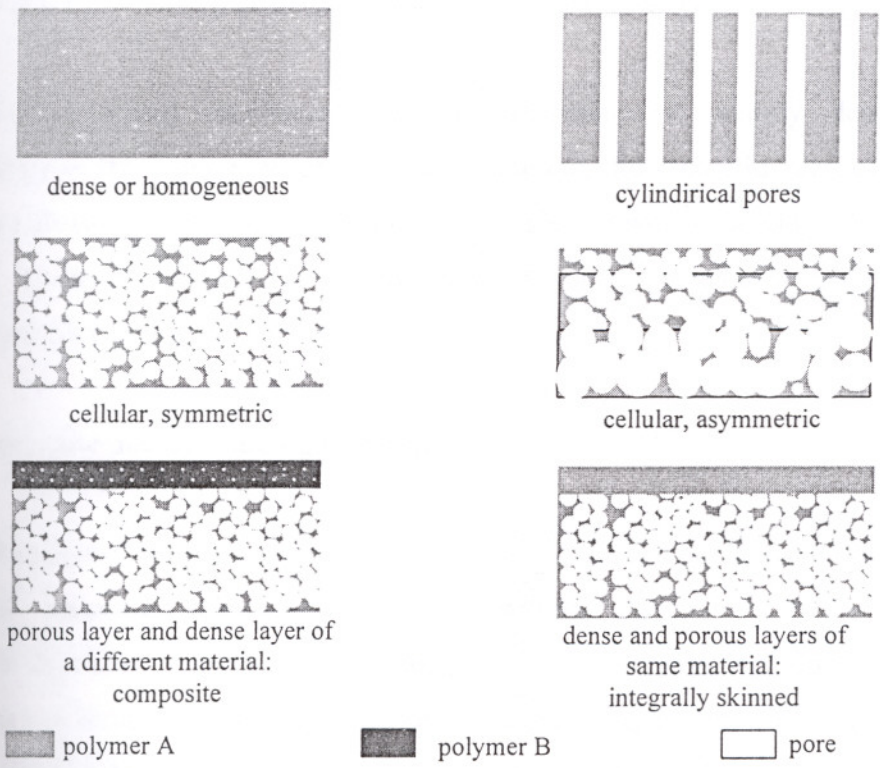

Figure 2.2. Cross sections of different membrane morphologies (Kools 1998).

The asymmetric membranes offer more advantages than the symmetric ones, therefore, they constitute a major place in separation processes. An asymmetric membrane can be defined as a structure in which two or more different morphological planes are observed under a scanning electron microscope as shown in Figure 2.3. The selectivity of the membrane is determined by dense thin skin layer and the mechanical strength is provided by thick porous layer. The thickness of the skin layer may vary between 0.1 and 1 μm and the porous sublayer can be as thick as 200 μm. The fraction of dense top layer and porous sublayer and the other structural characteristics of the membrane should be optimized based on the specific applications, desired purity of the permeate and operating costs.

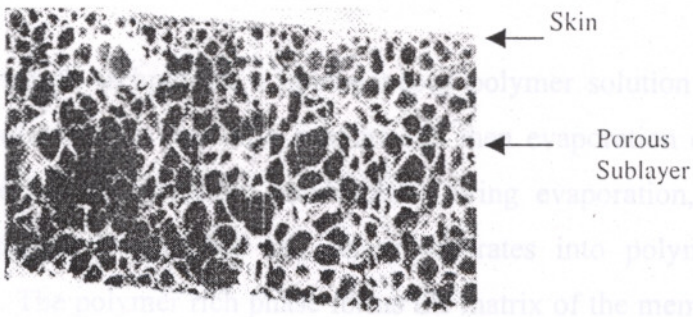

Figure 2.3. SEM picture of an asymmetric membrane (Altena 1982).

The transport mechanism within membranes is mainly determined by morphology of the membrane. In a dense membrane, the separation can occur only by solution diffusion mechanism. In porous membranes, however, in addition to molecular sieving, Knudsen diffusion and convective flow can contribute to the separation mechanism (Zolandz and Fleming 1992).

2.4. Membrane manufacturing techniques

Polymeric membranes can be produced by several techniques such as phase inversion, sintering, stretching and track etching. Asymmetric membranes with desirable structural features are obtained by phase inversion techniques. The phase inversion can be achieved through four principal methods and they will be discussed in detail in the following chapter.

CHAPTER 3

THERMODYNAMICS OF POLYMER SOLUTIONS AND PHASE INVERSION TECHNIQUES

The use of membranes were limited until Loeb and Sourirajan introduced the "phase inversion" technique in 1962. Since that time, the phase inversion technique became the most popular method to prepare polymeric membranes with asymmetric structures.

In phase inversion techniques, a homogeneous polymer solution consisting of solvent(s) and nonsolvent(s) is cast on a support and then evaporation of the casting solution takes place under convective conditions. During evaporation, the solution becomes thermodynamically unstable and phase separates into polymer lean and polymer rich phases. The polymer rich phase forms the matrix of the membrane, while, the polymer lean phase, rich in solvents and nonsolvents, fills the pores. After the polymer solidifies, the liquid in the pores is extracted.

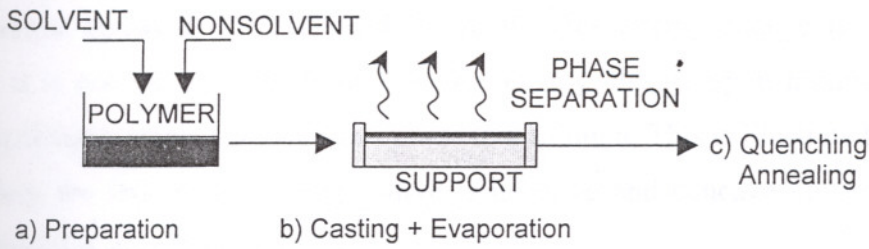

Figure 3.1. Basic steps in phase inversion techniques.

Based on the external effects, the phase inversion techniques can be classified into four main groups.

1. Immersion Precipitation (Wet casting)
2. Vapor induced phase separation
3. Thermally induced phase separation
4. Dry – casting (Air casting)

The theoretical treatment of membrane formation process by phase inversion technique consists of both thermodynamic and kinetic aspects. The composition and the

temperature at which the system becomes unstable are governed by thermodynamics whereas the rate of formation of phases and the mass transfer in the solution is a kinetic phenomena. The mechanism of asymmetric structure formation through phase separation is a rather complex phenomena and is altered by thermodynamic condition of the system during phase separation.

To make comment on the basic structures of the membrane formed, the phase diagram of the system needs to be constructed and the kinetic aspect must be coupled with the thermodynamic aspect of the system. Therefore, before going into details of phase inversion techniques, the thermodynamic of binary and ternary solutions will be discussed.

3.1. Phase behavior of polymer solutions

3.1.1. Phase behaviour of binary polymer solutions

A solution consisting of a polymer in a solvent or in a mixture of solvents can exhibit either single or multiple phases at particular composition and temperature ranges. The presence of single or multiple phases is mainly determined by the shape of the Gibbs free energy curve as a function of composition. It is known from basic thermodynamic knowledge that at equilibrium the free energy change is minimum. Although, it is not the only condition, the free energy change upon mixing must be negative to obtain a single homogeneous phase in a solution. This is illustrated in Figure 3.2, in which the free energy change curve is negative and concave upwards for all compositions of A and B components.

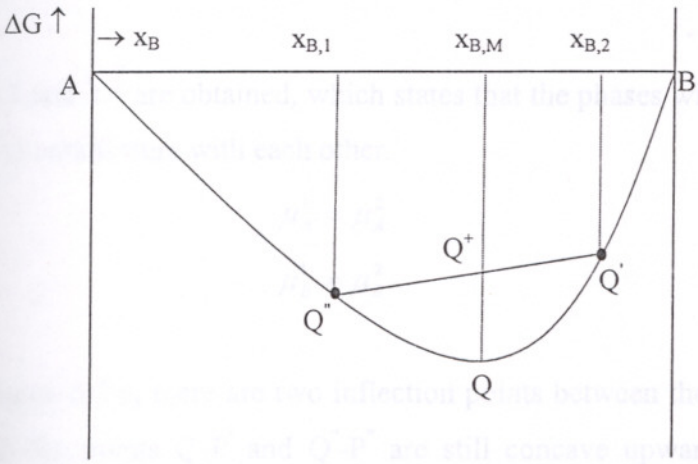

Figure 3.2. Free energy curve versus composition for a binary mixture.

If two mixtures with compositions $x_{B,1}$ and $x_{B,2}$ are mixed with an appropriate ratio, a solution can be obtained with a composition of $x_{B,M}$. The mixture will have a free energy value of Q, located on the curve, which is lower than the sum of the free energies value given by Q^+. Q is lower than Q^+; therefore there is an increase in free energy by separating a mixture with composition $x_{B,M}$ indicating that a homogeneous solution with composition $x_{B,M}$ is thermodynamically stable. In fact, the mixtures showing such a concave upwards free energy change curve is homogeneous at all compositions.

In Figure 3.3-a, although the free energy change is negative for all compositions, unlike the curve in Figure 3.2, it is concave downwards between the compositions $x_{B,1}$ and $x_{B,2}$. The free energy of the mixture may vary along the curve between points Q' and Q". The solution with a composition between $x_{B,1}$ and $x_{B,2}$ will have higher free energy than that of phase separated mixtures of these compositions. As a result a solution with in this composition range is not thermodynamically favored and will separate into two phases of composition $x_{B,1}$ and $x_{B,2}$.

The slope of the tangent line to both of the points Q' and Q" is equal to the first derivative of the change of free energy with composition. Using moles rather than mole fractions, it can be expressed as equation 3.1.

$$\left.\frac{\partial \Delta G}{\partial n_B}\right|_{n=n_{B,1}} = \left.\frac{\partial \Delta G}{\partial n_B}\right|_{n=n_{B,2}} \tag{3.1}$$

From the definition of chemical potential,

$$\frac{\Delta \mu_i}{RT} = \frac{\partial}{\partial n_i}\left(\frac{\Delta G^M}{RT}\right)_{n_{j,j\neq i}} \tag{3.2}$$

equations 3.3 and 3.4 are obtained, which states that the phases with mole fractions $x_{B,1}$ and $x_{B,2}$ are at equilibrium with each other.

$$\mu_A^1 = \mu_A^2 \tag{3.3}$$

$$\mu_B^1 = \mu_B^2 \tag{3.4}$$

In Figure 3.3-a, there are two inflection points between the points 1 and 2. The line between the points Q'-P' and Q"-P" are still concave upwards and is called the

metastable region, while the line between P' and P" corresponds to unstable two phase region.

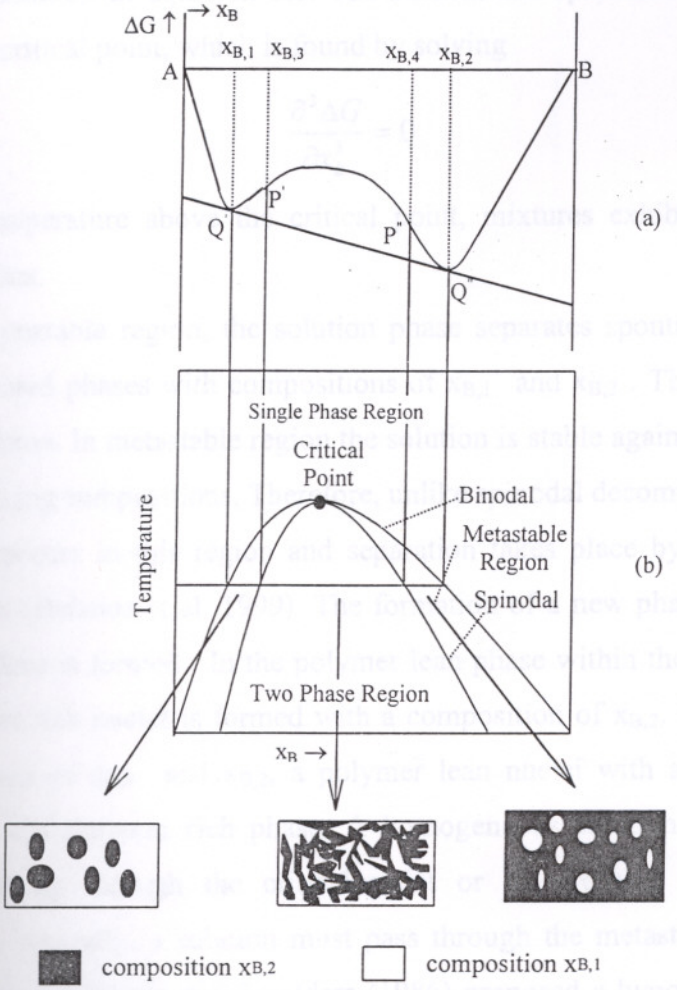

Figure 3.3. (a) Free energy curve and (b) Phase diagram for a binary system and possible structure formation in different parts of the phase diagram.

The points of inflection are determined by the second derivative of the free energy with respect to composition.

$$\frac{\partial^2 \Delta G}{\partial x_B^2} = 0 \tag{3.5}$$

$$\frac{\partial \Delta \mu_A}{\partial x_B} = \frac{\partial \Delta \mu_B}{\partial x_B} = 0 \tag{3.6}$$

In a typical binary phase diagram, the line called binodal forms the outer border of two phase region. Any two points on the binodal connected by a line correspond to compositions in two different phases that are in equilibrium. So at any temperature,

equilibrium compositions are determined by solving equation 3.3 or 3.4. Spinodal line forms a border between metastable and unstable two phase regions and it is calculated from the solution of equation 3.6. The binodal and spinodal lines coincide at a point called the critical point, which is found by solving

$$\frac{\partial^3 \Delta G}{\partial x_B^3} = 0 \tag{3.7}$$

At any temperature above the critical point, mixtures exhibit a single phase at all compositions.

In unstable region, the solution phase separates spontaneously into two small interconnected phases with compositions of $x_{B,1}$ and $x_{B,2}$. This is called the spinodal decomposition. In metastable region the solution is stable against separation into phases of neighboring compositions. Therefore, unlike spinodal decomposition, no spontaneous demixing occurs in this region and separation takes place by nucleation and growth mechanism (Beltsios et al. 1999). The formation of a new phase can only start after a stable nucleus is formed. In the polymer lean phase within the range of $x_{B,1}$ and $x_{B,3}$, the polymer rich nuclei is formed with a composition of $x_{B,2}$. In contrast, between the compositions of $x_{B,4}$ and $x_{B,2}$, a polymer lean nuclei with a composition of $x_{B,1}$ is formed in the polymer rich phase. A homogeneous solution can enter the unstable region directly through the critical point or by crossing the metastable region. Therefore, generally, a solution must pass through the metastable region to enter the unstable area. Wijmans and Smolders (1986) proposed a hypothesis that, the spinodal composition has no role in membrane formation, since the nucleation and growth mechanism which occurs in the metastable region is faster than the rate of mass transfer in the solution.

3.1.2. Phase behaviour of ternary polymer solutions

The phase diagram of a ternary system can be represented on a equilateral triangle as in Figure 3.4. Any point on this triangle represent a composition and the sum of the perpendicular distances from this point to all sides is unity. The corners of the triangle correspond to pure components whereas the points on the sides of the triangle represent the binary mixtures. The ternary phase diagrams also include binodal and spinodal lines, critical point, single phase, two phase and metastable regions.

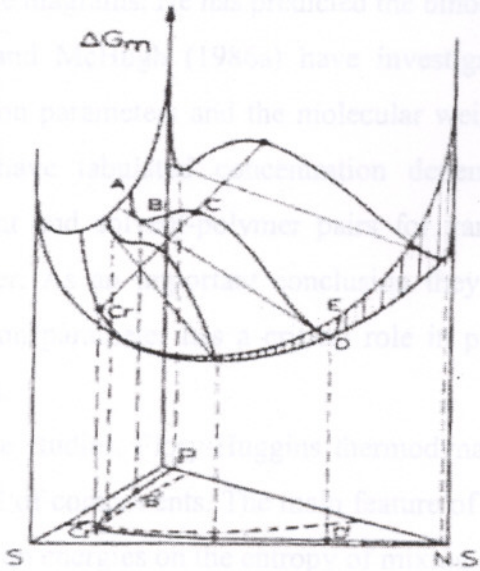

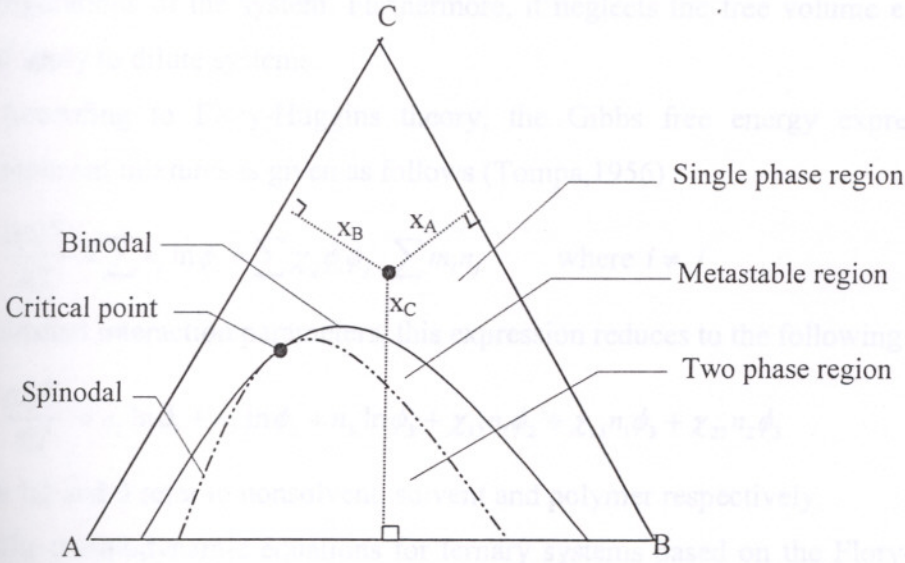

Figure 3.4. Sketch of change of Gibbs free energy surface for a ternary solution and ternary phase diagram.

3.2. Construction of ternary phase diagrams

The analyses on the construction of phase diagrams of ternary polymer solutions have been done by Tompa (1956), Altena (1982), Yilmaz and McHugh (1986a).

Tompa (1956) simplified the binodal, spinodal and critical point equations for ternary systems by assuming that polymer-solvent and polymer-nonsolvent interaction parameters as well as molar volumes of solvent and nonsolvent are the same.

Altena (1982) presented the binodal and spinodal equations with concentration dependent interaction parameters and studied the effect of interaction parameters on the shape of the phase diagrams. He has predicted the binodal only near the critical point.

Yilmaz and McHugh (1986a) have investigated the effect of constant and variable interaction parameters and the molecular weight of the polymer on the phase diagram. They have tabulated concentration dependent interaction parameters of solvent-nonsolvent and solvent-polymer pairs for variety of systems, including CA, acetone and water. As an important conclusion they have pointed out that solvent-polymer interaction parameter has a critical role in predicting the phase diagrams of polymer solutions.

In all these studies, Flory-Huggins thermodynamic theory was used to predict chemical potential of components. The main feature of this model is that it neglects the effects of interaction energies on the entropy of mixing and uses a lattice model to count the configurations of the system. Furthermore, it neglects the free volume effects and does not apply to dilute systems.

According to Flory-Huggins theory, the Gibbs free energy expression for multicomponent mixtures is given as follows (Tompa,1956) :

$$\frac{\Delta G^M}{RT} = \sum n_i \ln \phi_i + \sum \chi_{ij} \phi_i \phi_j \cdot \sum m_i n_i \qquad \text{where } i \neq j \tag{3.8}$$

Using constant interaction parameters, this expression reduces to the following form.

$$\frac{\Delta G^M}{RT} = n_1 \ln \phi_1 + n_2 \ln \phi_2 + n_3 \ln \phi_3 + \chi_{12} n_1 \phi_2 + \chi_{13} n_1 \phi_3 + \chi_{23} n_2 \phi_3 \tag{3.9}$$

in which 1,2 and 3 refer to nonsolvent, solvent and polymer respectively.

The thermodynamic equations for ternary systems based on the Flory-Huggins theory with variable interaction parameters are presented by Yilmaz (1986a). Using equation 3.2, and constant interaction parameters the chemical potential of the 3 components for constant interaction parameters can be expressed as follows:

$$\frac{\Delta \mu_1}{RT} = \ln \phi_1 + 1 - \phi_1 - \frac{v_1}{v_2}\phi_2 - \frac{v_1}{v_3}\phi_3 + (\chi_{12}\phi_2 + \chi_{13}\phi_3)(\phi_2 + \phi_3) - \chi_{23}\frac{v_1}{v_2}\phi_2\phi_3 \tag{3.10}$$

$$\frac{\Delta \mu_2}{RT} = \ln \phi_2 + 1 - \phi_2 - \frac{v_2}{v_1}\phi_1 - \frac{v_2}{v_3}\phi_3 + (\chi_{12}\frac{v_2}{v_1}\phi_1 + \chi_{23}\phi_3)(\phi_1 + \phi_3) - \chi_{13}\frac{v_2}{v_1}\phi_1\phi_3 \tag{3.11}$$

$$\frac{\Delta \mu_3}{RT} = \ln \phi_3 + 1 - \phi_3 - \frac{v_3}{v_1}\phi_1 - \frac{v_3}{v_2}\phi_2 + (\chi_{13}\frac{v_3}{v_1}\phi_1 + \chi_{23}\frac{v_3}{v_2}\phi_2)(\phi_1 + \phi_2) - \chi_{12}\frac{v_3}{v_1}\phi_1\phi_2 \tag{3.12}$$

At equilibrium the chemical potential of the components in two phases must be equal to each other.

$$\Delta\mu_{1,l} = \Delta\mu_{1,r} \tag{3.13}$$

$$\Delta\mu_{2,l} = \Delta\mu_{2,r} \tag{3.14}$$

$$\Delta\mu_{3,l} = \Delta\mu_{3,r} \tag{3.15}$$

The spinodal equation for a ternary system is given in equation 3.16.

$$G_{22}G_{33} = (G_{23})^2 \tag{3.16}$$

where

$$G_{ij} = \left(\frac{\partial^2 \Delta\overline{G}^M}{\partial\phi_i \partial\phi_j}\right)v_1 \tag{3.17}$$

and

$$\left(\frac{\partial \Delta\overline{G}^M}{\partial\phi_2}\right)_{T,P,\phi_3} = \frac{\Delta\mu_2}{v_2} - \frac{\Delta\mu_1}{v_1} \tag{3.18}$$

$$\left(\frac{\partial \Delta\overline{G}^M}{\partial\phi_3}\right)_{T,P,\phi_2} = \frac{\Delta\mu_3}{v_3} - \frac{\Delta\mu_1}{v_1} \tag{3.19}$$

Using equations 3.17 through 3.19 each term in equation 3.16 can be expressed as:

$$G_{22} = \frac{1}{\phi_1} + \frac{v_1}{v_2\phi_2} - 2\chi_{12} \tag{3.20}$$

$$G_{23} = \frac{1}{\phi_1} - (\chi_{12} + \chi_{13}) + \frac{v_1}{v_2}\chi_{23} \tag{3.21}$$

$$G_{33} = \frac{1}{\phi_1} + \frac{v_1}{v_3\phi_3} - 2\chi_{13} \tag{3.22}$$

The point at which the binodal and spinodal curves coincide can be calculated by solving equations 3.23 and 3.16 simultaneously.

$$G_{222}G_{33}^2 - 3G_{223}G_{23}G_{33} + 3G_{233}G_{23}^2 - G_{22}G_{23}G_{333} = 0 \tag{3.23}$$

where

$$G_{222} = \frac{1}{\phi_1^2} - \frac{v_1}{v_2\phi_2^2} \tag{3.24}$$

$$G_{223} = \frac{1}{\phi_1^2} \tag{3.25}$$

$$G_{233} = \frac{1}{\phi_1^2} \tag{3.26}$$

$$G_{333} = \frac{1}{\phi_1^2} - \frac{v_1}{v_3 \phi_3^2} \tag{3.27}$$

3.3. Method of computation for the construction of ternary phase diagram

In typical binary and ternary phase diagrams the compositions of the phases in equilibrium are shown by the tie line. The ends of this line are located on the binodal curve. Therefore, the combination of the tie lines gives the binodal. Arranging equations 3.13 through 3.15 and using material balance in both phases, the tie lines can be calculated by solving following set of equations.

$$F_i = \frac{\Delta\mu_{i,r} - \Delta\mu_{i,l}}{RT} \qquad i = 1,2,3 \tag{3.28}$$

$$F_4 = 1 - \sum_{i=1}^{3} \phi_{i,l} \tag{3.29}$$

$$F_5 = 1 - \sum_{i=1}^{3} \phi_{i,r} \tag{3.30}$$

The choice of one of the volume fractions in one of the phases as the independent variable leads to a system of 5 equations with 5 unknowns.

To construct the phase diagram, an appropriate objective function given by equation 3.31 was minimized using least square method (Hsu and Prausnitz 1973, Altena 1982, Yilmaz 1986).

$$OBJ = \sum \left(\frac{\Delta\mu_i^{'} - \Delta\mu_i^{''}}{RT} \right)^2 \tag{3.31}$$

The difficulties in computation have extensively been explained by Altena (1982) and Yilmaz (1986). Similar problems were also observed in this study. Due to the nature of polymer-nonsolvent interaction, the polymer concentration in the polymer-lean phase ($\phi_{3,l}$) approaches to zero for most of the equilibrium points. Yilmaz (1986) has reported $\phi_{3,l}$ as low as 10^{-30}. Within this region, the routine sometimes assumes a negative value for the polymer volume fraction, and it can cause the program to stop because of the logarithmic operation in the chemical potential expression.

To overcome this problem, the polymer volume fraction was assumed to be zero in the polymer lean phase. This reduces the chemical potential equations 3.10 and 3.11 for the polymer lean phase to equations 3.32 and 3.33.

$$\frac{\Delta\mu_{1,l}}{RT} = \ln(\phi_{1,l}) + (1-\frac{v_1}{v_2})\phi_{2,l} + \chi_{12}\phi_{2,l}^2 \tag{3.32}$$

$$\frac{\Delta\mu_{2,l}}{RT} = \ln(\phi_{2,l}) + (1-\frac{v_2}{v_1})\phi_{1,l} + \frac{v_2}{v_1}\chi_{12}\phi_{1,l}^2 \tag{3.33}$$

The choice one of the compositions as the independent variable in conjunction with the material balance, reduces the number of unknowns to three. For example, if one of the components in the polymer lean phase is chosen as the independent variable the functions to be minimized become as follows:

$$F_i = \frac{\Delta\mu_{i,l} - \Delta\mu_{i,r}}{RT} \qquad i = 1,2 \tag{3.34}$$

$$F_3 = 1 - \sum_{i=1}^{3} \phi_{i,r} \tag{3.35}$$

Near the critical point region, where the composition differences are not large, the routine can equate the volume fractions of the pairs in both phases. In order to avoid such a trivial solution, Hsu and Prausnitz (1973) modified the objective function into the form

$$OBJ = \sum_i \frac{(\Delta\mu_{i,l} - \Delta\mu_{i,r})^2 (RT)^{-2}}{(\phi_{i,l} - \phi_{i,r})^r} \tag{3.36}$$

where the value of r was recommended as 2 or 4. Yilmaz and McHugh(1986) have noted that, introducing such a penalty function has slightly improved their computational problems.

The calculation of the tie lines was started from near the polymer-nonsolvent line and proceeded through the critical point. The volume fraction of one component in one of the equilibrium phase was used as the initial guess in the calculation of the next tie line. So, in case the first tie line is calculated properly, the routine runs without any user input guess.

The number of unknowns in the spinodal equation are reduced to one by using material balance and choosing one of the volume fractions in one phase as the independent variable. Computational method for the spinodal line is similar to that used for the binodal line.

The critical or plait point was calculated by solving equations 3.16 and 3.23. This point was also approached as the distance between the end points of the tie line decreased. All equations used in constructing the ternary phase diagrams are nonlinear in nature and they were solved by using an IMSL routine called DNEQNF. The program codes written in Fortran were given in the Appendix.

3.4. Phase inversion techniques

3.4.1. Thermally induced phase separation (TIPS)

In TIPS process, a homogeneous polymer solution, comprising a solvent or a mixture of solvents and nonsolvents, is phase separated by lowering the temperature of the cast solution. Referring to Figure 3.3, when the temperature of the mixture is lowered below the critical point temperature, then the solution passes through the binodal curve and enters the metastable region (Witte et al. 1996). If the polymer is amorphous, microporous structures can be obtained by liquid-liquid phase separation followed by the gelation of the polymer (Laxminarayan et al. 1994). For semi-crystalline polymer, crystallization combined with liquid-liquid phase separation are responsible for structure formation (Caneba and Soong 1985).

3.4.2. Immersion Precipitation (Wet casting)

The first asymmetric membranes manufactured for reverse osmosis applications were produced using immersion precipitation technique by Loeb and Sourirajan in 1962. Since then, both experimental and modeling efforts in the area of asymmetric membrane formation have been focused on this technique. The analysis of immersion precipitation process is more complicated than the TIPS process, since the system is a ternary mixture.

The principal steps of immersion precipitation can be summarized as follows:

1. The preparation of the polymer solution consisting of a polymer and a solvent and/or a nonsolvent.
2. Casting of the homogeneous solution on a glass, metal or nonwoven textile fabric.
3. Evaporation step
4. Immersion of the cast solution into a nonsolvent bath

5. Extraction of the solvent and nonsolvent from the membrane and further treatment such as annealing.

In Table 3.1 a recipe for the production of cellulose acetate membrane by immersion precipitation method is given (Rautenbach and Albrecht 1989).

In wet casting technique, the structure and performance of the membrane is mainly controlled by immersion step. As illustrated in Figure 3.5, during an immersion step, casting solvent diffuses into the nonsolvent bath and counter-currently, nonsolvent in the bath penetrates into the polymer solution. Therefore, complex diffusion phenomena play an important role on the final structure.

For a specific polymer, solvent and nonsolvent, the morphology of the membrane, and consequently, separation characteristics, can be altered by changing concentration in the casting solution, evaporation time and conditions as well as temperature and composition in the bath.

Table 3.1. Recipe of a cellulose acetate membrane by immersion precipitation method. (Rautenbach and Albrecht 1989).

Casting Solution	Cellulose acetate	22.2 %
	Acetone	66.7 %
	Water	10.0 %
	$Mg(ClO_4)_2$	1.1 %
Precipitation Agent	Water	
Process Stage	Casting temperature	-7.5 to -16 ^{0}C
	Evaporation temperature	-7.5 to -16 ^{0}C
	Evaporation time	3 min
	Gel bath temperature	1-5 ^{0}C
	Annealing temperature	77-83 ^{0}C
	Annealing time	5 min

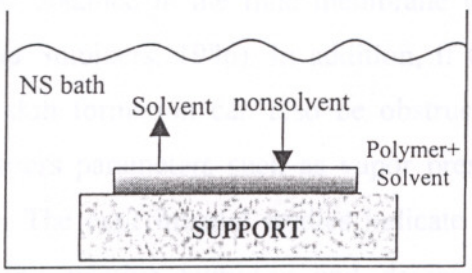

Figure 3.5. Schematic representation of the immersion step.

It was proposed that two types of demixing process, delayed and instantaneous precipitation, can take place in the immersed solution (Reuvers and Smolders 1987). In delayed precipitation, the demixing process does not occur at the instant of precipitation and the membrane is formed with a thick, dense skin and a sponge-type structure in the sublayer. Such membranes can be used in gas separation application where high selectivity is desired. In contrast, in the instantaneous precipitation, the demixing process starts at the instant of precipitation, which yields a thin skin layer over a highly porous layer. If the defects in the thin skin caused by the strong nonsolvent inflow can be prevented, a very rapid precipitation may result in the formation of closely packed spheres and nodules in the top layer (Tsay and McHugh 1992, Wienk et al. 1996).

The main discussion about immersion precipitation technique is the necessity of the evaporation step prior to immersion and its effects on final membrane structure. Based on the predicted composition paths shown in Figure 3.6; Tsay and McHugh (1992) proposed several structures produced by wet casting with and without prior evaporation step. Pinnau and Koros (1993) noted that, the formation of ultrathin and defect free skin layer is not possible without a forced evaporation step. Some experimental studies also suggest that an optimum evaporation time before quenching enhance the formation of defect free membranes with better separation characteristics (Pinnau and Koros 1991, Yamasaki et al. 1999).

3.4.3. Vapor induced phase separation

In vapor induced phase separation technique, the polymer solution is phase separated by the penetration of the nonsolvent from the vapor phase. The studies on this technique is fairly limited (Witte et al. 1996). In this technique, the mass transfer is much more slower than that in the immersion precipitation technique. So a flat concentration profile is obtained in the final membrane which yields to a symmetric structure (Wijmans and Smolders, 1986). In addition, if the vapor phase is saturated with the solvent, the skin formation can also be obstructed. The pore dimension is determined by the process parameters such as vapor pressure of the nonsolvent and polymer concentration. The experimental studies indicate that the more pores can be obtained with increasing relative humidity and decreasing polymer concentration (Matsuyama et al. 1999, Park et al. 1999).

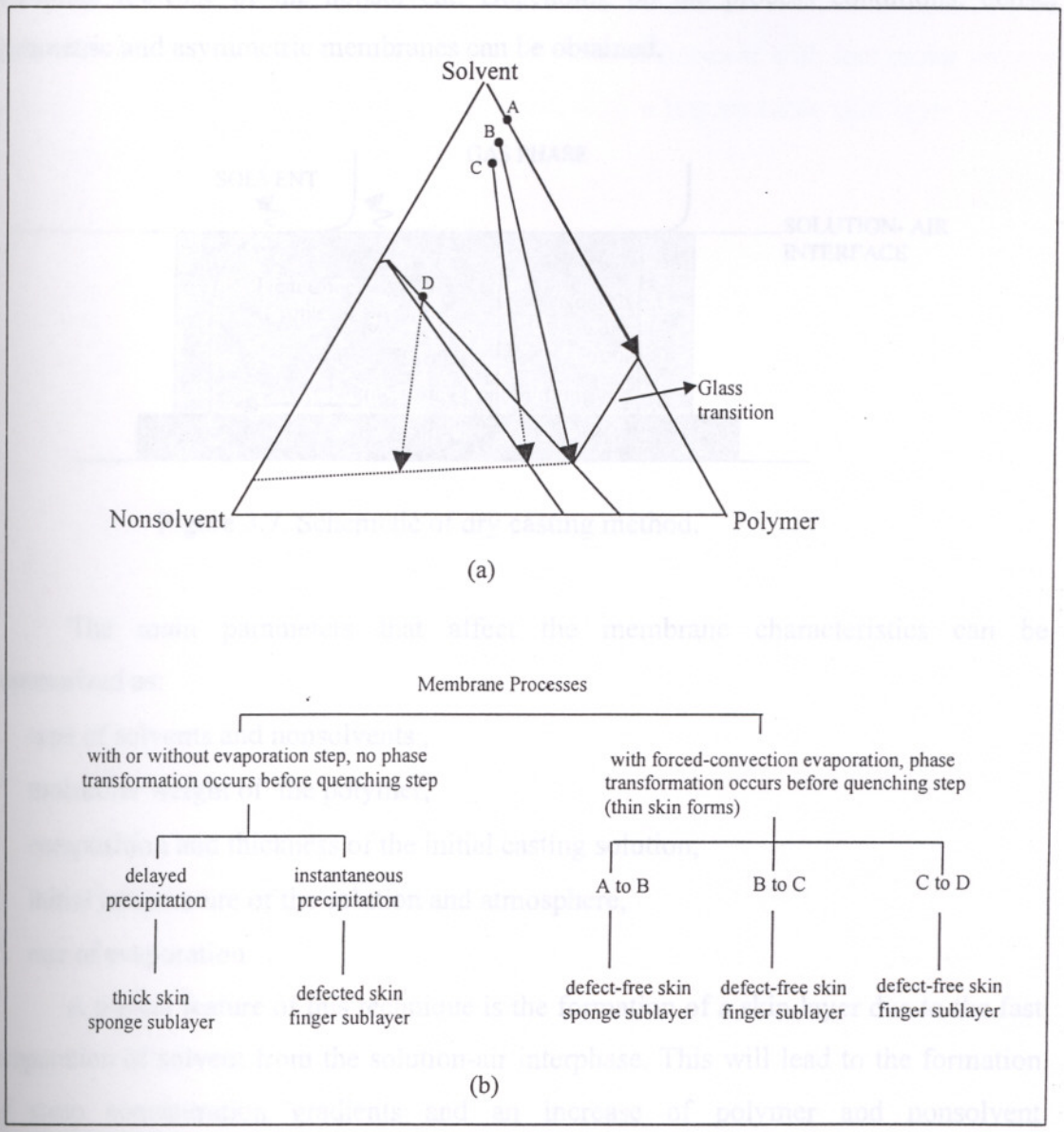

Figure 3.6. (a) Ternary phase diagram and concentration paths during membrane formation, (b) morphology-process relationship. (Reproduced from Tsay and McHugh, 1992)

3.4.4. Dry casting (Air casting)

Dry casting method, the subject of this thesis, involves the evaporation of solvent and nonsolvent from a at least ternary solution to manufacture a porous membrane. If the solvent used in the solution is more volatile than the nonsolvent, the

concentration of solvent decreases rapidly and phase separation is achieved due to fractional increase of the nonsolvent. Depending on the process conditions, dense, symmetric and asymmetric membranes can be obtained.

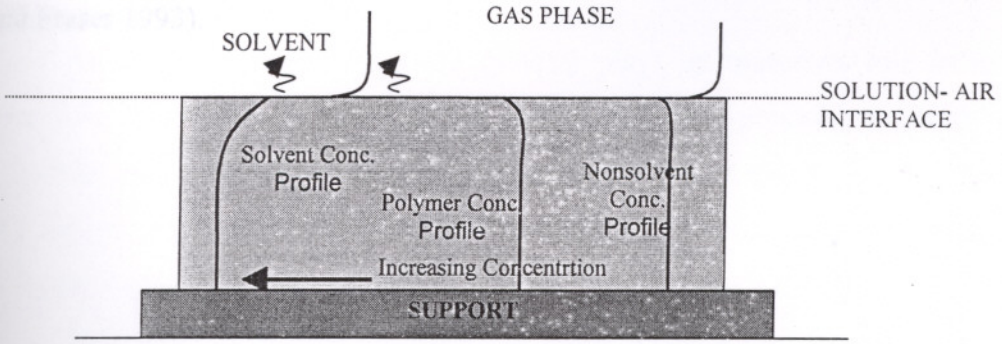

Figure 3.7. Schematic of dry casting method.

The main parameters that affect the membrane characteristics can be summarized as:

- type of solvents and nonsolvents ,
- molecular weight of the polymer,
- composition and thickness of the initial casting solution,
- initial temperature of the solution and atmosphere,
- rate of evaporation

A typical feature of this technique is the formation of a skin layer due to the fast evaporation of solvent from the solution-air interphase. This will lead to the formation of steep concentration gradients and an increase of polymer and nonsolvent concentrations at the surface as illustrated in Figure 3.7. In addition, the shrinkage of the film occurs due to solvent and nonsolvent loses. If the boiling point of the solvent is low enough significant evaporative cooling effects can be observed (Greenberg et al. 1995).

A wide range of morphology can be obtained with the dry cast membrane formation process. Main attempts were made on the investigation of the formation of macrovoids in the membrane. A number of hypotheses were proposed on the formation of macrovoids (Shojaie et al. 1994b). It was stated that, a macrovoid can be formed from a nuclei of a polymer-lean phase if the composition of the solution around the nuclei is stable. In addition, the polymer molar volume was found to be the key factor

for macrovoid formation. The experimental studies suggested that as the molar volume of the polymer increases the formation of macrovoids decreases and interconnected pore structures can be obtained. On the contrary, the use of polymer with low molar volume leads to macrovoid formation in the membrane with a impermeable skin layer (Zeman and Fraser 1993).

CHAPTER 4

DIFFUSION IN POLYMER SOLUTIONS

Diffusion in polymer solvent systems plays an important role in membrane formation processes as well as in other polymer processing steps such as devolatilization of residual solvents, formation of films, coatings etc. The fundamental physical property required to design and optimize these processes is the mutual diffusion coefficient, so, prediction of diffusion coefficients is crucial.

Several theories exist for predicting and correlating the diffusion coefficients of small molecules in liquids and gases. However, these theories are not applicable for polymer-solvent mixtures due to complex chain like structure of polymers. In contrast to low molecular weight systems, the diffusivities in polymer solutions are strong function of temperature and composition.

Different formalisms, based on the free volume theory, have been developed to predict self diffusion coefficients in polymer solvent systems. However, not self but mutual diffusion coefficients are required in defining most processes of industrial interest. Therefore, a few models have been proposed for relating the self diffusion coefficients to the mutual ones in multicomponent system.

In the first part of the chapter, the basis of free volume theory and then Vrentas-Duda (Vrentas and Duda 1984) free volume theory will be outlined. In the second part, the relationships between self and mutual diffusion coefficients in both binary and ternary mixtures will be given.

4.1. Free-volume theory

The free volume theory was first introduced by Cohen and Turnbull in 1959 (Kumins and Kwei 1968). In this theory, the small molecules are assumed as hard spheres, and if one of the spheres moves in any direction and leaves a space behind it, another sphere may jump to this vacancy. Such displacements in a bulk of liquid result in diffusive motion. Hence, the diffusion constant can be related to the average number of jumps per unit time and the jump distance. According to this theory, diffusion

coefficient is proportional to the probability of finding a hole of sufficient size and it is given in equation 4.1.

$$D_1 = A\exp\left[\frac{-\gamma V^*}{V^f}\right] \qquad (4.1)$$

where V^* is the minimum hole size into which molecule can jump and V^f is the average hole free volume per sphere. The proportionality constant A is related to the gas kinetic velocity and γ is the overlap factor to account for the overlap between free volume elements.

Numerous investigators have extended Cohen and Turnbull's free volume concepts to describe molecular transport in concentrated polymer solutions. Among these formulations, the most successful one was derived by Vrentas-Duda and it will be main focus of the next section.

4.2. Vrentas-Duda free volume theory

In Vrentas-Duda free volume theory, total volume of the liquid is divided into two parts: occupied volume and free volume, as shown in Figure 4.1. Total free volume is also splitted into two parts: hole free volume which is available for molecular transport and interstitial free volume which is unavailable for molecular transport.

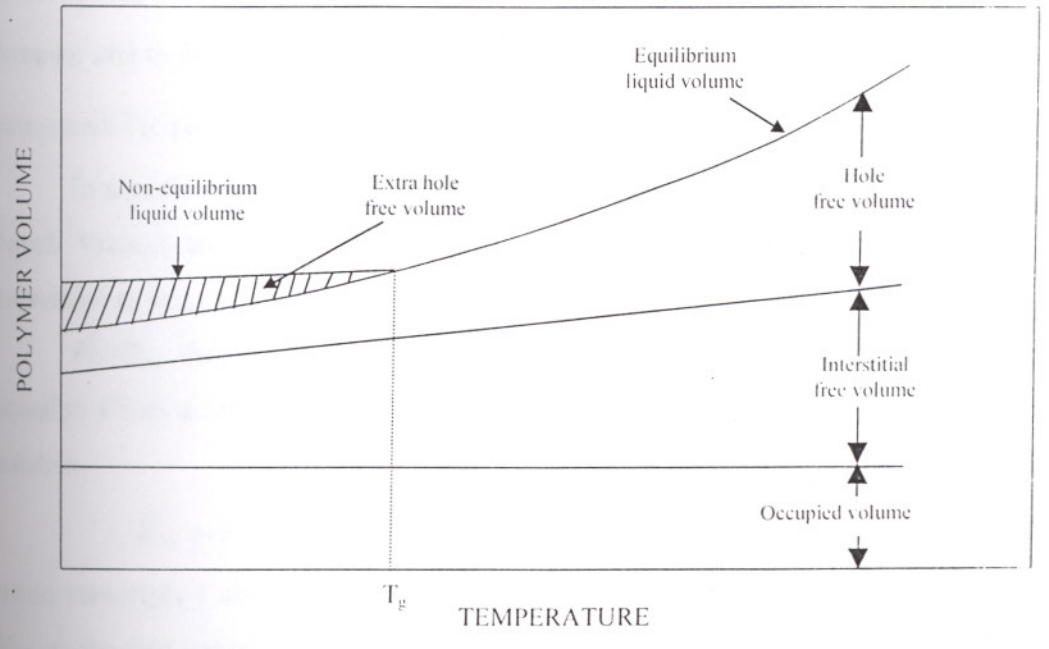

Figure 4.1. Characteristics of the volume of a polymer above and below the glass transition temperature.

To describe the self diffusion coefficient of a single component in a binary mixture, Vrentas and Duda modified equation 4.1 as follows:

$$D = D_{01} \exp\left[\frac{-\gamma\ \widetilde{V}_1^*}{\widetilde{V}_{FH}}\right] \tag{4.2}$$

in which $\widetilde{V}_1^*$ is the critical molar free volume for a jumping unit of species 1 to migrate and $\widetilde{V}_{FH}$ is the free volume per mole of all individual jumping units in the solution and is given by the following equation.

$$\widetilde{V}_{FH} = \frac{\hat{V}_{FH}}{\left[\frac{\omega_1}{M_{1j}} + \frac{\omega_2}{M_{2j}}\right]} \tag{4.3}$$

where,

$\hat{V}_{FH}$ = average specific hole free volume per gram of mixture.

$M_{i,j}$ = molecular weight of jumping unit of species i.

Combining equations 4.2 and 4.3 they derived following expression for solvent self diffusion coefficient in polymer solution.

$$D_1 = D_{01} \exp\left[-\frac{E}{RT}\right] \exp\left[\frac{-\gamma(\omega_1 \hat{V}_1^* + \omega_2 \xi \hat{V}_2^*)}{\hat{V}_{FH}}\right] \tag{4.4}$$

in which D_{01} is the pre-exponential factor, E is the activation energy required for a jumping unit to be free from its neighbors, $\hat{V}_i^*$ is the specific critical hole free volume of component i required for a jump and $\xi = \widetilde{V}_{1j}^* / \widetilde{V}_{2j}^*$.

In equation 4.4, the critical point is the determination of the free volume of the liquid. Vrentas and Duda have proposed a fully predictive theory that relates this expression to some properties of solvent and polymer.

Finally, they defined an expression for the specific hole free volume as in equation 4.5 as a function of volumetric characteristics of the pure components in the solution.

$$\hat{V}_{FH} = \omega_1 K_{11}(K_{21} - T_{g1} + T) + \omega_2 K_{12}(K_{22} - T_{g2} + T) \tag{4.5}$$

where subscripts 1 and 2 denote solvent and polymer respectively. K_{11}, K_{21} and K_{12}, K_{22} are the free volume parameters of solvent and polymer, respectively and T_g is the glass transition temperature.

The basic free volume expression for a binary system has been extended for a ternary system by considering the distribution of available hole free volume among all jumping units of solvent 1, solvent 2, and polymer 3, and the contributions to the hole free volume from two solvents as well as the polymer (Ferguson and Meerwall 1980, Vrentas et al. 1984). Including these modifications, self diffusion coefficients of solvent 1 and 2 in a ternary mixture are given as follows:

$$D_1 = D_{01} \exp\left(-\frac{\gamma(\omega_1 \hat{V}_1^* + \omega_2 \hat{V}_2^* \xi_{13}/\xi_{23} + \omega_3 \hat{V}_3^* \xi_{13})}{\hat{V}_{FH}} \right) \tag{4.6}$$

$$D_2 = D_{02} \exp\left(-\frac{\gamma(\omega_1 \hat{V}_1^* \xi_{23}/\xi_{13} + \omega_2 \hat{V}_2^* + \omega_3 \hat{V}_3^* \xi_{23})}{\hat{V}_{FH}} \right) \tag{4.7}$$

$$\hat{V}_{FH} = K_{11}(K_{21} + T - T_{g1})\omega_1 + K_{12}(K_{22} + T - T_{g2})\omega_2 + K_{13}(K_{23} + T - T_{g3})\omega_3 \tag{4.8}$$

4.3. Estimation of free volume parameters

The free volume parameters can be estimated if chemical structure of both solvents and polymers, viscosity of each pure component and density of pure solvents at different temperatures, critical molar volume of the solvents and the glass transition temperature of the polymer are known.

The critical molar volume of each component, $\hat{V}_1^*$, is estimated as the specific volumes of that components at 0 ^{0}K. The group contribution methods can be used to estimate the molar volumes at 0 ^{0}K.

The free volume parameters of the polymer are determined by fitting viscosity data of pure polymer and solvent to the expression which relates the viscosity to the hole free volume of the system (Doolittle 1951).

$$\ln \eta_2 = \ln A_2 + \frac{\left(\frac{\gamma \hat{V}_2^*}{K_{12}}\right)}{(K_{22} - T_{g2}) + T} \tag{4.9}$$

where, η_2 is the viscosity of the polymer.

If the polymer's glass transition temperature is known the Williams-Landel-Ferry (WLF) equation is an alternative expression for predicting the free volume parameters

of the polymer (Duda et al. 1982). For most of the polymers the WLF constants are predicted from viscosity temperature data (Ferry 1980) and can be related to free volume parameters as in equations 4.10 and 4.11.

$$K_{22} = C_{22}^{WLF} \tag{4.10}$$

$$\frac{K_{12}}{\gamma} = \frac{\hat{V}_2^*}{2.303(C_{12}^{WLF})(C_{22}^{WLF})} \tag{4.11}$$

The other parameters in equations 4.4 and 4.5, D_0, E, K_{11}/γ, and $K_{21} - T_{g1}$, can be estimated using equation 4.12 which is obtained by equating the Dullien's expression to the Vrentas-Duda free volume equation (Zielinski and Duda 1992, Hong 1995).

$$\ln\left(\frac{0.124\times10^{-16}\tilde{V}_1^{*2/3}RT}{\eta_1 M_1 \hat{V}_1}\right) = \ln D_0 - \frac{E(\omega_1 \to 1)}{RT} - \frac{\frac{\gamma\hat{V}_1^*}{K_{11}}}{K_{21} - T_{g1} + T} \tag{4.12}$$

where M_1 and $\tilde{V}_1^*$ are the solvent's molecular weight and critical molar volume respectively.

In this equation the only temperature dependent parameters are the viscosity ($\eta_1, g/cm.s$), and the specific volume ($\hat{V}_1, cm^3/g$) of the pure solvent. The $0.124^{\times}10^{-16}$ is a constant and has a units of $mol^{2/3}$. The energy effects can be assumed as negligible and in such a case E can be equated to zero. As a result, equation 4.12 becomes a three parameter regression problem.

The only remaining parameter to be estimated in equation 4.4 is the ratio (ξ) of the molar volume of the solvent jumping unit to that of the polymer jumping unit. Assuming that solvents move as a whole unit, then it may be expressed as:

$$\xi = \frac{\tilde{V}_1^0(0)}{\tilde{V}_{2j}} = \frac{M_1\hat{V}_1^*}{M_{2j}\hat{V}_2^*} \tag{4.13}$$

in which, M_{2j} represents the molecular weight of the jumping unit of the polymer. Zielinski and Duda (1992) proposed a relationship in which the size of a polymer jumping unit is independent of the solvent and is polymer specific as given by the equation 4.14.

$$\frac{\gamma \hat{V}_2^* \xi}{K_{12}} = \beta \tilde{V}_1^0(0) \tag{4.14}$$

According to this relationship, once β is known for a specific polymer the ξ parameter for any solvent in that polymer can be determined.

4.4. Determination of the mutual diffusion coefficients

4.4.1. Solvent-Polymer: Binary systems

The formalism derived for predicting mutual diffusion coefficient of a solvent in the binary solution is well established and has been successfully used. According to this formulation, mutual diffusion coefficient is a function of the self diffusivity and the thermodynamic factor as given by equation 4.15.

$$D = \frac{D_1 \omega_1 \omega_2}{RT} \left(\frac{\partial \mu_1}{\partial \omega_1} \right)_{T,P} \tag{4.15}$$

The chemical potential of the solvent is represented by μ_1. For polymer solutions there are several thermodynamic models to determine concentration dependence of chemical potentials, however, Flory-Huggins theory is the most widely used one. When the chemical potential of the solvent is represented by Flory-Huggins theory,

$$\frac{\mu_1 - \mu_1^0}{RT} = \ln \phi_1 + (1 - \frac{v_1}{v_2})\phi_2 + \chi_{12}\phi_2^2 \tag{4.16}$$

then equation 4.15 reduces to:

$$D = D_1(1-\phi_1)^2(1-2\chi\phi_1) \tag{4.17}$$

In equation 4.16 and 4.17, ϕ_1 and ϕ_2 represent the volume fraction of the solvent and polymer respectively and χ is the interaction parameter between solvent and polymer.

4.4.2. Solvent-Solvent-Polymer: Ternary systems

Diffusion in multicomponent systems is commonly encountered in practical applications. However, there are only a few models available in the literature to predict

multicomponent diffusivities. The lack of formulations is due to increasing number of diffusion coefficients as well as due to lack of enough experimental data to validate the models. If the multicomponent flux equations are written using the Fick's law as in equations 4.18 and 4.19 for a ternary system, it can be seen that four independent diffusion coefficients are required. The diagonal terms, D_{11}, D_{22} are called main diffusivities and the off-diagonal terms D_{12}, D_{21} are called cross diffusion coefficients.

$$J_1^* = -D_{11}\frac{\partial \rho_1}{\partial x} - D_{12}\frac{\partial \rho_2}{\partial x} \tag{4.18}$$

$$J_2^* = -D_{21}\frac{\partial \rho_1}{\partial x} - D_{22}\frac{\partial \rho_2}{\partial x} \tag{4.19}$$

For a n component system $(n-1)^2$ diffusion coefficients are needed.

Recently, two alternative methods, based on the Bearman' s statistical mechanical theory (Bearman 1961), have been proposed by Alsoy (1998) relating both main and cross mutual diffusion coefficients to self diffusion coefficients and thermodynamic data .

In the Bearman' s approach the frictional force, the right hand side of the equation 4.20, is a function of the velocity difference and the friction coefficient between two species.

$$\frac{d\mu_i}{dx} = -\sum_{j=1}^{N}\frac{\rho_j}{M_j}\zeta_{ij}(v_i - v_j) \tag{4.20}$$

According to this equation the chemical potential gradient, which is the actual driving force for diffusion, is equal in magnitude and opposite in sign to the frictional force.

In Bearman' s formulation, the self diffusion coefficients can be expressed in terms of five friction coefficients, which provide a link between self and mutual diffusivities. The practical application of Bearman's theory is currently not possible since the concentration and the temperature dependence of friction coefficients are not known. To overcome this problem, Alsoy (1998) proposed two different diffusion formalisms by imposing some assumptions through individual friction coefficients.

In the first case, it was assumed that the ratio of the friction coefficients is equal to the ratio of their molar volumes. With such an assumption, the main and cross diffusion coefficients are given by the equations 4.21-4.24.

$$D_{11} = \frac{D_1\rho_1}{RT}\left(\frac{\partial \mu_1}{\partial \rho_1}\right) \tag{4.21}$$

$$D_{12} = \frac{D_1 \rho_1}{RT}\left(\frac{\partial \mu_1}{\partial \rho_2}\right) \tag{4.22}$$

$$D_{21} = \frac{D_2 \rho_2}{RT}\left(\frac{\partial \mu_2}{\partial \rho_1}\right) \tag{4.23}$$

$$D_{22} = \frac{D_2 \rho_2}{RT}\left(\frac{\partial \mu_2}{\partial \rho_2}\right) \tag{4.24}$$

In the second case, the friction coefficients among all of the solute molecules are identically equal to zero (i.e, $\zeta_{11}=\zeta_{22}=\zeta_{12}=0$). Then the mutual diffusion coefficients are given by equations 4.25-4.28.

$$D_{11} = \rho_1(1-\rho_1\hat{V}_1)D_1\left(\frac{1}{RT}\frac{\partial \mu_1}{\partial \rho_1}\right) - \rho_1\rho_2\hat{V}_2 D_2\left(\frac{1}{RT}\frac{\partial \mu_2}{\partial \rho_1}\right) \tag{4.25}$$

$$D_{12} = \rho_1(1-\rho_1\hat{V}_1)D_1\left(\frac{1}{RT}\frac{\partial \mu_1}{\partial \rho_2}\right) - \rho_1\rho_2\hat{V}_2 D_2\left(\frac{1}{RT}\frac{\partial \mu_2}{\partial \rho_2}\right) \tag{4.26}$$

$$D_{21} = \rho_2(1-\rho_2\hat{V}_2)D_2\left(\frac{1}{RT}\frac{\partial \mu_2}{\partial \rho_1}\right) - \rho_1\rho_2\hat{V}_1 D_1\left(\frac{1}{RT}\frac{\partial \mu_1}{\partial \rho_1}\right) \tag{4.27}$$

$$D_{22} = \rho_2(1-\rho_2\hat{V}_2)D_2\left(\frac{1}{RT}\frac{\partial \mu_2}{\partial \rho_2}\right) - \rho_1\rho_2\hat{V}_1 D_1\left(\frac{1}{RT}\frac{\partial \mu_1}{\partial \rho_2}\right) \tag{4.28}$$

In each case, multicomponent mutual diffusivities are related to self diffusivities and thermodynamic factors, both of which can be predicted using free volume and Flory-Huggins thermodynamic theories. The validity of both formulations were implicitly tested for ternary polymer solutions (Alsoy and Duda 1999).

4.5. Determination of Flory-Huggins interaction parameters

Predicting mutual diffusion coefficients from self diffusivities and thermodynamic factors requires to know the Flory-Huggins interaction parameters

between the species. This parameter, χ, can be determined from solubility data in which the equilibrium weight fraction of the solvent in the polymer is known as a function of solvent vapor pressure, P_1, using the Flory-Huggins equation.

$$\frac{P_1}{P_1^0} = \phi_1 \exp(\phi_2 + \chi\phi_2^2) \tag{4.29}$$

where P_1^0 is the solvent saturation vapor pressure. The solvent weight and volume fractions are related through :

$$\phi_1 = \frac{\varpi_1 \hat{V}_1}{\omega_1 \hat{V}_1 + \omega_2 \hat{V}_2} \tag{4.30}$$

If solubility data is available; χ can be predicted by using Bristow's (Bristow and Watson 1958) semi-empirical equation.

$$\chi = 0.35 + \frac{\tilde{V}_1}{RT}(\delta_1 - \delta_2)^2 \tag{4.31}$$

where δ_i is the solubility parameter of component i. Extensive tables for the solubility parameters of both polymer and solvent are reported in Polymer's Handbook (Grulke 1999).

In this work, the interaction parameters for CA/water, CA/acetone and acetone/water were obtained from Dabral et al. (1998) as, 1.4, 0.5 and 1.3, respectively.

4.6. Calculation of free volume parameters of CA/Acetone/Water system

The free volume parameters of acetone and water were reported in the literature by Zielinski and Duda (1992) and Hong (1995). These values were regressed from molar volume and viscosity data and tabulated in Table 4.1.

Table 4.1. Free volume parameters of acetone and water

	$\hat{V}^*$ cm^3/g	$\tilde{V}^0(0)$ cm^3/mol	(K_{11}/γ) $cm^3/g.K$	$K_{21}-T_{g1}$ K	D_{01} cm^2/s	Reference
Acetone	0.943	54.77	9.83×10^{-4}	-12.12	14.3×10^{-4}	Zielinski and Duda(1992)
Acetone	0.943	-	1.86×10^{-3}	-53.33	3.6×10^{-4}	Hong (1995)
Water	1.071	-	2.18×10^{-3}	-152.29	8.55×10^{-4}	Hong (1955)

However, neither free volume parameters nor WLF constants for cellulose acetate (CA) were reported in the literature. To determine these polymer specific parameters, K_{13}/γ,

$K_{23} - T_{g3}$, as well as the mixture parameter $\hat{V}_3^* \xi_{23}$, the experimental self diffusion data of Anderson and Ullman (1973) and Park (1961) were fitted to Vrentas-Duda free volume theory. In the expression, the free volume parameters of acetone were obtained from Hong (1995) and energy effects were assumed to be negligible. The comparison of experimental data with the correlation is given in Figure 4.2 and the fitted parameters are tabulated in Table 4.2. The accuracy of the regressed values is high since the calculated self diffusion coefficients are in good agreement with the experimental data. The product of critical molar volume of polymer with the ratio of jumping unit of water to that of polymer, $\hat{V}_3^* \xi_{13}$, was obtained from the following equation

$$\hat{V}_3^* \xi_{13} = \frac{\hat{V}_1^* M_1}{M_{3j}} \tag{4.32}$$

in which jumping unit of polymer, M_{3j}, was calculated as follows using the values determined for acetone.

$$M_{3j} = \frac{\hat{V}_2^* M_2}{\hat{V}_3^* \xi_{23}} \tag{4.33}$$

The summary of all free volume parameters and Flory-Huggins interaction parameters is given in Table 4.3.

Table 4.2. Free volume parameters of CA/acetone and CA/water systems

	(K_{12}/γ) $cm^3/g.K$	K_{22}-T_{g2} K	$\xi_{i3}\hat{V}_3^*$ cm^3/g
CA / Acetone	3.64×10^{-4}	-240.0	0.715
CA / Water	3.64×10^{-4}	-240.0	0.252

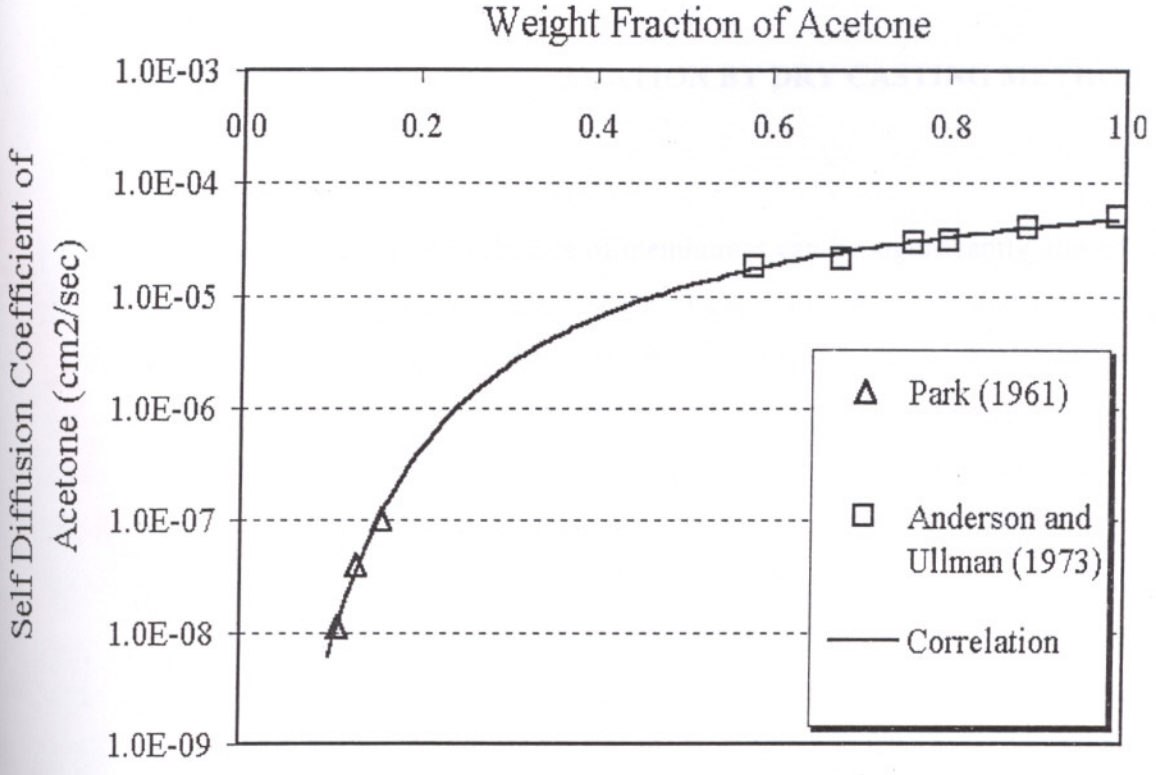

Figure 4.2. The self diffusion coefficient of acetone in cellulose acetate as a function of weight fraction. Comparison of the experimental data (Anderson and Ullman 1973, Park 1961) with the calculated self diffusion coefficients.

Table 4.3. Free volume and Flory-Huggins interaction parameters used in diffusivity correlations.

Parameter	**CA/Acetone**	**CA/Water**
D_0 cm^2/sec	3.6 10^{-4}	8.55 10^{-4}
E_i J/mol	0	0
K_{11}/γ cm^3/gK	0.00186	0.00218
K_{12}/γ cm^3/gK	0.000364	0.000364
K_{21}-T_{g1} K	-53.33	-152.29
K_{22}-T_{g2} K	-240	-240
$\hat{V}_1^*$ cm^3/gr	0.943	1.071
$\xi_{13}\hat{V}_3^*$	0.715	0.252
χ	0.5	1.4

CHAPTER 5

MODELING OF MEMBRANE FORMATION BY DRY CASTING METHOD

The morphology and performance of membranes can be significantly altered by both processing and casting conditions. Slight changes in the membrane fabrication recipes can greatly influence the final membrane morphology. A fully predictive mathematical model provides a convenient means of investigating the effect of different parameters on the final membrane structure and eliminates the extensive trial and error experimentation. These facts are considerable motivations for the development of mathematical models.

The modeling of membrane formation process by dry casting method is complicated due to phase separation, simultaneous heat and mass transfer controlled by complex thermodynamic and transport properties of polymer solutions. Most of the work in literature has focused on the modeling of wet casting method. There exist only a few models on the dry casting technique. The models developed for the wet-cast method cannot be used as a basis for modeling dry cast process, since the latter process involves coupled heat and mass transport. Hence, in this thesis, a fully predictive model was used for the formation of membranes through the dry cast process.

Theoretical treatment of membrane formation process requires to combine kinetics and thermodynamics of the system simultaneously. Thermodynamic consideration is necessary to draw a phase boundary line, to formulate boundary conditions and diffusivity relations. On the other hand, kinetic consideration is necessary to predict the composition paths in the membrane. When these paths are plotted on the phase diagram, they provide information about the final membrane structure.

This chapter consists three parts. In the first part, previous studies on phase inversion techniques were criticized, detailed derivation of the dry casting model equations was given, and computational method for solving these equations was discussed. In the previous chapter, most of the model parameters (free volume parameters and the Flory-Huggins interaction parameters) were given. In the final part of this chapter, methods to calculate remaining model parameters, heat and mass

transfer coefficients and interface pressures, were discussed and all physical properties used in the calculations were tabulated.

5.1. Previous studies on phase inversion and evaporative casting techniques

5.1.1. Binary solution-Evaporation models

The studies on the immersion precipitation have mainly focused on the modeling of evaporation step. The first evaporation model was developed by Anderson and Ullman (1973). They predicted the solvent concentration in the film by assuming semi-infinite film thickness, unidirectional isothermal mass transfer perpendicular to the surface, negligible film shrinkage and specified constant surface concentration. The differential equation, initial and boundary conditions are given by equations 5.1 through 5.4.

$$\frac{\partial \phi_2}{\partial t} = \frac{\partial}{\partial x}\left(D \frac{\partial \phi_2}{\partial x} \right) \tag{5.1}$$

$$\phi_2(x,0) = \phi_0 \tag{5.2}$$

$$\phi_2(0,t) = \phi_s \tag{5.3}$$

$$\phi_2(\infty,t) = \phi_s \tag{5.4}$$

They performed their calculations for two cases. In the first case, it was assumed that polymer response to the change is instantaneous and concentration dependence of the diffusion coefficient, D, is given by the following equation 5.5 (Fujita 1968).

$$D = D(0)\exp\left(\frac{\phi_2}{(A\phi_2 + B)} \right) \tag{5.5}$$

in which the constants A and B were regressed from the experimental self diffusivity data. In the second case, they assumed that the process is controlled by solvent diffusion and rate of polymer response. Therefore, the diffusion coefficient was defined as a function of both composition and time. However, in both models, they used the self diffusion coefficient rather than the mutual diffusion coefficient. According to the predicted time dependent solvent concentration profiles in the film, they have concluded that, to obtain a very thin skin layer, the polymer response should be fast and the solvent diffusion coefficient should decrease dramatically with increasing polymer concentration.

Castellari and Ottani (1981) improved some of the assumptions of Anderson and Ullman (1973). They assumed a finite film thickness and took into account the film shrinkage. Additionally, the surface concentration was allowed to vary in time by using an empirical expression which involves an evaporation rate constant. Similar to the previous model, they used the same expression for the concentration dependence of diffusion coefficients. Their results indicated that the evaporation time and the evaporation rate are critical parameters in determining the thickness of the skin layer of a membrane. In addition, they concluded that conditions in the drying atmosphere play an important role on the formation of asymmetric structures.

Ataka and Sasaki (1982) performed gravimetric experiments on cellulose acetate and acetone binary casting solutions, to investigate the effect of initial casting compositions, the thickness and ambient temperature on the rate of solvent evaporation. To compare the experimental results with theory, they derived an analytical solution assuming constant diffusion coefficient, isothermal process and no film shrinkage.

On the contrary to the previous models, in the evaporation model developed by Krantz et al. (1986), a surface boundary condition was used in which mass transfer from the surface to the ambient phase is proportional to the mass transfer coefficient. In addition, the excess volume of mixing effect was incorporated in the model. The self diffusion coefficient was correlated by Fujita's expression (equation 5.5), however, unlike prior models, it was related to the mutual diffusion coefficient by a semi-empirical function. They also studied the cellulose acetate-acetone system and obtained the necessary self diffusion data from Anderson and Ulmann's (1973) study.

Tsay and McHugh (1991) developed a fully predictive model for the evaporation of binary solution consisting of cellulose acetate and acetone. They took into account the moving interface, concentration dependent mutual diffusion coefficients and time dependent mass transfer coefficients. In predicting the self diffusion coefficient of acetone, Vrentes and Duda free volume theory was used in conjunction with the experimental diffusion data of Anderson and Ulmann (1973). They investigated the effects of initial compositions, casting film thickness, surface area, and the composition of the solvent in the vapor phase on the evaporation rates. In addition they compared their numerical results with the experimental studies of Ataka and Sasaki (1982) and with the analytical solution obtained for fixed finite thickness, constant diffusion coefficients and constant volume flux at the solution-air interface.

5.1.2. Ternary solution- Dry casting and Evaporation models

The modeling studies for the evaporation of ternary solution are limited due to increasing complexity of equations and the lack of experimental multicomponent diffusion data. In all models that have been discussed in previous section, it was assumed that membrane formation process is a isothermal process. This is not a very realistic assumption since evaporative cooling effects can be significant. Greenberg et al. (1995) have observed a decrease in membrane temperature from an initial casting temperature of 25 ^{0}C to 0 ^{0}C during the evaporation of acetone from cellulose acetate.

The first non-isothermal model on dry-casting method for a ternary mixture was developed by Shojaie et al. (1994a). In their model, equations were formulated using mass average velocity and excess volume of mixing effects were incorporated. The change in thickness of the film was considered and is a function of both position and time. They have used cellulose acetate-acetone-water as a model system and Fujita's expression to predict self diffusion coefficients. The constants of Fujita's expression were obtained by regressing the experimental data of Anderson and Ullman (1973) and Roussis (1981). The self diffusion coefficients were related to mutual diffusion coefficients using friction coefficients. The water/acetone and acetone/cellulose acetate friction coefficients were related to the available binary-diffusion coefficients, whereas the water/cellulose acetate friction coefficients were related to acetone/cellulose acetate friction coefficients. In constructing the phase diagram and as well as in defining the boundary condition at the solution-air interface, Flory-Huggins theory was used with variable interaction parameters. The heat and mass transfer coefficients were predicted using empirical correlation derived for free convection. The effects of initial composition and casting thickness were investigated and the numerical results were compared with the experimental results (Shojaie et al. 1994b). The total mass loss due to both solvent and nonsolvent evaporation and temperature of the film were measured by microbalance and infrared camera respectively. In addition final membrane morphologies were determined with the SEM pictures and results were compared with the model predictions.

Matsuyama et al. (1997) performed modeling studies to investigate the effects of nonsolvent type used in the casting solution. Although the system is ternary, they

assumed that the nonsolvent evaporation is negligible and therefore used binary diffusion equation.

The model developed by Alsoy and Duda (1999) describes the multicomponent drying behavior of polymer solutions. Unlike previous studies, in this model the problem is cast in terms of volume average velocity instead of mass average velocity. This choice significantly reduced the complexity of the equations. In addition, the temperature was assumed to be a function of time only. The experimental and modeling studies of Shojaie et al (1994a, 1994b) are consistent with this assumption. The model equations consist of coupled unsteady state heat and mass transfer equations, film shrinkage and boundary conditions. The main and cross mutual diffusion coefficients were expressed in terms of thermodynamic factors and self diffusivities using Flory-Huggins and Vrentas-Duda free volume theories respectively. The details of this study will be given later in this chapter under the section of development of model equations.

5.1.3. Immersion precipitation and vapor induced phase separation models.

In immersion precipitation and vapor induced phase separation techniques, initially homogeneous polymer, solvent and/or nonsolvent mixture is phase separated by the inflow of the nonsolvent either from the liquid phase or vapor phase. Therefore, both systems of interest are ternary and in principle, the main difference between the models arises in determining the boundary condition at the solution-air or liquid interface.

In most of the modeling studies of quenching step of immersion precipitation techniques, the system is treated as an isothermal process. This assumption is reasonable, if the temperature of the quenching medium is kept constant. In addition, it has been usually assumed that no polymer dissolves in the coagulation bath and instantaneous equilibrium exists between the film side and bath side.

The first model on immersion precipitation was developed by Cohen et al. (1979) and it was based on steady state diffusion model. Predicted composition paths were plotted on the ternary phase diagram to make comments on the final membrane morphology.

Yilmaz and McHugh (1986b) developed a unidirectional pseudobinary diffusion equation formalism for constant partial molar volumes and negligible bath dynamics. For a semi-infinite film thickness, they assumed constant surface flux at the film-bath

interface. Their experimental studies have indicated that a fast convective flow of solvent occurs in the bath due to density fluctuations. Therefore, they argued that their model is applicable for short times prior to skin formation.

In the model of Reuvers and Smolders (1987), the bath dynamics has also been taken into account. The mass transfer in the bath was assumed to be diffusion controlled. The ternary diffusion equations were derived from binary diffusion and thermodynamic data. Their analyses are applicable only for short period of time after immersion step, because in the derivation of the equations they assumed semi finite film thickness and constant interfacial concentrations.

A more complete model was developed by Tsay and McHugh (1990) which incorporates film shrinkage and variable interface compositions. They investigated the initial polymer concentration, addition of nonsolvent in the casting solution prior to quenching, addition of solvent in the coagulation bath, polymer molecular weight, initial film thickness and thermodynamic interaction parameters on the final structure membranes cast from cellulose acetate/acetone system.

Cheng et al. (1994) considered the convective mass transfer in the coagulation bath and investigated the effects of the parameters, used in defining the diffusion coefficients on the precipitation times.

The only modeling study on the vapor induced phase separation technique was performed by Matsuyama et al (1999). In fact the modeling of this technique is similar to that of dry casting. In that study, they investigated the concentration profiles of polymer in the film during the penetration of the nonsolvent from the vapor phase to a initially homogeneous polymer-solvent solution. Due to the low concentration of nonsolvent in the film, they derived their diffusion equations for quasi binary system.

5.2. Development of model equations

The assumptions and model equations derived here for the dry casting technique are based on the modeling study of Alsoy (1998) originally developed for the drying behavior of multicomponent polymer solutions. The equations are developed for the system geometry shown in Figure 5.1.

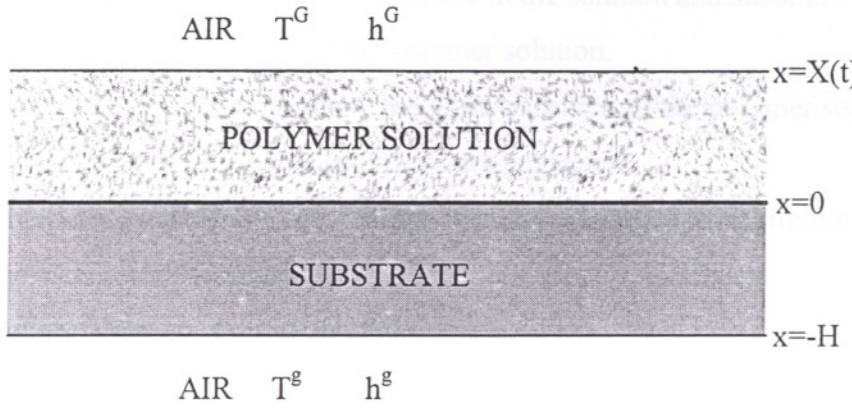

Figure 5.1. Schematic of dry casting process.

The polymer solution is cast on a substrate with a thickness of H. The cast solution thickness, X, is time dependent. The polymer solution and substrate have interfaces with air. The air facing the polymer solution has a temperature of T^G and a heat transfer coefficient of h^G. These values for the air next to the substrate are T^g and h^g respectively.

5.2.1. Assumptions

The model equations derived in this thesis are based on the following assumptions.

1. Both heat and mass transfers are unidirectional since the width of the film is much greater than the thickness.
2. The density of the solution is a function of the composition, while, the partial specific volumes are independent of composition and temperature. Hence, there is no volume change on mixing.
3. No reaction occurs in the system .
4. The average values for the density, heat capacity, and thermal conductivity of the solution are used.
5. The substrate is impermeable. Therefore, there is no mass transfer at the solution-substrate interface.
6. Gravitational effects are neglected.
7. The polymer solution behaves as a Newtonian fluid.
8. Heat transfer by the radiative mode is neglected.

9. The temperature is a function of time only, since the resistance to heat transfer in the gas phase is much greater than the resistance in the solution and substrate.
10. There is no viscous dissipation in the polymer solution.
11. The temperature of the film is above the glass transition of the polymer solution.
12. The kinetic energy effects at the interfaces are neglected.
13. The convective exchange of momentum at phase interfaces is negligible compared to the forces at phase boundaries.
14. The gas phase does not exert drag on the solution.
15. Gas phase is ideal.

The heat and mass transfer equations are uncoupled by the aid of assumption 4 and as a result, the complex fluid mechanics problem is avoided (Vrentas and Vrentas 1994).

5.2.2. Derivation of equations

5.2.2.1. Species continuity equation

The species continuity equation for component i:

$$\frac{\partial \rho_i}{\partial t} + \left(\frac{\partial n_{i,x}}{\partial x} + \frac{\partial n_{i,y}}{\partial y} + \frac{\partial n_{i,z}}{\partial z} \right) = R_i \tag{5.6}$$

Using assumptions 1 and 3 the continuity equation can be simplified into:

$$\frac{\partial \rho_i}{\partial t} = -\frac{\partial n_{i,x}}{\partial x} \tag{5.7}$$

Here, mass flux $n_{i,x}$ can be expressed in terms of volume average velocity υ^*.

$$n_i = \rho_i \upsilon_i = \rho_i \upsilon^* + \rho_i (\upsilon_i - \upsilon^*) \tag{5.8}$$

where,

$$\upsilon^* = \sum \hat{V}_i \rho_i \upsilon_i \tag{5.9}$$

In equation 5.8 the first term on the right hand side represents the flux of component i moving with the bulk stream. The second term is the diffusive flux relative to the bulk stream and can be expressed by Fick's law.

For an N component system the diffusive flux is given by equation 5.10:

$$j_i^{*} = \rho_i(\upsilon_i - \upsilon^{*}) = \sum_{j=1}^{N-1}(-D_{ij}\frac{\partial \rho_j}{\partial x}) \tag{5.10}$$

and total continuity equation is given by equation 5.11.

$$\frac{\partial \rho}{\partial t} = -\frac{\partial}{\partial x}\cdot\sum_{i=1}^{3}\rho_i\upsilon_i \tag{5.11}$$

If species continuity equation written for each component in equation 5.7 is multiplied by partial specific volume of each component, $\hat{V}_i$, and if these equations are summed from i=1 to N, then

$$\sum_{i=1}^{N}\frac{\partial}{\partial t}(\rho_i\hat{V}_i) + \sum_{i=1}^{N}\frac{\partial}{\partial x}(\rho_i\upsilon_i\hat{V}_i) = 0 \tag{5.12}$$

Using equation 5.9 and definition of volume fraction, $\sum_{i=1}^{N}\rho_i\hat{V}_i = 1$, then, equation 5.12 reduces to the following form:

$$\frac{\partial \upsilon^{*}}{\partial x} = 0 \tag{5.13}$$

Since the substrate is impermeable (assumption 5), the velocity of species at the solution substrate interface are zero. Therefore, using equation 5.13 it can be stated that the volume average velocity is zero at that interface. Since the volume average velocity gradient was found to be zero, then the volume average velocity is zero throughout the cast solution. Thus, the convective term can be neglected and the total flux of component i can be expressed as follows:

$$n_{i,x} = \rho_i\upsilon_i = \rho_i(\upsilon_i - \upsilon^{*}) = \sum_{j=1}^{N-1}(-D_{ij}\frac{\partial \rho_j}{\partial x}) \tag{5.14}$$

Consequently, the species continuity equation can be simplified into the following form.

$$\frac{\partial \rho_i''}{\partial t} = \frac{\partial}{\partial x}\left[\sum_{j=1}^{2}D_{ij}\frac{\partial \rho_j''}{\partial x}\right] \tag{5.15}$$

To solve equation 5.15 two boundary conditions and one initial condition are needed. At the instant of casting, the solution is homogeneous and the concentrations of the species in the cast film do not vary with position.

$$\text{At } t=0 \quad \rho_i''(0,x) = \rho_{i0}'' \tag{5.16}$$

At the solution-substrate interface the mass transfer rate is zero (assumption 5).

$$n_i^p\Big|_{x=0} = 0 = j_i^{\neq} = -\sum_{j=1}^{N-1}(D_{ij}\frac{\partial \rho_j}{\partial x}) \tag{5.17}$$

Thus, one of the boundary conditions can be expressed as:

$$\text{at} \qquad x=0 \qquad \frac{\partial \rho_i^p}{\partial x} = 0 \tag{5.18}$$

The other boundary, the solution-air interface, moves due to shrinkage of the film. Appropriate boundary condition at this interface is obtained from jump mass balance, expressed by equation 5.19.

$$\rho_i^p(\mathbf{v}_i^p \cdot \mathbf{n}^* - \mathbf{U}^* \cdot \mathbf{n}^*) = \rho_i^G(\mathbf{v}_i^G \cdot \mathbf{n}^* - \mathbf{U}^* \cdot \mathbf{u}^*) \tag{5.19}$$

in which $\mathbf{n}^*$ is the unit normal vector pointing from polymer solution phase to gas phase (denoted by superscripts p and G respectively), $\mathbf{v}_i^J$ is the velocity vector of component i in phase J and $\mathbf{U}^*$ is the velocity vector of the phase interface.

The change of the film thickness with respect to time can be expressed as:

$$\mathbf{U}^*.\mathbf{n}^* = \frac{dX}{dt} \tag{5.20}$$

The mass transfer to the gas phase, the right hand side of equation 5.19, can be approximated using the analogy given in equation 5.21.

$$\rho_i^G(\mathbf{v}_i^G \cdot \mathbf{n}^* - \mathbf{U}^* \cdot \mathbf{n}^*) = k_i^G(P_{ii}^G - P_{ib}^G) = \rho_i^p \mathbf{v}_i^p.\mathbf{n}^* - \rho_i^p \mathbf{U}^*.\mathbf{n}^* \tag{5.21}$$

According to equation 5.21, the rate of mass transfer is proportional to the mass transfer coefficient and the difference between the partial pressure of volatile component at the interface and in the bulk. Combining equations 5.20 and 5.21, and noting that $n_i = \rho_i^p \mathbf{v}_i^p \cdot \mathbf{n}^*$ then, equation 5.21 can be expressed as follows:

$$k_i^G(P_{ii}^G - P_{ib}^G) = n_i\Big|_{x=X(t)} - \rho_i^p\Big|_{x=X(t)}\frac{dX}{dt} \tag{5.22}$$

Inserting the definition of n_i, one can define the second boundary condition at the solution-air interface as follows:

$$\text{at } x=X(t) \qquad -\left[\sum_{j=1}^{2} D_{ij}^p \frac{\partial \rho_j^p}{\partial x}\right] - \rho_i^p \frac{dX}{dt} = k_i^G(P_{ii}^G - P_{ib}^G) \tag{5.23}$$

5.2.2.2. Heat transfer equation

The one dimensional unsteady state heat transfer equation in terms of transport properties of the solution and substrate phases can be written as follows:

$$\rho^p C_p^p \frac{\partial T^p}{\partial t} = \mathrm{k}^p \frac{\partial^2 T^p}{\partial x^2} \tag{5.24}$$

$$\rho^s C_p^s \frac{\partial T^s}{\partial t} = \mathrm{k}^s \frac{\partial^2 T^s}{\partial x^2} \tag{5.25}$$

If equation 5.24 is integrated from x=0 to x=X(t) and equation 5.25 from x=0 to x=-H, the following expressions are obtained

$$\rho^p C_p^p \frac{\partial T^p}{\partial t} X(t) = k^p \frac{dT^p}{dx}\bigg|_{x=0}^{x=X(t)} \tag{5.26}$$

$$\rho^s C_p^s \frac{\partial T^s}{\partial t} H = k^s \frac{dT^s}{dx}\bigg|_{x=-H}^{x=0} \tag{5.27}$$

The addition of these two expressions yield equation 5.28

$$\rho^p C_p^p \frac{\partial T^p}{\partial t} X(t) + \rho^s C_p^s \frac{\partial T^s}{\partial t} H = k^p \frac{dT^p}{dx}\bigg|_{x=0}^{x=X(t)} + k^s \frac{dT^s}{dx}\bigg|_{x=-H}^{x=0} \tag{5.28}$$

To derive final form of heat transfer equation, the heat fluxes at the substrate-air (x=-H), substrate-solution (x=0) and solution-air (x=X(t)) interfaces must be defined. They are basically obtained from the jump energy balances which is applied at each interface. Equation 5.29 shows this expression written at the interfaces of phases A and B.

$$\begin{aligned} &\rho^A \hat{U}^A (\mathbf{v}^A \cdot \mathbf{n}^A - \mathbf{U}^* \cdot \mathbf{n}^*) + \mathbf{q}^A \cdot \mathbf{n}^* - \mathbf{v}^A \cdot (\mathbf{T}^A \cdot \mathbf{n}^*) \\ &= \rho^B \hat{U}^B (\mathbf{v}^B \cdot \mathbf{n}^B - \mathbf{U}^* \cdot \mathbf{n}^*) + \mathbf{q}^B \cdot \mathbf{n}^* - \mathbf{v}^B \cdot (\mathbf{T}^B \cdot \mathbf{n}^*) \end{aligned} \tag{5.29}$$

in which, $\mathbf{v}^J$ and $\mathbf{T}^J$ are the mass average velocity vector and stress tensor in phase J respectively. For the substrate-solution interface this expression can be simplified into equation 5.30 considering that the interface is not moving and the velocities of the species are zero. At x=0

$$\begin{aligned} \mathbf{U}^* \cdot \mathbf{n}^* &= 0 \\ \mathbf{v}^p \cdot \mathbf{n}^* = \mathbf{v}^s \cdot \mathbf{n}^* &= 0 \\ \mathbf{q}^s \cdot \mathbf{n}^* &= \mathbf{q}^p \cdot \mathbf{n}^* \end{aligned} \tag{5.30}$$

where, $\mathbf{q}^J$ is the conductive heat flux vector in phase J. Using Fourier's law of heat conduction, the jump energy balance at x=0 becomes:

$$-\mathrm{k}^p \left.\frac{\partial T^p}{\partial x}\right|_{x=0} = -\mathrm{k}^s \left.\frac{\partial T^s}{\partial x}\right|_{x=0} \tag{5.31}$$

Similarly, for the gas-substrate interface (x = -H), the jump energy balance reduces to:

$$\mathbf{q}^s \cdot \mathbf{n}^* = \mathbf{q}^g \cdot \mathbf{n}^* \tag{5.32}$$

Heat transfer from the gas phase to the substrate is described by Newton's law of cooling. Then equation 5.32 becomes as follows.

$$-k^s \left.\frac{\partial T^s}{\partial x}\right|_{x=-H} = h^g (T^g - T^s) \tag{5.33}$$

At the solution-gas interface (x=X(t)), the jump energy balance must be coupled with jump mass balance equation. If total jump mass balance equation is equated to Q,

$$Q = \rho^p (\mathbf{v}^p \cdot \mathbf{n}^* - \mathbf{U}^* \cdot \mathbf{n}^*) = \rho^G (\mathbf{v}^G \cdot \mathbf{n}^* - \mathbf{U}^* \cdot \mathbf{u}^*) \tag{5.34}$$

then, jump energy balance can be written as follows:

$$Q(\hat{U}^G - \hat{U}^p) = \mathbf{q}^p \cdot \mathbf{n}^* - \mathbf{q}^G \cdot \mathbf{n}^* + \mathbf{v}^G \cdot (\mathbf{T}^G \cdot \mathbf{n}^*) - \mathbf{v}^p \cdot (\mathbf{T}^p \cdot \mathbf{n}^*) \tag{5.35}$$

The internal energy ($\hat{U}$)can be defined as a function of enthalpy($\hat{H}$), pressure and density.

$$\hat{U} = \hat{H} - \frac{P}{\rho} \tag{5.36}$$

Multiplying both sides of the equation with Q yields

$$Q\hat{H} = Q\hat{U} + P\upsilon \tag{5.37}$$

Stress tensors in both phases can be written as follows using assumption 15:

$$\mathbf{T}^G_{xx} \cdot \mathbf{n}^* = -\mathbf{P}^G \qquad \mathbf{T}^p_{xx} \cdot \mathbf{n}^* = -\mathbf{P}^p \tag{5.38}$$

Combining equations 5.35, 5.37 and 5.38 gives,

$$Q(\hat{H}^G - \hat{H}^p) = \mathbf{q}^p \cdot \mathbf{n}^* - \mathbf{q}^G . \mathbf{n}^* \tag{5.39}$$

The term, $Q(\hat{H}^G - \hat{H}^p)$, represents total amount of energy lost due to evaporation; so it can be defined as follows:

$$Q(\hat{H}^G - \hat{H}^p) = \sum_{i=1}^{N-1} k_i^G (P_{ii}^G - P_{ib}^G) \Delta \hat{H}_{vi} \tag{5.40}$$

The heat flux in the polymer phase $\mathbf{q}^p \cdot \mathbf{n}^*$, is described by Fourier's law of conduction and heat flux in the gas phase is defined by Newton's law of cooling, as follows:

$$\mathbf{q}^p \cdot \mathbf{n}^* = -k\frac{\partial T}{\partial x} \qquad \mathbf{q}^G \cdot \mathbf{n}^* = h^G(T^p - T^G) \tag{5.41}$$

If equations 5.40 and 5.41 are inserted into equation 5.39, then the heat transfer boundary condition at x=X(t) is obtained as follows:

$$\text{At x=X(t)} \quad \sum_{i=1}^{N} k_i^G (P_{ii}^G - P_{ib}^G)\Delta\hat{H}_v = -k^p \frac{\partial T^p}{\partial x} - h^G(T^p - T^G) \tag{5.42}$$

It is generally assumed that the temperature is continuos at the phase boundary.

$$T^p = T^s \tag{5.43}$$

If equations 5.31, 5.33, 5.42 and 5.43 are substituted into equation 5.28, then the final form of the heat transfer equation is obtained as follows:

$$\frac{dT}{dt} = -\left[\frac{h^G(T - T^G) + \sum_{i=1}^{N-1} k_i^G \Delta\hat{H}_{vi}(P_{ii}^G - P_{ib}^G) + h^g(T - T^g)}{\rho^p \hat{C}_p^p X(t) + \rho^s \hat{C}_p^s H}\right] \tag{5.44}$$

To solve equation 5.44 an initial condition is needed and it is assumed that initially the cast solution has a temperature of T_0 .

$$\text{at } t = 0 \qquad T(0) = T_0 \tag{5.45}$$

5.2.2.3. Time dependence of boundary position

Time dependence of boundary position is obtained from the jump mass balance for the polymer.

$$\rho_3^p(\mathbf{v}_3^p \cdot \mathbf{n}^* - \mathbf{U}^* \cdot \mathbf{n}^*) = \rho_3^G(\mathbf{v}_3^G \cdot \mathbf{n}^* - \mathbf{U}^* \cdot \mathbf{n}^*) \tag{5.46}$$

Since the polymer is non volatile:

$$\rho_3^G(\mathbf{v}_3^G \cdot \mathbf{n}^* - \mathbf{U}^* \cdot \mathbf{n}^*) = 0 \tag{5.47}$$

Using equations 5.8, 5.10 and 5.20 at x=X(t) one can write:

$$n_3^p\Big|_{x=X(t)} = \rho_3^p \mathbf{v}_3^p.\mathbf{n}^* = \rho_3^p \frac{dX}{dt} = j_3^{\neq} \tag{5.48}$$

By definition, for an N component system, the sum of the products of the diffusive flux with respect to volume average velocity and specific volume is equal to zero.

$$\sum_{i=1}^{N} j_i^{\neq} \hat{V}_i = 0 \tag{5.49}$$

Combining equations 5.48 and 5.49 yields:

$$\frac{dX}{dt} = -\frac{\sum_{i=1}^{2} j_i^p \hat{V}_i^p}{\rho_3^p \hat{V}_3^p} \tag{5.50}$$

The denominator of the right hand side of equation 5.50 express the volume fraction of the polymer. Therefore the time dependence of the boundary position can be written in terms of diffusive fluxes and mass densities of the volatile components.

$$\frac{dX}{dt} = -\left[\frac{\sum_{i=1}^{2} j_i^p \hat{V}_i^p}{1-\sum_{i=1}^{2} \rho_i^p \hat{V}_i^p}\right] \tag{5.51}$$

The initial condition for the thickness of the cast film can be expressed as follows:

$$\text{at } t = 0 \qquad X(0) = L \tag{5.52}$$

5.2.2.4 Coordinate transformation and dimensionless variables

To facilitate the numerical solution of the equations the interface should be mobilized and this was done by using a coordinate transformation as follows:

$$\eta = \frac{x}{X(t)} \tag{5.53}$$

In addition, temperature, compositions, time and the thickness of the film can be expressed in terms of dimensionless variables by using equations 5.54 through 5.57.

$$C_i = \frac{\rho_i^p}{\rho_{i0}^p} \tag{5.54}$$

$$t^* = \frac{tD_{11,0}^p}{L^2} \tag{5.55}$$

$$T^* = \frac{T - T_0}{T^G - T_0} \tag{5.56}$$

$$X^* = \frac{X(t)}{L} \tag{5.57}$$

To express the species continuity equation in terms of dimensionless variables, some mathematical manipulations and rearrangements must be done. The total derivatives of dimensionless compositions and immobilized position can be written as:

$$dC_i = \left(\frac{\partial C_i}{\partial x}\right)dx + \left(\frac{\partial C_i}{\partial t}\right)dt \tag{5.58}$$

$$dC_i = \left(\frac{\partial C_i}{\partial \eta}\right) d\eta + \left(\frac{\partial C_i}{\partial t}\right) dt \tag{5.59}$$

$$d\eta = \left(\frac{\partial \eta}{\partial x}\right) dx + \left(\frac{\partial \eta}{\partial t}\right) dt \tag{5.60}$$

If one substitutes equation 5.60 into equation 5.59 and compare it with equation 5.58,

$$\frac{\partial \eta}{\partial x} = -\frac{x\dfrac{dX}{dt}}{X(t)^2} \tag{5.61}$$

$$dt = \frac{L^2}{D_{11,0}^p} dt^* \tag{5.62}$$

when equations 5.54, 5.55, 5.57, 5.61 and 5.62 are inserted into equation 5.15, the new form of the species continuity equation becomes :

$$\frac{\partial C_i}{\partial t^*} - \frac{\eta}{X^*}\frac{dX^*}{dt^*}\frac{\partial C_i}{\partial \eta} = \frac{1}{X^{*2}}\frac{\partial}{\partial \eta}\left[\sum_{j=1}^{2} \frac{D_{ij}^p}{D_{11,0}^p}\frac{\rho_{j0}^p}{\rho_{i0}^p}\frac{\partial C_j}{\partial \eta}\right] \tag{5.63}$$

The dimensionless form of the time dependence of the boundary position and the dimensionless initial and boundary conditions can be expressed by equations 5.64 through 5.68.

$$\eta = 0 \qquad \frac{\partial C_i}{\partial \eta} = 0 \tag{5.64}$$

$$\eta = 1 \quad -\frac{1}{X^*}\left[\sum_{j=1}^{N-1} \frac{D_{if}^p}{D_{11,0}^p}\frac{\rho_{j0}^p}{\rho_{i0}^p}\frac{\partial C_j}{\partial \eta}\right] - C_i\frac{dX^*}{dt^*} = \frac{k_i^G(P_{ii}^G - P_{ib}^G)L}{\rho_{i0}^p D_{11,0}^p} \tag{5.65}$$

$$\eta = 1 \quad X^*\frac{dX^*}{dt^*} = \frac{\sum_{i=1}^{2} \hat{V}_i^p \sum \dfrac{D_{ij}^p}{D_{11,0}^p}\rho_{j,0}^p \dfrac{\partial C_j}{\partial \eta}}{1 - \sum_{i=1}^{N-1} \rho_{i0}^p C_i \hat{V}_i^p} \tag{5.66}$$

$$t^* = 0 \qquad C_i(0,\eta) = 1 \tag{5.67}$$

$$t^* = 0 \qquad X^*(0) = 1 \tag{5.68}$$

The boundary conditions given in equations 5.65 and 5.66, can be further rearranged to avoid the numerical estimation of concentration derivatives. Since it is expected that, due to the nature of the system, the change of concentration is very steep near the solution-air interface, to avoid the calculation of the concentration derivatives numerically at the surface the equation 5.63 can be integrated from $\eta = 0$ to $\eta = 1$.

$$\int_0^1 \frac{\partial C_i}{\partial t^*} d\eta - \int_0^1 \frac{\eta}{X^*} \frac{dX^*}{dt^*} \frac{\partial C_i}{\partial \eta} d\eta = \frac{1}{X^{*2}} \int_0^1 \frac{\partial}{\partial \eta} \left[\sum_{j=1}^{2} \frac{D_{ij}^p}{D_{11,0}^p} \frac{\rho_{j0}^p}{\rho_{i0}^p} \frac{\partial C_j}{\partial \eta} \right] d\eta \tag{5.69}$$

$$\int_0^1 \frac{\partial C_i}{\partial t^*} d\eta - \frac{1}{X^*} \frac{dX^*}{dt^*} \int_0^1 \eta \frac{\partial C_i}{\partial \eta} d\eta = \frac{1}{X^{*2}} \left[\sum_{j=1}^{2} \frac{D_{ij}^p}{D_{11,0}^p} \frac{\rho_{j0}^p}{\rho_{i0}^p} \frac{\partial C_j}{\partial \eta} \right]_{\eta=0}^{\eta=1} \tag{5.70}$$

Using equations 5.64 and 5.65 the new form of the boundary condition becomes as follows:

$$\text{At} \quad \eta = 1 \qquad \frac{d}{dt} \left[X^* \int_0^1 C_i d\eta \right] = - \frac{k_i^G (P_{ii}^G - P_{ib}^G) L}{\rho_{io}^p D_{11,0}^p} \tag{5.71}$$

Similarly, the integrated form of equation 5.63 can be substituted into equation 5.66 and using equations 5.67 and 5.68, following explicit form of dimensionless thickness of the film is obtained.

$$X^* = \frac{1 - \sum_{i=1}^{2} \rho_{i0}^p \hat{V}_i^p}{1 - \sum_{i=1}^{2} \rho_{i0}^p \hat{V}_i^p \int_0^1 C_i d\eta} \tag{5.72}$$

Time dependence of the temperature of the film, can be expressed in terms of dimensionless variables defined in equations 5.73 through 5.76.

$$A = \frac{L(h^G + h^g)}{D_{11,0}^p \rho^p \hat{C}_p^p} \tag{5.73}$$

$$B = - \frac{L \sum_{i=1}^{N-1} k_i^G \Delta \hat{H}_{vi} (P_{ii}^G - P_{ib}^G)}{\rho^p \hat{C}_p^p D_{11,0}^p (T^G - T_0)} \tag{5.74}$$

$$E = \frac{L h^g (T^g - T^G)}{D_{11,0}^p \rho^p \hat{C}_p^p (T^G - T_0)} \tag{5.75}$$

$$F = \frac{\rho^s \hat{C}_p^s H}{\rho^p \hat{C}_p^p H} \tag{5.76}$$

$$\frac{dT^*}{dt^*} = \frac{A(1 - T^*) + E + B}{F + X^*} \tag{5.77}$$

The initial condition becomes:

$$\text{at} \qquad t^* = 0 \qquad T^*(0) = 0 \tag{5.78}$$

5.3. Numerical solution of the model equations

The equations 5.63, 5.64, 5.71, 5.72, 5.77 and 5.78 are highly nonlinear ordinary and partial differential equations and it is not possible to derive an analytical solution. Therefore, these equations were solved numerically by using finite difference technique.

The nonlinear partial differential equations were first transformed into a finite system of nonlinear algebraic equations by discretizing them with finite difference technique. Rewriting the species continuity in the finite difference form yields expressions 5.79 through 5.80 in which, i and j represent space and time respectively.

$$\frac{(C_1)_i^{j+1}-(C_1)_i^{j}}{\Delta t^*}=\frac{\eta_i}{X^{*j+1}}\frac{(X^{*j+1}-X^{*j})}{\Delta t^*}\frac{(C_1)_{i+1}^{j+1}-(C_1)_i^{j+1}\left[1-\left(\frac{h_i}{h_{i-1}}\right)^2\right]-(C_1)_{i-1}^{j+1}\left(\frac{h_i}{h_{i-1}}\right)^2}{h_i\left(1+\frac{h_i}{h_{i-1}}\right)}$$
$$+\frac{2}{(X^{*j+1})^2 D_{11,0}(h_{i-1}+h_i)}\left[\begin{array}{l}\left((D_{11})_{i+1/2}^{j+1}\frac{(C_1)_{i+1}^{j+1}-(C_1)_i^{j+1}}{h_i}-(D_{11})_{i-1/2}^{j+1}\frac{(C_1)_i^{j+1}-(C_1)_{i-1}^{j+1}}{h_{i-1}}\right)\\ +\frac{\rho_{20}}{\rho_{10}}\left((D_{12})_{i+1/2}^{j+1}\frac{(C_2)_{i+1}^{j+1}-(C_2)_i^{j+1}}{h_i}-(D_{12})_{i-1/2}^{j+1}\frac{(C_2)_i^{j+1}-(C_2)_{i-1}^{j+1}}{h_{i-1}}\right)\end{array}\right] \quad (5.79)$$

$$\frac{(C_2)_i^{j+1}-(C_2)_i^{j}}{\Delta t^*}=\frac{\eta_i}{X^{*j+1}}\frac{(X^{*j+1}-X^{*j})}{\Delta t^*}\frac{(C_2)_{i+1}^{j+1}-(C_2)_i^{j+1}\left[1-\left(\frac{h_i}{h_{i-1}}\right)^2\right]-(C_2)_{i-1}^{j+1}\left(\frac{h_i}{h_{i-1}}\right)^2}{h_i\left(1+\frac{h_i}{h_{i-1}}\right)}$$
$$+\frac{2}{(X^{*j+1})^2 D_{11,0}(h_{i-1}+h_i)}\left[\begin{array}{l}\frac{\rho_{10}}{\rho_{20}}\left((D_{21})_{i+1/2}^{j+1}\frac{(C_1)_{i+1}^{j+1}-(C_1)_i^{j+1}}{h_i}-(D_{21})_{i-1/2}^{j+1}\frac{(C_1)_i^{j+1}-(C_1)_{i-1}^{j+1}}{h_{i-1}}\right)\\ +\left((D_{22})_{i+1/2}^{j+1}\frac{(C_2)_{i+1}^{j+1}-(C_2)_i^{j+1}}{h_i}-(D_{22})_{i-1/2}^{j+1}\frac{(C_{21})_i^{j+1}-(C_2)_{i-1}^{j+1}}{h_{i-1}}\right)\end{array}\right] \quad (5.80)$$

These equations along with discretized form of heat transfer equation were solved simultaneously by the aid of a subroutine called DNEQNF from IMSL. This subroutine solves the system of nonlinear equations using a modified Powell hybrid algorithm. To check the accuracy of numerical solution, the total number of grid points

were increased and the time steps were decreased until the change in the numerical results was negligible. The numerical simulation was performed using a PC based computer. The codes were written in Fortran and given in the Appendix.

To facilitate the numerical solution of the equations, variable grid sizes were used instead of uniform ones, since the concentrations of the components change drastically at the solution-air interface. By using an appropriate function, smaller increments near the solution-air interface and coarser increments near the solution-substrate interface can be obtained as shown in Figure 5.2. Equations 5.81 and 5.82 were used to generate variable grid sizes.

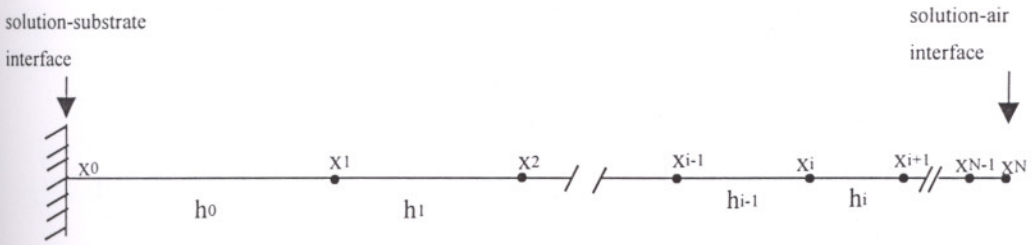

Figure 5.2. Illustration of variable grid spacing for N grid points.

$$h_i = h_{i-1}\left[1+\frac{\varepsilon}{L}\left[\frac{L-x_i}{L}\right]^{\sigma} h_{i-1}\right] \tag{5.81}$$

where L is the total length and h_i is the grid size.

$$\sum_{i=0}^{N-1} h_i = L \tag{5.82}$$

The constants, ε and σ in these equations were chosen to obtain optimum grid size distribution through the solution and their values were determined as –4 and 1 respectively. The number of grid points was chosen as 100 above which numerical values of calculated model results did not change.

The effects of ε and σ on the grid size distribution were illustrated in Figure 5.3 and 5.4. The length of the first and last grids was calculated as 0.04593 and 0.005987 by an iterative solution using 100 grid points and the values of –4 and 1 for ε and σ respectively.

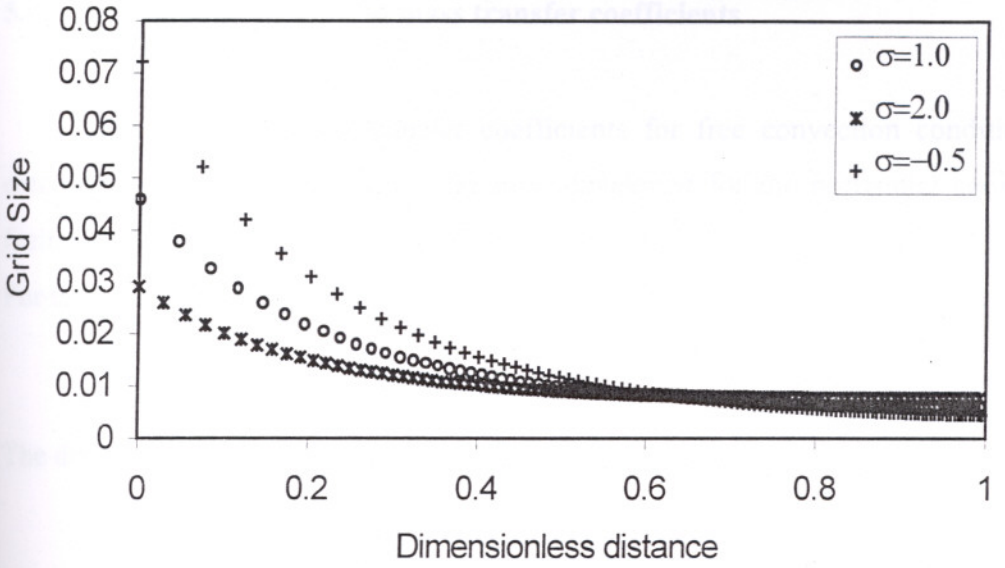

Figure 5.3. Variation of grid sizes with σ ($\varepsilon = -4.0$ and # Grid Points=100)

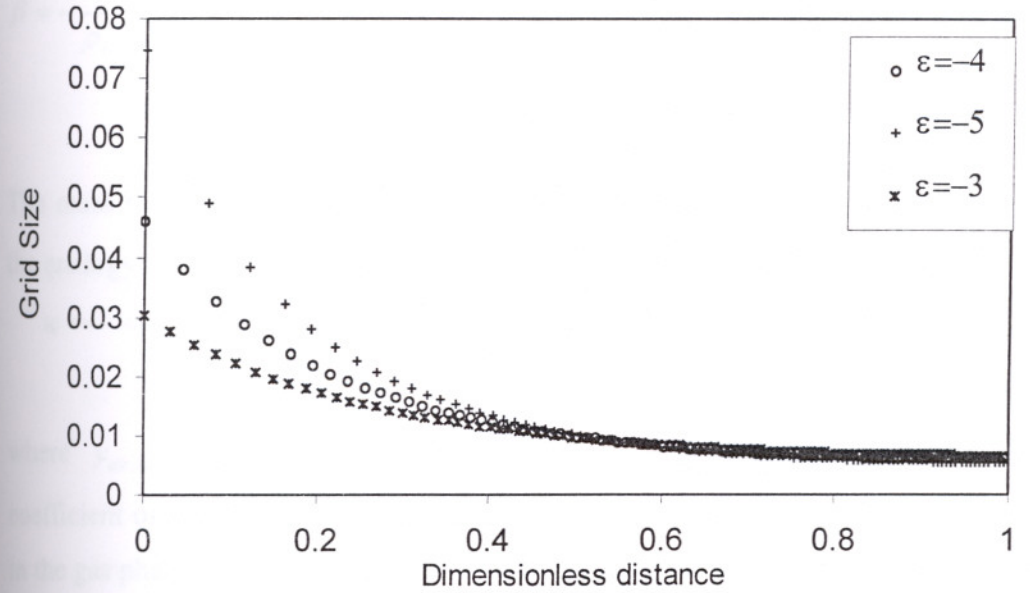

Figure 5.4. Variation of grid sizes with ε ($\sigma = 1.0$ and # Grid Points=100)

5.4. Determination of other model parameters

5.4.1. Estimation of heat and mass transfer coefficients

The heat and mass transfer coefficients for free convection conditions were determined using an empirical correlation developed for the horizontal cooled plates facing upward in the laminar range (McAdams 1954).

For the heat transfer coefficient (h);

$$\frac{hL_c}{k^G} = 0.27(Gr \cdot \mathrm{Pr})^{0.25} \tag{5.83}$$

The dimensionless Grashof and Prandtl numbers are equal to:

$$Gr = \frac{g\rho_G^2 \beta(\Delta T)L_c^3}{\mu_G^2} \tag{5.84}$$

$$\mathrm{Pr} = \frac{C_p \mu}{k^G} \tag{5.85}$$

where the expansion coefficient,

$\beta = -\frac{1}{\rho_G}\left(\frac{\partial \rho_G}{\partial T}\right)_P$ and for perfect gas, it reduces to the following form:

$$\beta = \frac{1}{T} \tag{5.86}$$

The mass transfer coefficient (k_i[=]sec/cm) of each component was determined using the analogy between the heat and mass transfer (Tsay and McHugh 1991).

$$\frac{k_i L_c y_{air,lm} \hat{V}_{i,G} P}{D_{i,G}} = 0.27(Gr \cdot Sc)^{0.25} \tag{5.87}$$

where $y_{alr,lm}$, $D_{i,g}$, $\hat{V}_{i,g}$, P are the log mean mole fraction difference, diffusion coefficient of component i in the gas phase, the partial specific volume of component i in the gas phase and total pressure, respectively. The Grashof and Schmidt numbers can be expressed as:

$$Gr = \frac{g\rho_G^2 L_c^3 \left|\zeta(y_{i,i} - y_{i,G})\right|}{\mu_G^2} \tag{5.88}$$

and

$$Sc = \frac{\mu_G}{\rho_G D_{i,G}} \tag{5.89}$$

where the coefficient ζ which represents the effect of mole fraction of component i on the gas density is equal to:

$$\zeta = -\frac{1}{\rho_G}\left(\frac{\partial \rho_G}{\partial y_i}\right)_{P,T} \tag{5.90}$$

For the case of forced convection conditions the heat and mass transfer coefficient were calculated by the correlations given in equations 5.91 and 5.92 (Incropera and DeWitt 1990).

$$\frac{hL_c}{k^G} = 0.664\,\mathrm{Re}^{1/2}\,\mathrm{Pr}^{1/3} \tag{5.91}$$

$$\frac{k_i L_c \hat{V}_{i,G} P}{D_{i,G}} = 0.664\,\mathrm{Re}^{1/2} \cdot Sc^{1/3} \tag{5.92}$$

The Reynods number has its standard definition as:

$$\mathrm{Re} = \frac{\rho_G L_c \upsilon_G}{\mu_G} \tag{5.93}$$

where υ_G represents the velocity of the bulk air stream

5.4.2. Calculation of interface pressure of volatile components

The partial pressure of the volatile components at the solution-gas interface, was calculated from the following relationship.

$$P_{ii} = a_i P_i^{sat} \tag{5.94}$$

where the activity of component i can be defined as:

$$a_i = \exp\left(\frac{\Delta \mu_i}{RT}\right) \tag{5.95}$$

The saturated vapor pressure of acetone and water (P^{sat}) at any temperature (T) was calculated by expression given in equation 5.96 (Reid et al. 1977). The constants A, B, C and D are reported in Table 5.1.

$$\ln\frac{P^{sat}}{P_c} = (1-T_r)^{-1}\left[AT_r + BT_r^{1.5} + CT_r^3 + DT_r^6\right] \tag{5.96}$$

where,

$$T_r = 1 - \frac{T}{T_c} \tag{5.97}$$

Table 5.1. The constants used in the calculation of vapor pressures of acetone and water.

	Water	Acetone
A	-7.76451	-7.45514
B	1.45838	1.20200
C	-2.77580	-2.43926
D	-1.23303	-3.35590
T_c (K)	647.3	508.1
P_c (bar)	221.2	47

5.5. Physical parameters of the model

The physical properties of water, acetone, CA, polymer solution, support and air were obtained from different sources and given in Tables 5.2 through 5.4 (Shojaie et al. 1994a, Incropera and Dewitt 1990, Perry and Chilton 1973).

Table 5.2. Physical properties of water, acetone and CA.

	Water	Acetone	CA
Density (g/cm^3)	1.00	0.79	1.31
Molecular Weight (g/mol)	18.0	58.08	40000
Molar Volume (cm^3/mol)	18.0	73.92	30532
Heat of vaporization @ 20 ^{0}C (J/g)	2444	552	-

Table 5.3. Physical properties of polymer solution, substrate and air.

Glass Support	
Density[1] g/cm^3	2.5
Heat Capacity[1] J/gK	0.75
Polymer Solution	
Heat Capacity[2] J/gK	2.5
Air	
Thermal Conductivity[1] W/cmK	$2.55\ 10^{-4}$

[1]Incropera and Dewitt (1990)

[2]Shojaie et al. (1994a)

Table 5.4. The parameters used in the calculation of heat and mass transfer coefficients

Density of air ρ_G (g/cm^3)	1.19×10^{-3}
Viscosity of air μ_G (g/cm.s)	1.85×10^{-4}
Diffusivity of water in air[1] D_{1G} (cm^2/s)	0.280
Diffusivity of acetone in air[1] D_{2G} (cm^2/s)	0.125
Characteristic length of casting area L_c (cm)	10
η_1 Coefficient for water[2] in Equation 5.*	-1.0
η_2 Coefficient for acetone[2] in Equation 5.*	0.38

[1]Incropera and Dewitt (1990)

[2]Calculated from ideal gas law.

5.6. Test of the predictability of the model

The measurement of variables in real time for the membrane formation is very difficult and such analysis requires highly sophisticated techniques. Shoajaie et al. (1994b) and Greenberg et al. (1995) used the infrared thermography technique which provides both gravimetric and thermal information. In addition, by the light-intensity measurements the onset and duration of the phase separation were determined. In this work, the experimental aspect of the thesis consists of three parts. First, the validity of the model is confirmed using the measurement of total evaporation rate by monitoring the overall mass change as a function of time. Second, the morphology of the prepared membranes is investigated using scanning electron microscope pictures. Finally, the water vapor permeability and density of membranes are measured.

For all experimental studies CA was supplied from Aldrich with a molecular weight of 50,000 and an acetyl content of 38.9%. A high purity acetone and deionized-distilled water was used. The CA was dried in an oven above 100^0C for several hours before used. No further purification was applied to the materials.

Since acetone is very volatile, the fraction of it in the solution was controlled. First, the binary solution of acetone and CA was prepared by stirring until a homogeneous solution was obtained. Acetone, evaporated during preparation was added to the solution. After the addition of water, the beaker was kept closed so mass loss due

to evaporation was prevented. The ternary solution was stirred for one day before casting.

Gravimetric measurements were carried out by casting the polymer solutions on a 10 cm wide square glass supports with the aid of a film applicator. After casting, the glass support was carried to the microbalance within 15 seconds. At the initial stages of evaporation, the data was collected with 5 seconds intervals. In all experiments, the lower side of the glass plate was insulated so, the heat transfer from that surface was prevented. The accumulation of the volatile components in the gas phase was not allowed by using an open chamber, as a result, the concentration in the gas phase was kept constant.

Morphological studies were conducted using JEOL 5200 type scanning electron microscope at the School of Dentistry, Ege University. The membranes were cut with the aid of a very sharp knife and then coated with gold.

CHAPTER 6

RESULTS AND DISCUSSION

The model equations were solved numerically to investigate the effects of different parameters on the membrane formation. The predictions from the model provide composition paths in terms of volume fraction, temperature and the thickness of the membrane. The compositions at the solution-substrate, the solution-air interface and at a point just below the free surface were plotted on the ternary phase diagrams. The times at which composition paths cross the binodal line as well as the difference in times at which the solution on the substrate and air sides enter into the binodal were noted. The interpretation of composition paths plotted on the phase diagrams and the concentration profile of the polymer through the membrane provided information on the final structure of the membrane. In the following sections, first of all predictive ability of the model is tested by comparing the experimental data with simulation results. Secondly, the effect of different parameters on the membrane formation is investigated. Finally, the scanning electron microscope pictures of the membranes prepared under different conditions are evaluated.

6.1. Test of predictive ability of the model

The major test of any model is to determine how accurately it can predict process variables that are measured experimentally. In this section, ternary model predictions are compared to the experimental results that include total mass loss. Three sets of quantitative comparisons corresponding to cases R1, R2, R3 in Table 6.1 are shown in Figures 6.1 through 6.3. These figures show the predicted and measured total polymer solution mass as a function of time. The initial thickness of the solution could not be properly adjusted, therefore, it was calculated by extrapolating the mass loss data to zero time. As can be seen, the agreement between the model and experimental data is excellent for cases R1 and R2 shown in Figures 6.1 and 6.2. However, a slight deviation is observed for case R3 in Figure 6.3.

Table 6.1. The initial conditions, the processing parameters and code numbers of the numerical results.

Code # of Model Results	Volume Fractions			Initial Casting Temperature of film (^{0}C)	Temperature of air (^{0}C)	Initial Casting Thickness (μm)	% RH	Mode of convection / velocity of air (cm/sec)	Mass Transfer Coefficients (sec/cm)		Heat Transfer Coefficients (W/cm^2.K)	
	Water	Acetone	CA						Water	Acetone	Film Side	Substrate Side
R1	0.05	0.85	0.10	23	24	140	50	Free	9.7×10^{-11}	5.9×10^{-10}	2.5×10^{-4}	Insulated
R2	0.10	0.80	0.10	23	24	120	50	Free	6.4×10^{-11}	5.5×10^{-10}	2.2×10^{-4}	Insulated
R3	0.15	0.80	0.05	23	24	166	60	Free	8.8×10^{-11}	4.9×10^{-10}	2.2×10^{-4}	Insulated
R4	0.10	0.80	0.10	23	24	200	0	Free	$1.2.\times10^{-10}$	5.5×10^{-10}	2.2×10^{-4}	Insulated
R5	0.15	0.75	0.10	23	24	200	0	Free	$1.3.\times10^{-10}$	5.1×10^{-10}	2.2×10^{-4}	Insulated
R6	0.02	0.88	0.10	23	24	200	0	Free	$9.2.\times10^{-11}$	6.2×10^{-10}	2.2×10^{-4}	Insulated
R7	0.10	0.80	0.10	23	24	120	0	Free	1.2×10^{-10}	5.5×10^{-10}	2.2×10^{-4}	Insulated
R8	0.10	0.80	0.10	23	24	250	0	Free	1.2×10^{-10}	5.5×10^{-10}	2.2×10^{-4}	Insulated
R9	0.10	0.80	0.10	23	24	120	25	Free	1.1×10^{-10}	5.5×10^{-10}	2.2×10^{-4}	Insulated
R10	0.10	0.80	0.10	23	24	120	0	Forced/20	3.7×10^{-10}	7.5×10^{-10}	5.3×10^{-4}	Insulated
R11	0.10	0.80	0.10	23	24	120	0	Forced/50	5.9×10^{-10}	1.2×10^{-9}	8.4×10^{-4}	Insulated

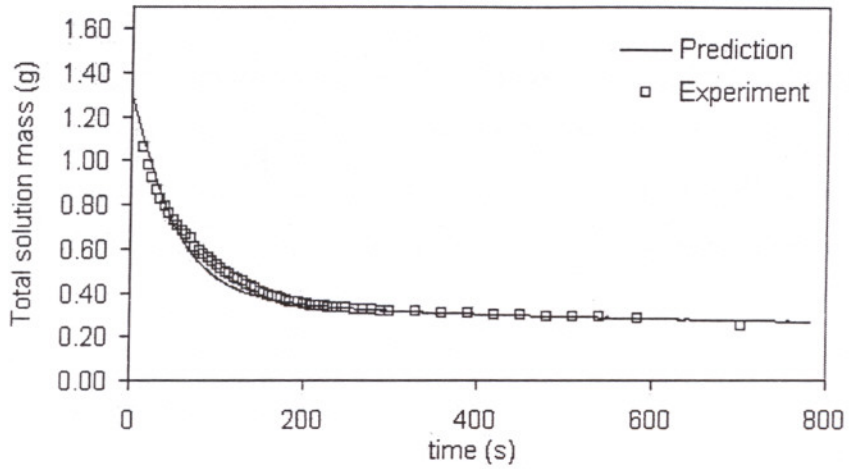

Figure 6.1. Predicted(-) and measured () total solution mass as a function of time for a membrane cast from a CA/Acetone/Water solution for case R1.

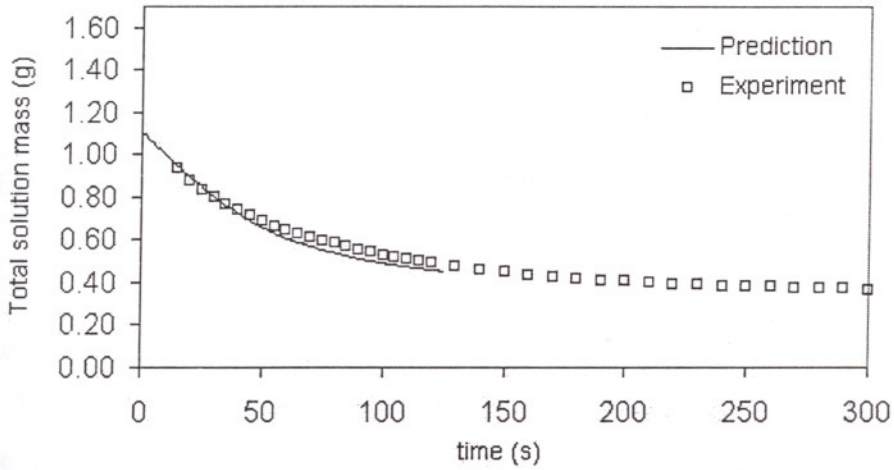

Figure 6.2. Predicted(-) and measured () total solution mass as a function of time for a membrane cast from a CA/Acetone/Water solution for case R2.

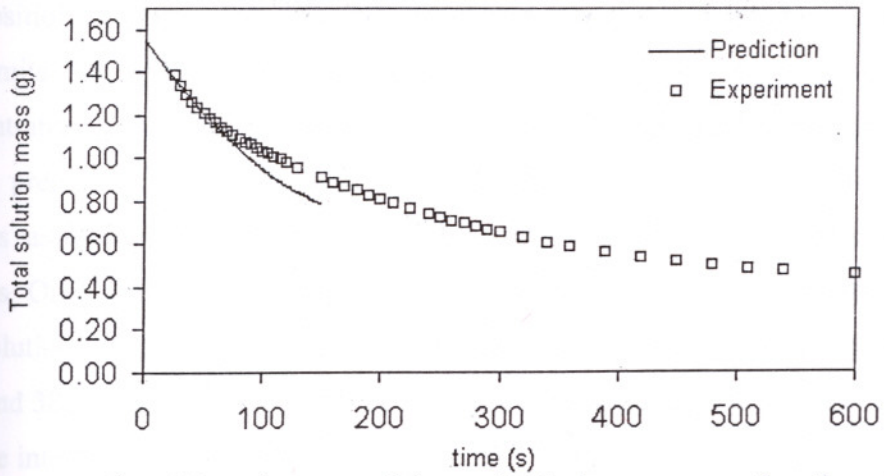

Figure 6.3. Predicted(-) and measured () total solution mass as a function of time for a membrane cast from a CA/Acetone/Water solution for case R3.

The dry cast model used in this study does not include any adjustable parameters, that is, the predictions are only based on conservation laws, solution thermodynamics and measured and correlated values of the relevant physical and transport properties. Therefore, it is a very useful tool to optimize membrane formation process.

6.2. Comparison of different cases

Simulations have been done for different cases to illustrate the power of the model and to investigate the effect initial compositions and the thickness of the solution, relative humidity and mode of convection on the final membrane structure. The input data for these cases are given in Table 6.1.

6.2.1 Effect of volume fraction of water in the casting solution

In cases R4 through R6, the volume fraction of CA was kept constant while the volume fraction of water was adjusted as 0.1, 0.15 and 0.02.

The predictions for the instantaneous concentrations, expressed in terms of volume fractions, are plotted on the ternary phase diagram as shown in Figure 6.4. The point shown as a dot represents the initial composition of the casting solution. Concentration paths in time are shown for the substrate/solution, solution/air interface and for the point just below the solution/air interface. A typical phase diagram including composition paths provides valuable information about the membrane formation. First, it permits assessing whether a phase separation occurs which requires that the concentration paths cross the binodal curve of the phase diagram. This type of plot also allows predicting the inception time and duration of the phase separation. Finally it permits assessing the type of morphology which results from a particular casting process. One observes from Figure 6.4 that the concentration paths of the solution/air and solution/substrate interfaces cross the binodal curve at markedly different times (424 and 383 s respectively). Also, as illustrated in Figure 6.5, the concentrations of CA at three interfaces significantly differ from each other. In fact, the difference in volume fractions of cellulose acetate at the surface and at a point just below the surface is about 0.2 although the distance between these points is only 0.006 in dimensionless

coordinates. Hence, one might expect that this casting conditions represented by R4 will produce a porous asymmetric membrane in which the upper surface is much denser than its lower surface.

The volume fraction profiles of CA, water and acetone in Figures 6.5, 6.6 and 6.7, show that at the initial stages of membrane formation, the rate of evaporation is very fast compared to that of water. Thus, the concentration of CA increases rapidly at the surface and sharp concentration gradients are observed. This phenomena leads to decrease in the diffusion of the volatile components in CA. Figure 6.5 indicates that, the concentration of CA at the substrate side starts to change only after 200 seconds. Similar trends can also be seen from the overall composition paths in Figure 6.8. Although there is loss of water, due to the fast evaporation of acetone, the volume fraction of water increases.

The thickness of the membrane for case R4 decreases asymptotically from 200 μm to about 50 μm in 420 seconds as illustrated in Figure 6.9. Due to the fast evaporation of acetone and associated evaporative cooling effect, the temperature of the cast solution decreased about 9 ^{0}C in 400 seconds as shown in Figure 6.10.

In case R5 the initial concentration of water was increased to 0.15. For these casting conditions the substrate/solution and the solution/air interfaces reach the phase boundary at 340 and 365 seconds, respectively, earlier than the previous case R4 as shown in Figure 6.11. The concentration profile of CA at 350 second in Figure 6.12 indicates that these casting conditions should lead to a highly asymmetric membrane structure. Unlike case R4, in case R5 the concentration of water in the solution changed remarkably, showing a higher volume fraction at the substrate side as seen in Figure 6.13 . The average volume fraction of water shown in Figure 6.15, exhibits an increase from 0.15 to about 0.25 in 350 seconds. Comparing Figures 6.8 and 6.15, one can see that the rate of evaporation of acetone in case R5 is slower than that in case R4. This is mainly due to higher diffusional resistance in the membrane indicated by sharp concentration profiles in Figures 6.12, 6.13 and 6.14, respectively. Although, the initial volume fraction of acetone is lower in case R5, it is higher (0.5 compared to 0.4 in case R4) at the time of precipitation. Consequently, a thicker membrane will be obtained in this case with a thickness of 80 μm.

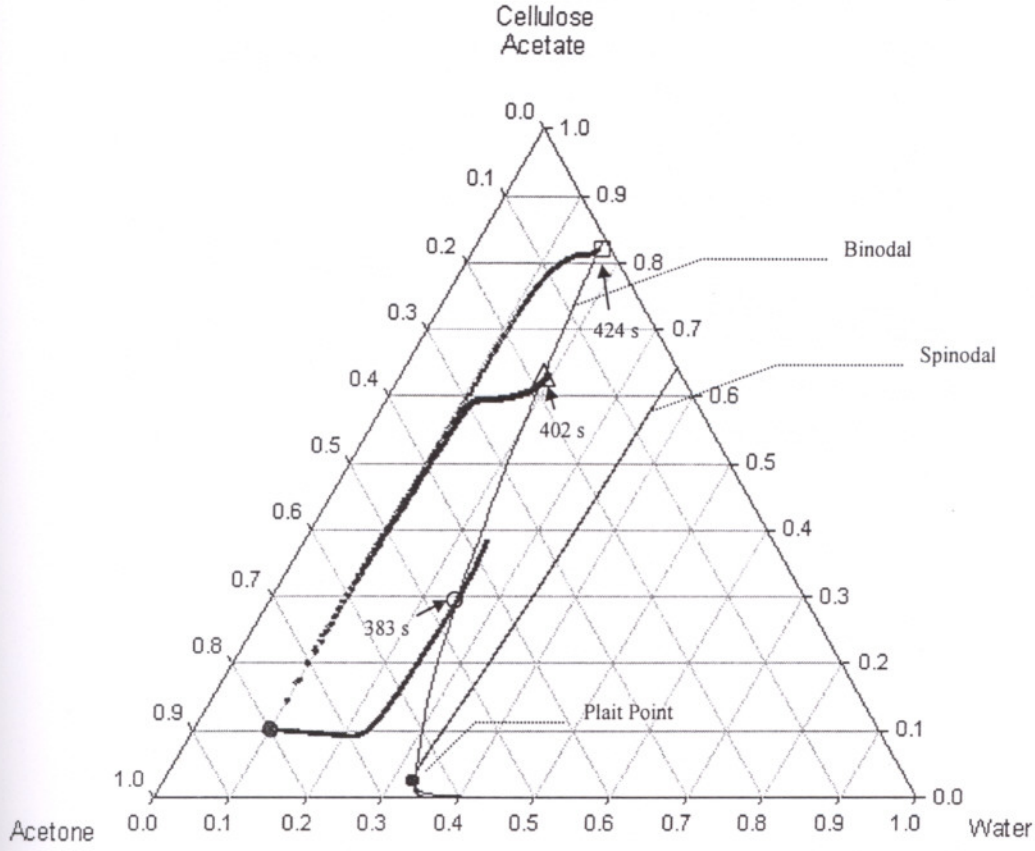

Figure 6.4. Concentration paths of water, acetone and CA for case R4 (O: solution/substrate interface, □: solution/air interface Δ: point just below solution/air interface).

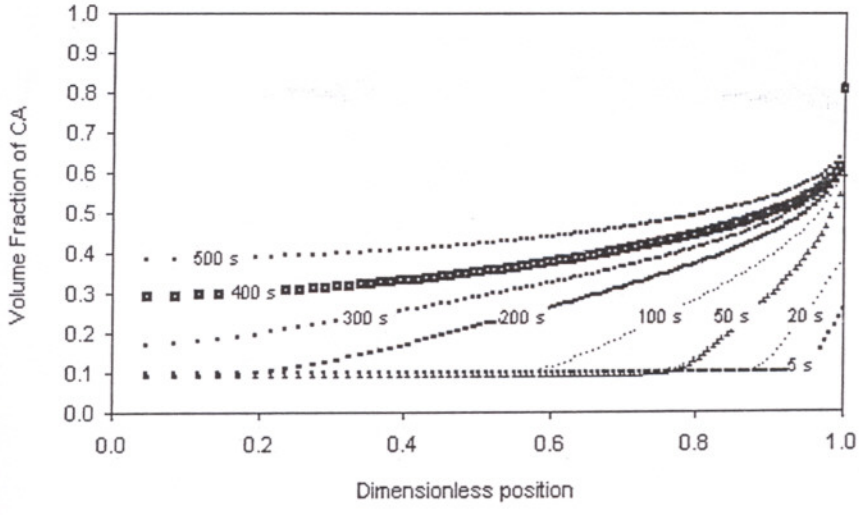

Figure 6.5. Volume fraction profiles of CA for case R4.

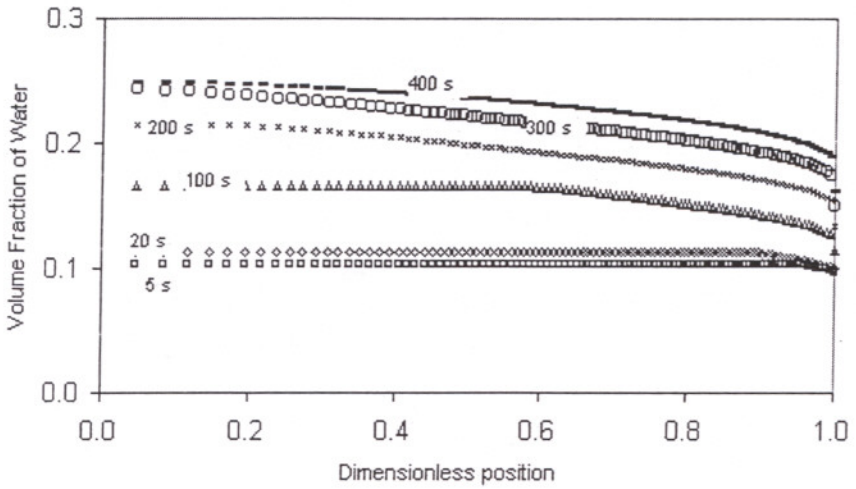

Figure 6.6. Volume fraction profiles of water for case R4.

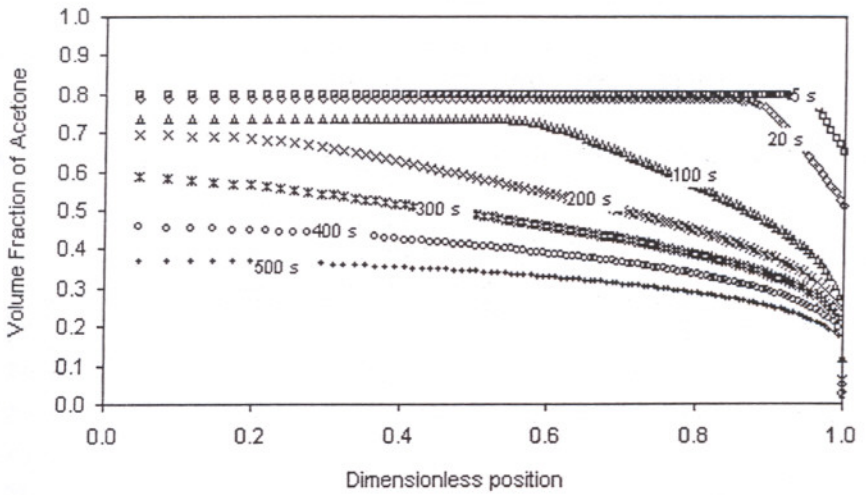

Figure 6.7. Volume fraction profiles of acetone for case R4.

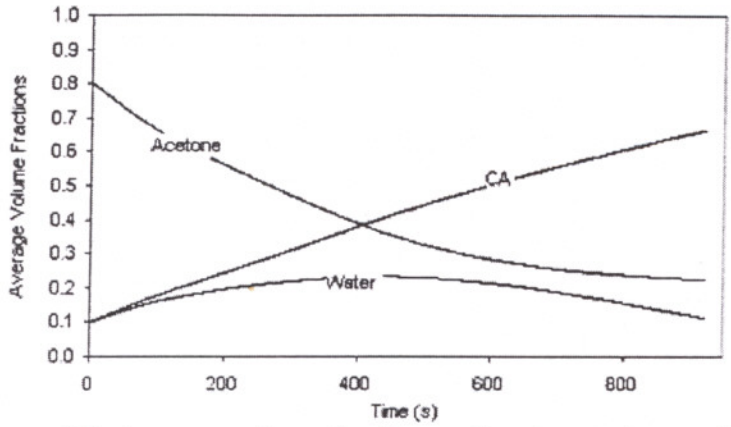

Figure 6.8. Average volume fractions of water, acetone and CA during membrane formation for case R4.

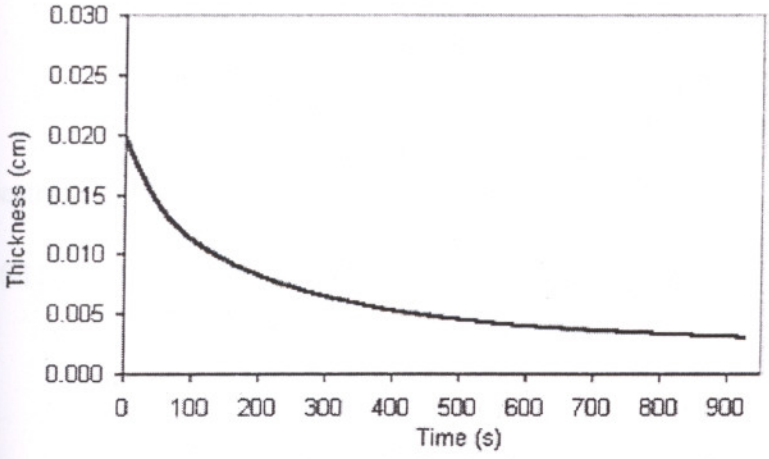

Figure 6.9. Thickness of the solution during membrane formation for case R4.

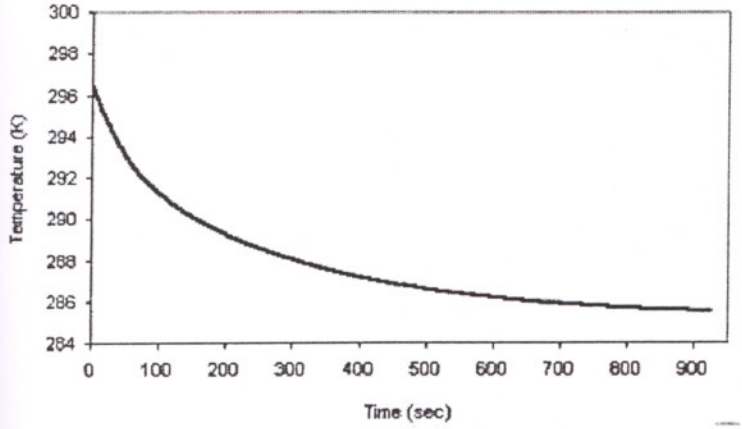

Figure 6.10. Temperature of the solution during membrane formation for case R4.

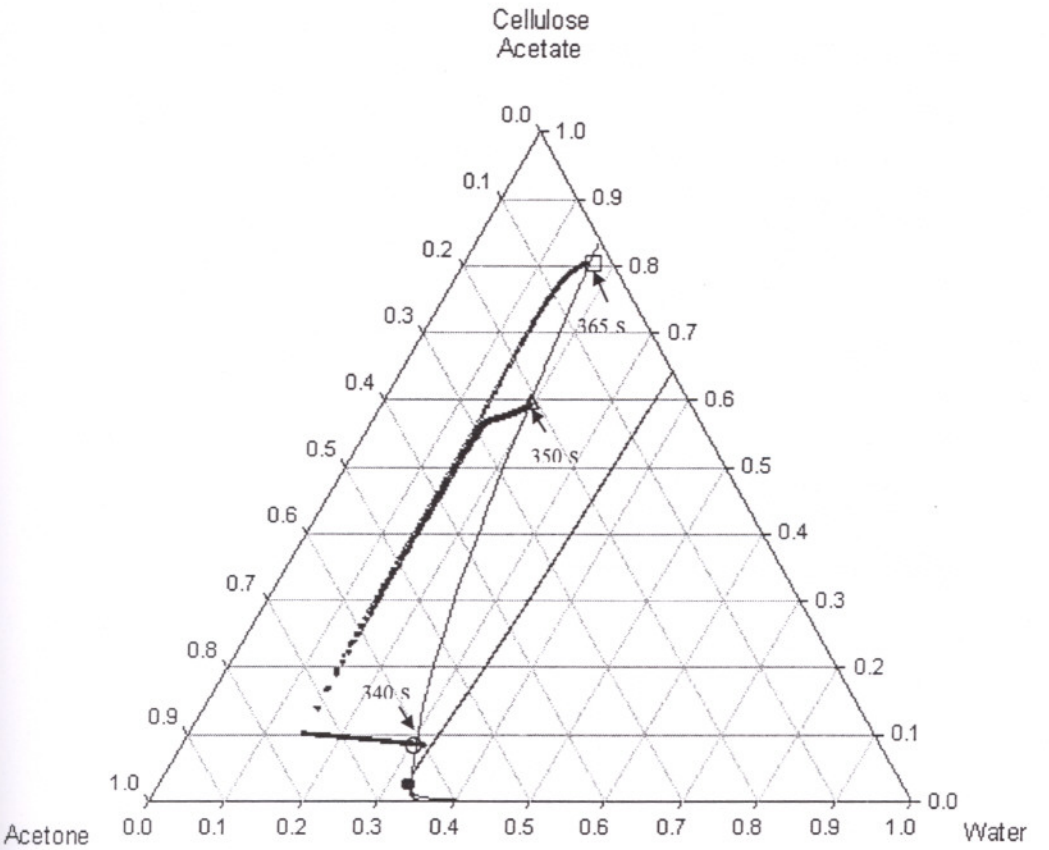

Figure 6.11. Concentration paths of water, acetone and CA for R5 (O: solution/substrate interface, □ solution/air interface, Δ: point just below solution/air interface).

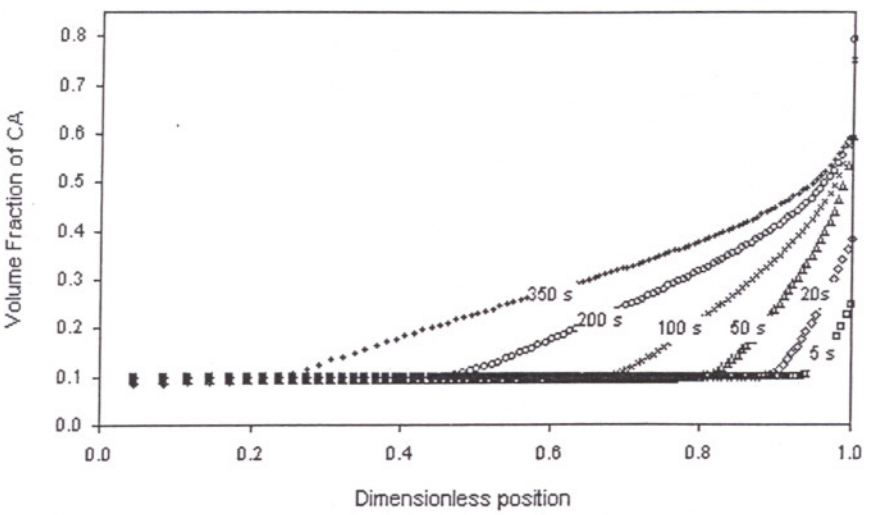

Figure 6.12. Volume fraction profiles of CA for case R5.

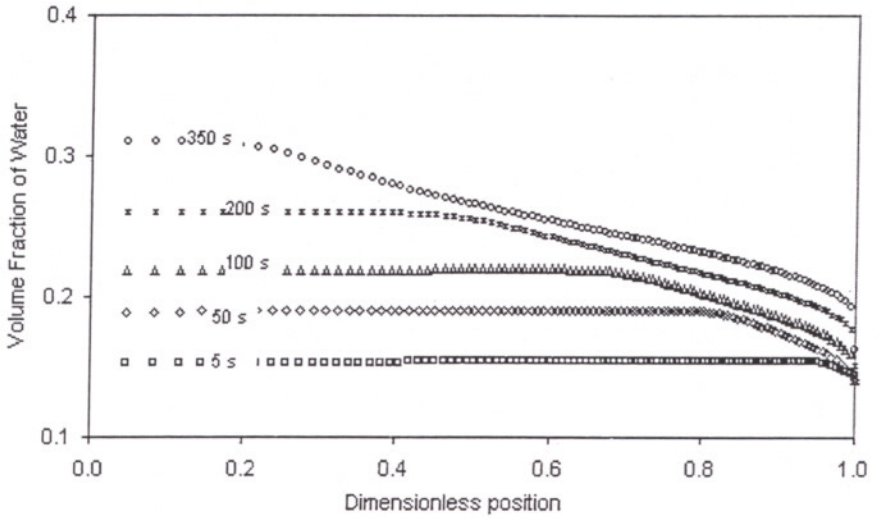

Figure 6.13. Volume fraction profiles of water for case R5.

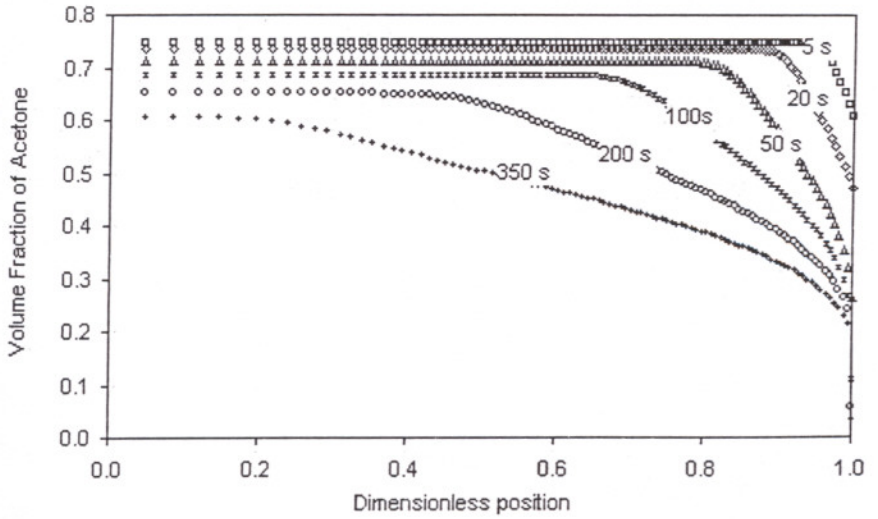

Figure 6.14. Volume fraction profiles of acetone for case R5.

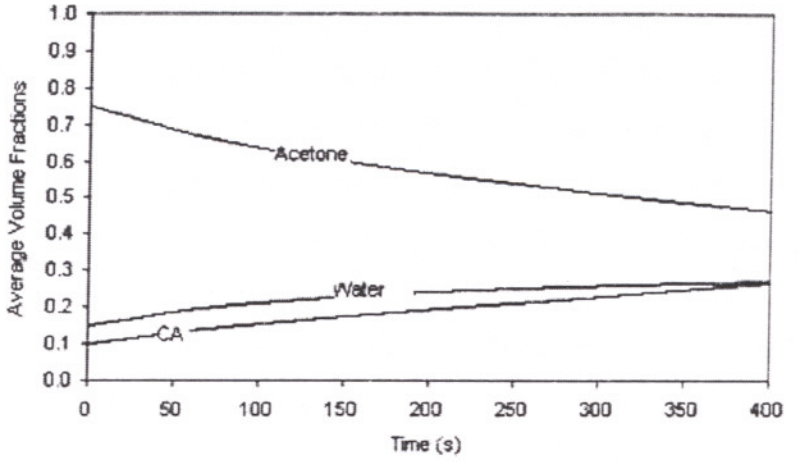

Figure 6.15. Average volume fractions of water, acetone and CA during membrane formation for case R5.

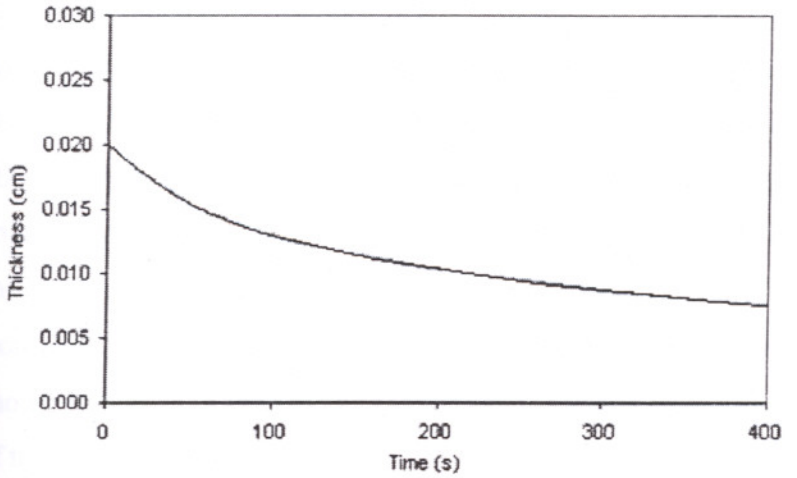

Figure 6.16. Thickness of the solution during membrane formation for case R5.

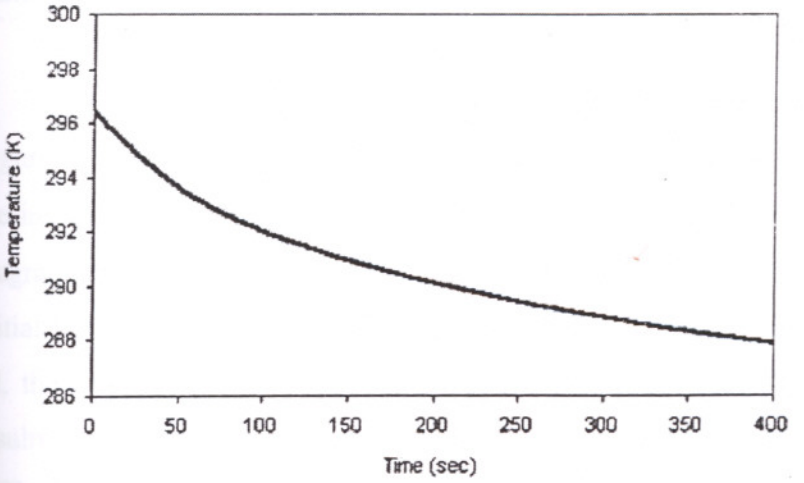

Figure 6.17. Temperature of the solution during membrane formation for case R5.

To investigate the effect of different conditions on the membrane structure, the surface skin thickness was defined as the distance between the air/solution interface, and the point where the concentration of polymer decreased by 10%. According to this criteria, as the concentration of water in the casting solution increases the percentage of dense top skin layer decreases. The percent skin layer was calculated as 4.2% and 3.0% for cases R4 and R5, respectively.

The temperature of the solution decreased about 8^0C until metastable region was reached as shown in Figure 6.17.

In case R6 the water volume fraction decreased to a very small amount as 0.02. As illustrated in Figure 6.18, neither the gas side nor the support side entered the metastable region. This model prediction implies that at such conditions the phase separation does not take place and a dense nonporous film is obtained rather than a porous membrane. The concentration profiles in Figures 6.19, 6.20, 6.21 show that concentration gradients of CA and acetone decreased after 200 seconds of evaporation. Due to fast evaporation of acetone, concentration of water reached a maximum around 200 seconds and then started to decrease. Compared to previous cases, no sharp concentration gradients of water were observed through the entire solution. Figure 6.23 shows that during 300 seconds of evaporation, the thickness of the solution decreased from 200 μm to 25 μm. The temperature of the solution decreased from about 9 ^{0}C as shown in Figure 6.24. Due to a decrease in acetone loss after 300 seconds, temperature of the solution starts to increase.

6.2.2 Effect of initial film thickness

The effect of initial film thickness on membrane formation process is shown in Figures 6.25 and 6.26 where the conditions are identical to those in case R4 except that the initial film thickness are 120 μm and 250 μm, respectively. Comparing the phase diagrams in Figure 6.4 (case R4) and Figure 6.25 (case R7) indicates that decreasing the initial film thickness in case R7 affects the formation process in 2 major ways. First of all, the onset of phase transition is faster since decreasing the initial film thickness results in a decrease in the total mass of acetone. So, shorter time is required to remove sufficient amount of acetone to allow entire casting solution to cross the binodal.

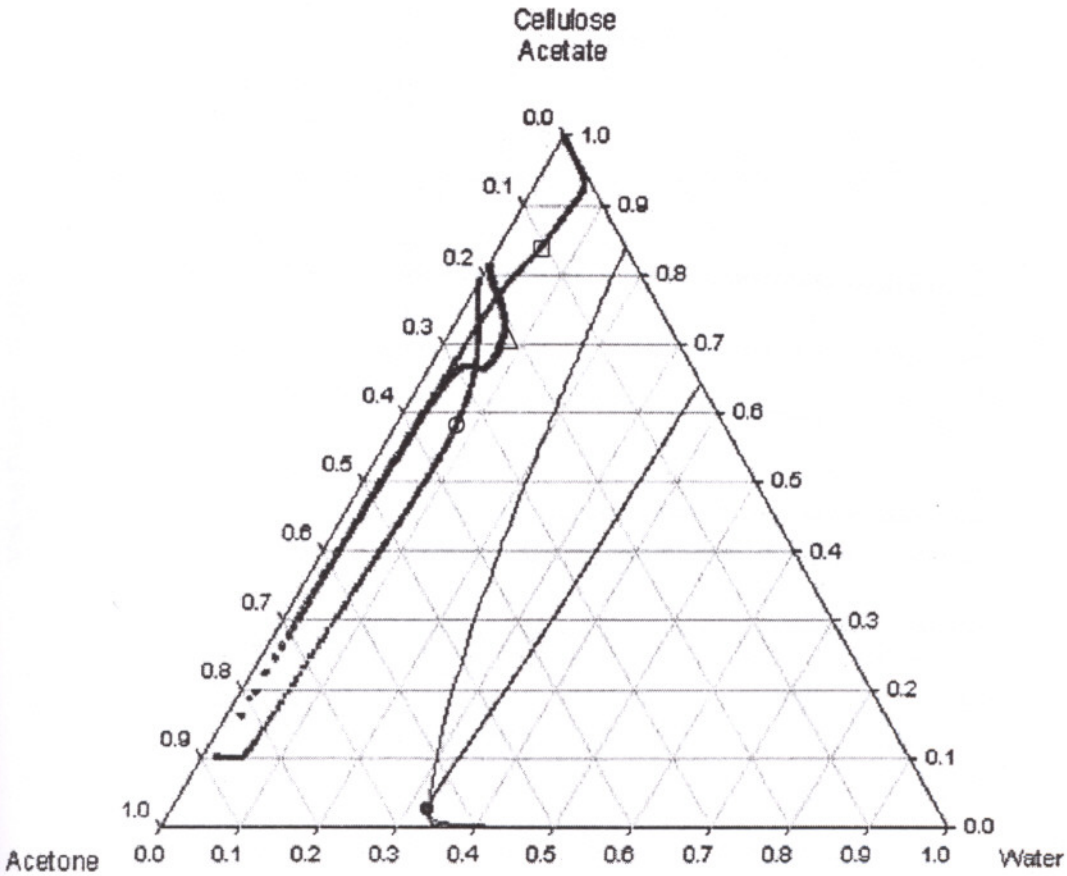

Figure 6.18. Concentration paths of water, acetone and CA for case R6 (O: solution/substrate interface, : solution/air interface, Δ: point just below solution/air interface).

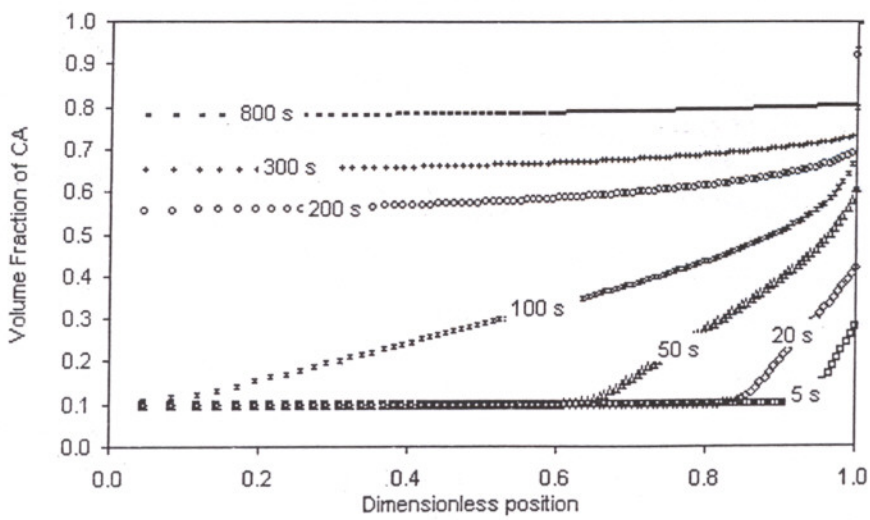

Figure 6.19. Volume fraction profiles of CA for case R6.

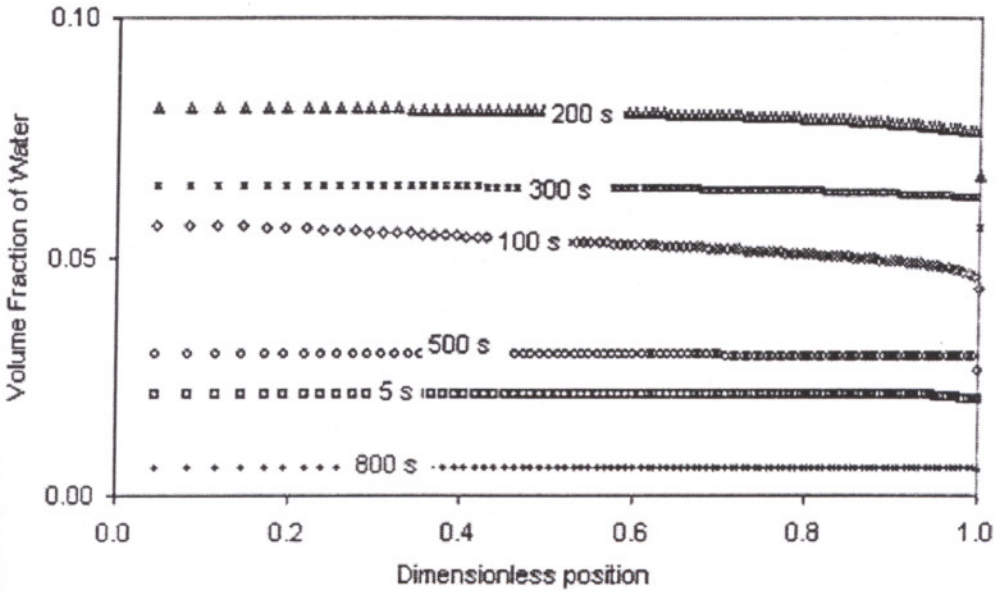

Figure 6.20. Volume fraction profiles of water for case R6.

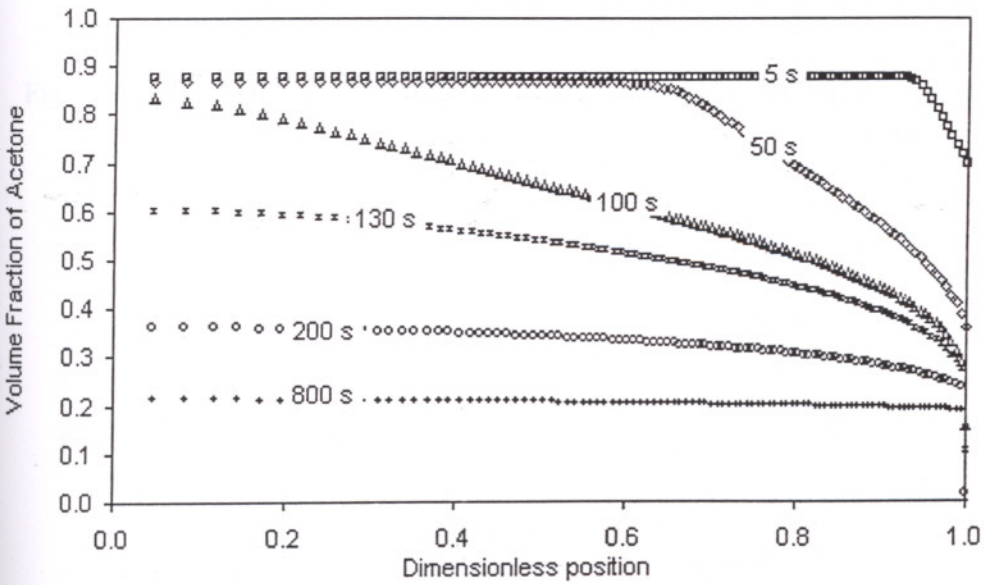

Figure 6.21. Volume fraction profiles of acetone for case R6.

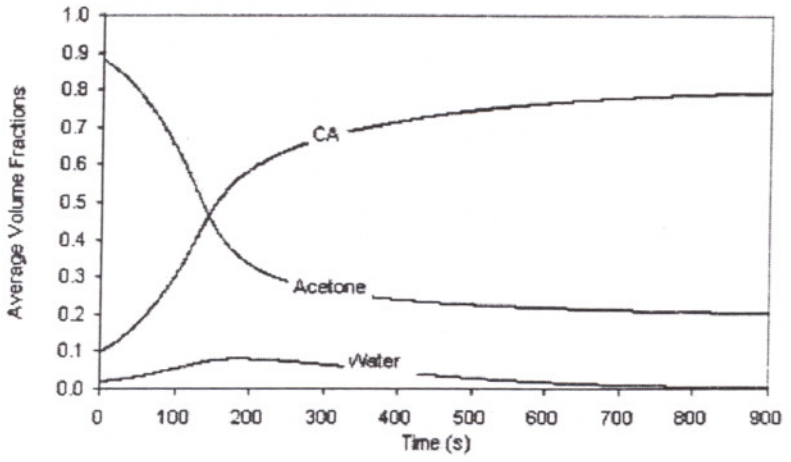

Figure 6.22. Average volume fractions of water, acetone and CA during membrane formation for case R6.

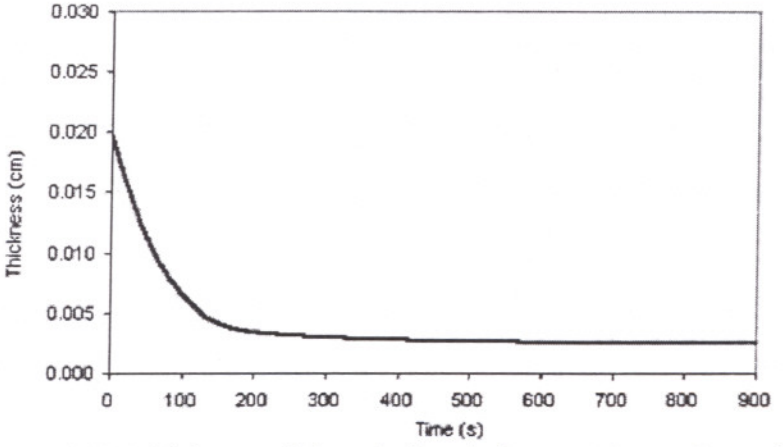

Figure 6.23. Thickness of the solution during membrane formation for case R6.

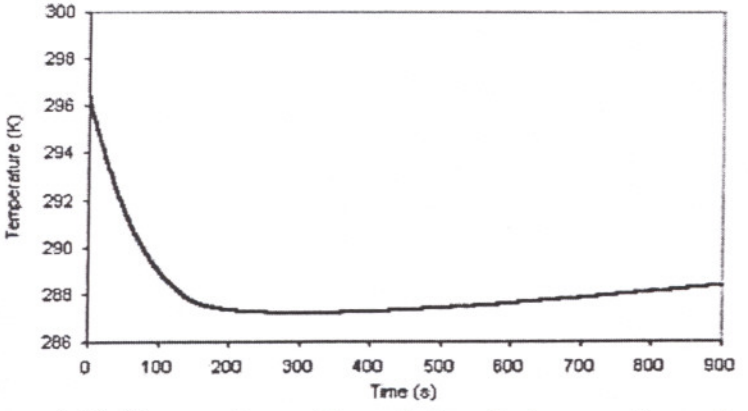

Figure 6.24. Temperature of the solution during membrane formation for case R6.

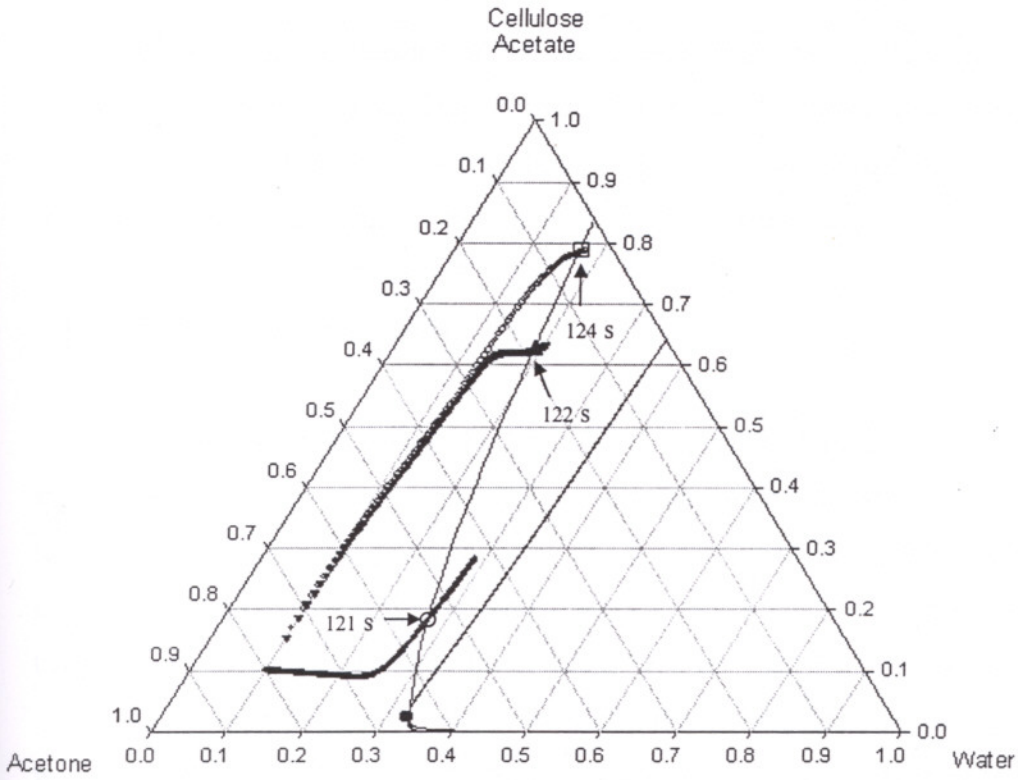

Figure 6.25. Concentration paths of water, acetone and CA for case R7 (O: solution/substrate interface, □: solution/air interface, Δ: point just below solution/air interface).

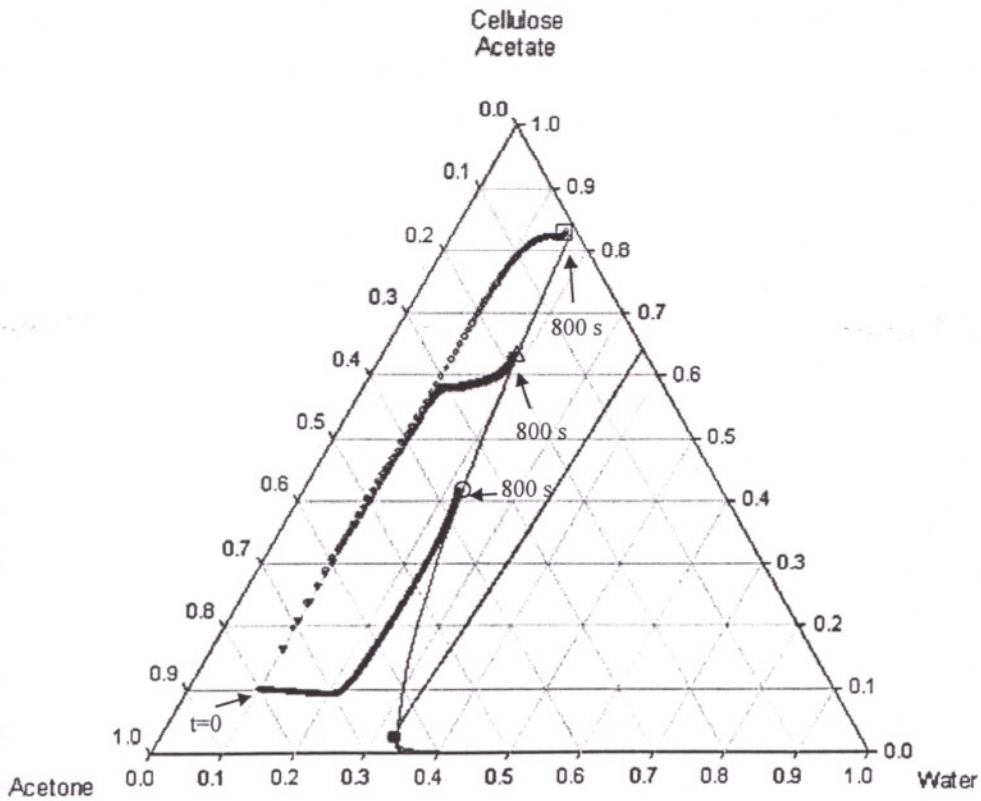

Figure 6.26. Concentration paths of water, acetone and CA for case R8 (O: solution/substrate interface, □: solution/air interface, Δ: point just below solution/air interface).

Also, with decreasing initial film thickness, the difference in polymer concentrations at the top and bottom interfaces is smaller, implying less asymmetry in the final membrane structure with a thinner skin. The percentage of dense skin layer was calculated as 4.2% and 3 %for cases R4 and R7, respectively.

6.2.3 Effect of relative humidity

To investigate the effect of relative humidity on the final membrane structure, % relative humidity was increased to 25% in case R9, where all other conditions are the same as those in case R7. Similarly, one of the experimental conditions represented in case R2 are the same as those in case R7, except that % relative humidity is 50 %. So; the phase diagrams of these three cases, R2, R7 and R9, respectively were compared.

As the relative humidity in air increases, the driving force for the evaporation of water decreases consequently; the residual amount of water in the solution increases. Comparing the phase diagrams in Figure 6.27 and 6.28 indicate that increasing the relative humidity affects the formation process in two ways. First, solution/air and solution/substrate interfaces enter into the phase diagram more rapidly, and not at the same time. Second, increasing the relative humidity will lead to a membrane structure with thinner skin layer. The percentage of dense skin layer was calculated as 3% and 2.4% for cases R9 and R2, respectively.

6.2.4. Effect of convection mode

In all the cases reported so far, the heat and mass transfer from the cast polymer solution to the gas phase were controlled by free convection process. In this section, the effect of velocity of air, in other words, the effect of forced convection on the membrane formation was investigated. For this purpose, conditions in cases R10 and R11 were kept identical to those in case R7 except that velocity of air was changed as 20 and 50 cm/sec, respectively. The results in Figures 6.29 and 6.30 show that with increasing air velocity, phase separation is completely suppressed and a uniformly dense coating devoid of substantial microstructure will result.

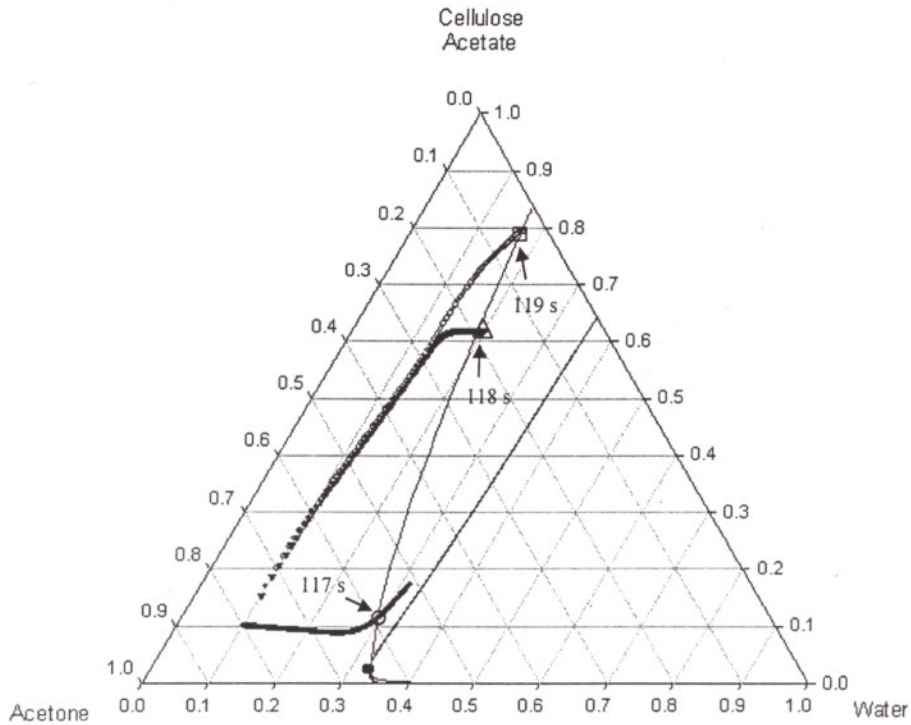

Figure 6.27. Concentration paths of water, acetone and CA for case R9 (O: solution/substrate interface, □: solution/air interface, Δ: point just below solution/air interface).

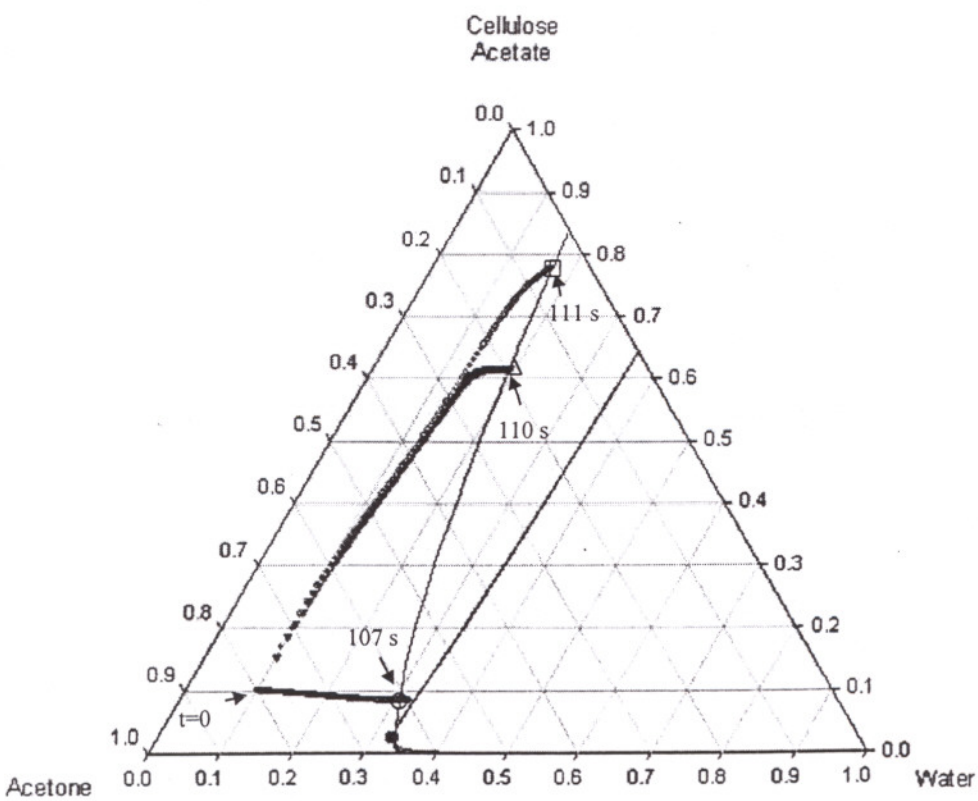

Figure 6.28. Concentration paths of water, acetone and CA for case R2 (O: solution/substrate interface, □: solution/air interface, Δ: point just below solution/air interface).

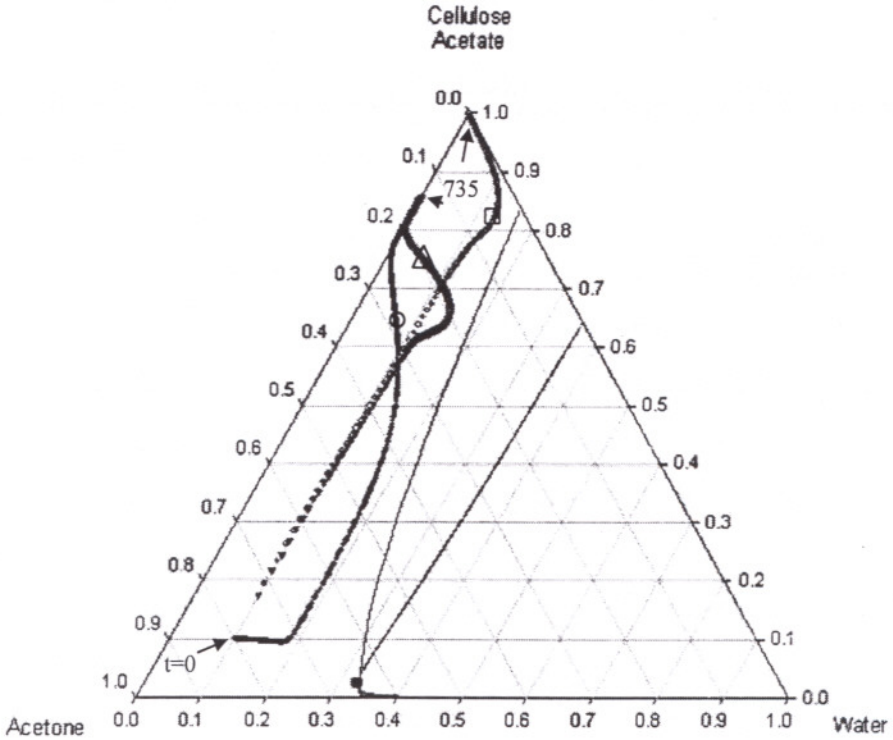

Figure 6.29. Concentration paths of water, acetone and CA for case R10 (O: solution/substrate interface, □: solution/air interface, Δ: point just below solution/air interface).

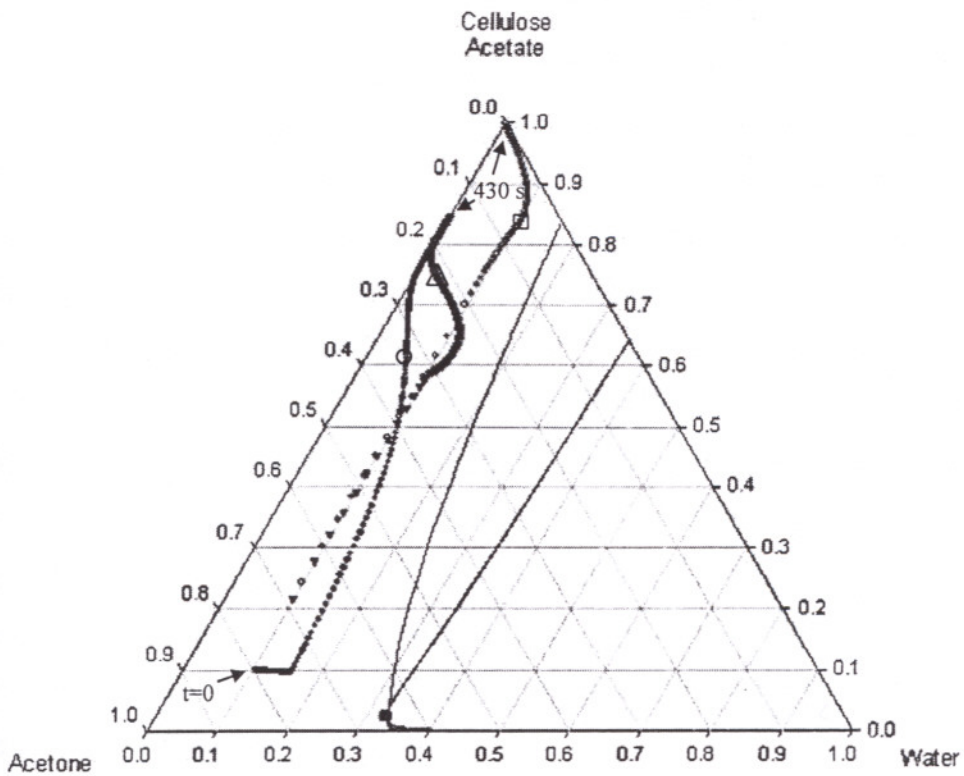

Figure 6.30. Concentration paths of water, acetone and CA for case R11 (O: solution/substrate interface, □: solution/air interface, Δ: point just below solution/air interface).

6.2.5. Effect of free volume parameters and diffusion formalism on the model results

The accurate formulation of the prediction of the diffusion equations and analysis of predictions therefrom forms the basis and heart of the membrane formation modeling. The diffusion formalism used in this study combines thermodynamic and self diffusion data, therefore its accuracy mainly depends on availability of these data. In this section, the effects of free volume parameters and cross diffusion coefficients on model predictions were evaluated.

In Figures 6.31 through 6.33, the model results were compared with the experimentally obtained mass loss data during dry casting. In these figures curve A represents the result which was obtained using different free volume parameters while curve B represents the prediction when the cross coefficients are assumed to be negligible.

In the study of Verros and Malamataris (1999), CA free volume parameters, K_{13}/γ and $\xi_{23}\hat{V}_3^*$, were regressed as 0.0005 and 0.638 respectively using the binary drying curves of CA and acetone. Using the regressed value of ξ_{23}, ξ_{13} was calculated as 0.225. These values are different than those calculated and reported in this work in Table 6.1 Predictions were then performed by inserting Verros and Malamataris's free volume parameters into the model. As illustrated in Figures 6.31 through 6.33 using free volume parameters reported in this work gives much better predictions when compared with the experimental data corresponding to case R1, R2, R3 respectively. This is due to the fact that in Verros and Malamataris's study, temperature dependent free volume parameters, K_{13}/γ, was regressed using data collected at just one temperature. Included in Figures 6.31-6.33 are predictions from equations 4.25 through 4.28 but using the principal diffusion coefficients (i.e., the cross diffusion coefficients were set equal to zero). On the basis of results evident in these figures, one can conclude that cross diffusion coefficients are not negligible and strongly influence the predictions of membrane formation modeling.

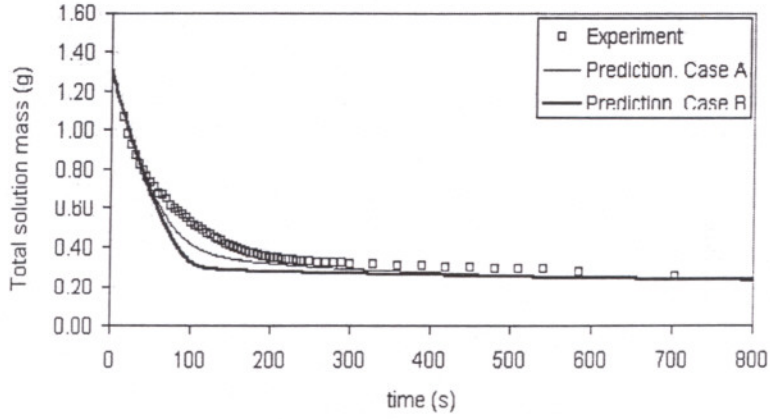

Figure 6.31. Experimental corresponding to case R1, and simulation results for total solution mass as a function of time. The line corresponds to full model, whereas the dashed solid line represents the solution when the cross diffusion coefficients are assumed to be negligible.

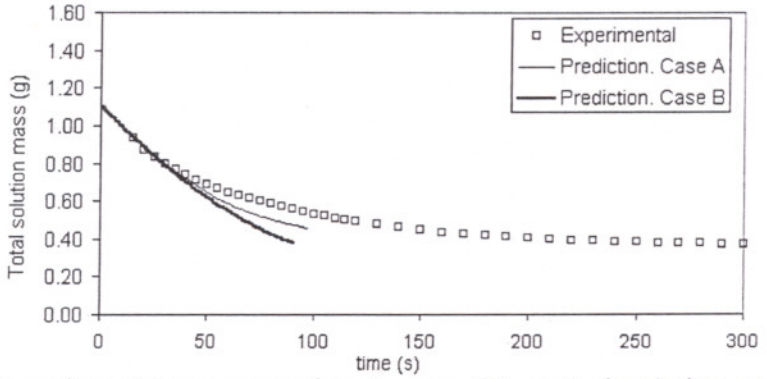

Figure 6.32. Experimental corresponding to case R2, and simulation results for total solution mass as a function of time. The line corresponds to full model, whereas the dashed solid line represents the solution when the cross diffusion coefficients are assumed to be negligible.

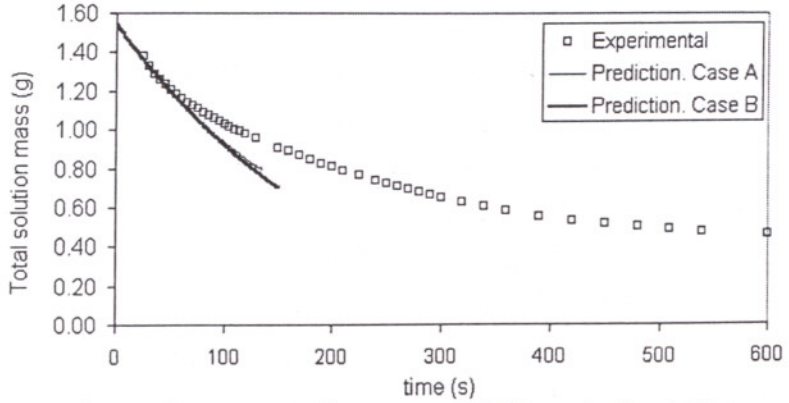

Figure 6.33. Experimental corresponding to case R3, and simulation results for total solution mass as a function of time. The line corresponds to full model, whereas the dashed solid line represents the solution when the cross diffusion coefficients are assumed to be negligible.

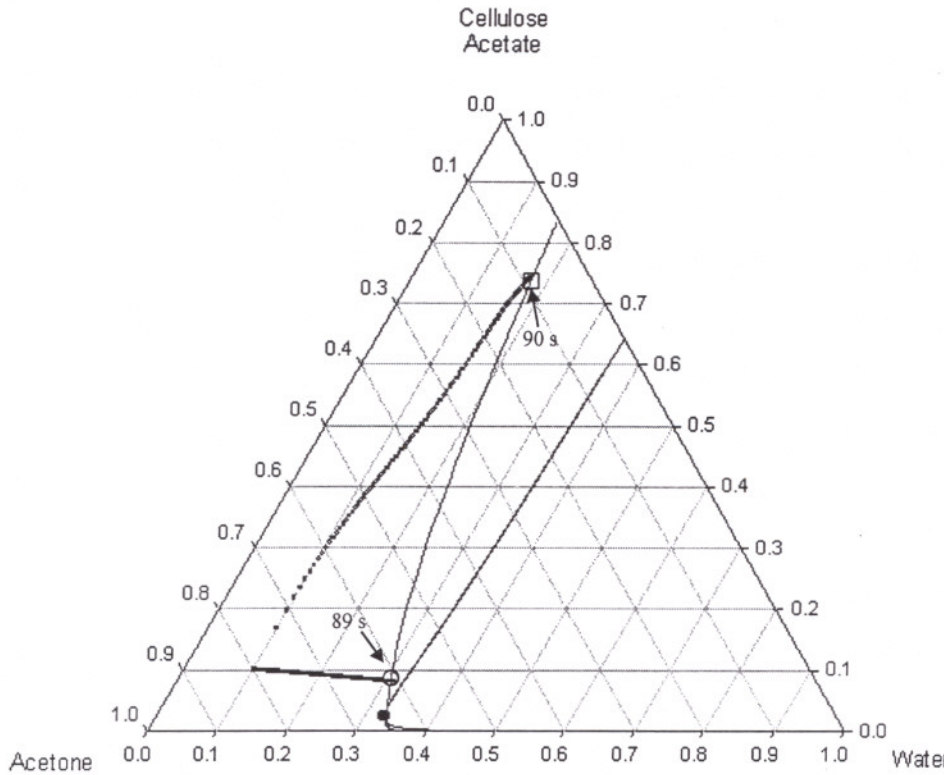

Figure 6.34. Concentration paths of water, acetone and CA for case A (O: solution/substrate interface, □: solution/air interface).

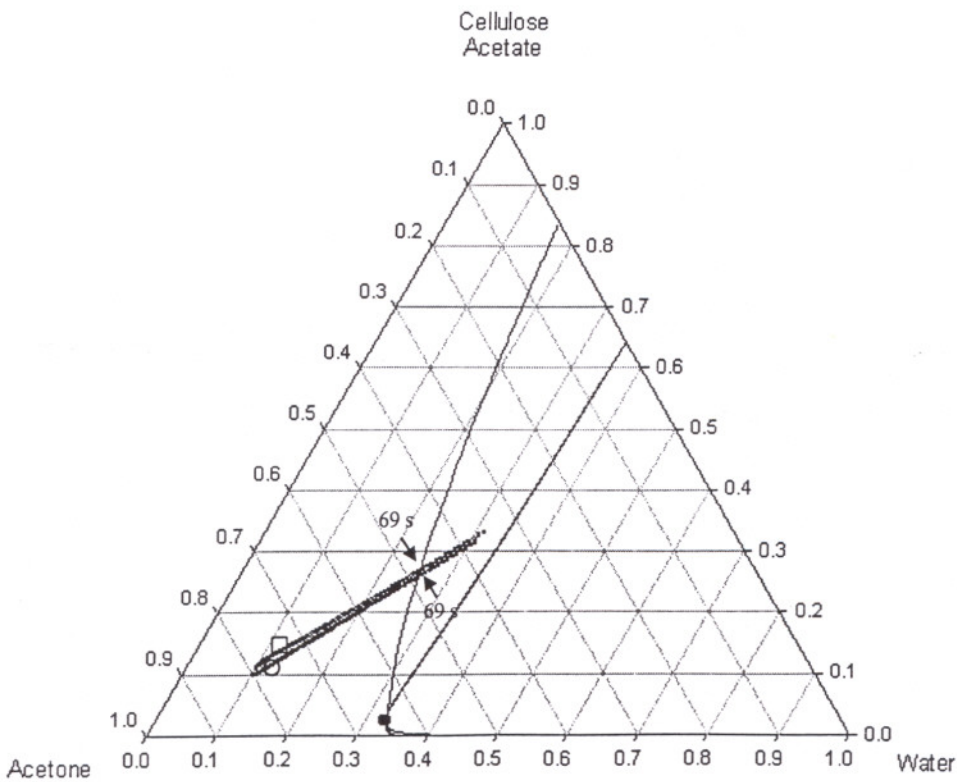

Figure 6.35. Concentration paths of water, acetone and CA for case B (O: solution/substrate interface, □: solution/air interface).

To investigate the effect of free volume parameters and cross diffusion coefficients on the prediction of structure formation, composition paths calculated for case A and B were plotted on the phase diagrams as shown in Figure 6.34 and 6.35, respectively. Compositions in these figures are predictions corresponding to the experimental condition, case R2. The phase diagram corresponding to this case was plotted previously in Figure 6.28 in which prediction of compositions was based on free volume parameters reported in Table 6.1 and diffusion formalism including both main and cross diffusion coefficients. Comparing Figure 6.28 with Figure 6.34 shows that the precipitation times decreased about 10 % when different free volume parameters were used. When the diffusion coefficients were set to zero, both the precipitation times and composition paths at the substrate and surface regions changed drastically. A comparison between concentration paths in Figure 6.28 and 6.35 indicates that the morphology obtained in Figure 6.28 has much greater asymmetry than that obtained in Figure 6.35. In fact the predictions in Figure 6.35 suggests that final membrane structure will be symmetric and porous. This prediction is completely different than that shown in Figure 6.28. Consequently the results shown in this section indicate that cross diffusion coefficients should not be neglected, otherwise, predictions of final membrane structure can be very misleading.

6.3 Morphological studies

Structural studies on cellulose acetate membranes, prepared from two different compositions, were conducted using scanning electron microscopy. Although several membranes were prepared with dry casting and immersion precipitation techniques at different processing conditions, specific structures could not be obtained at the first trials due to deficiencies in sample preparation techniques for SEM analysis.

Figures 6.36 and 6.37 show the SEM pictures taken at two different magnifications. Membranes were cast at 20 ^{0}C from CA solution containing 17 % water, 76 % acetone and 7 % CA and prepared by dry casting technique. In these pictures, gray parts represent the polymer matrix, while the black parts are porous regions. Higher magnification shown in Figure 6.37 indicates that membrane has a sponge like structure and pores in the structure are interconnected. This is a desired structure for applications, which require high permeabilities. The SEM pictures could

not be used to determine the thickness of dense skin layer over a porous sublayer since air and substrate sides of prepared membranes were not marked before the analysis.

Figure 6.38 shows the cross section of the membrane cast from a solution containing 10 % water, 80 % acetone and 10 % CA. Comparing Figure 6.36 and 6.38 indicates that decreasing water concentration in the casting solution also decreases the porosity of the membrane. The model also predicted that % of porous layer decreased from 77.0 % to 75.8 % as volume fraction of water was decreased from 0.15 to 0.10. This result was also verified by density measurements in which density of membrane decreased from 0.7 to 0.4 gr/cm^3 while initial water volume fraction was increased from 0.1 to 0.18.

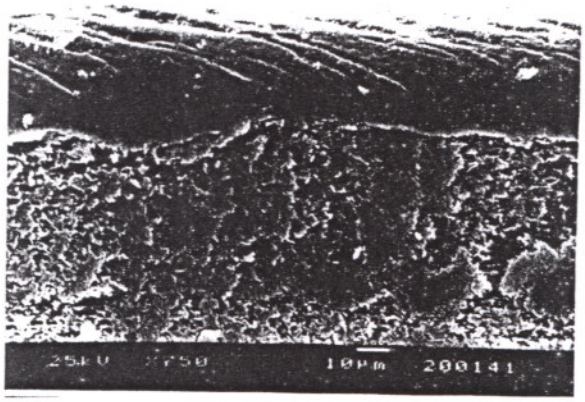

Figure 6.36. SEM picture of cross section of a membrane. Initial composition: %17 Water, %76 Acetone, % 7 Cellulose Acetate. Magnification×750.

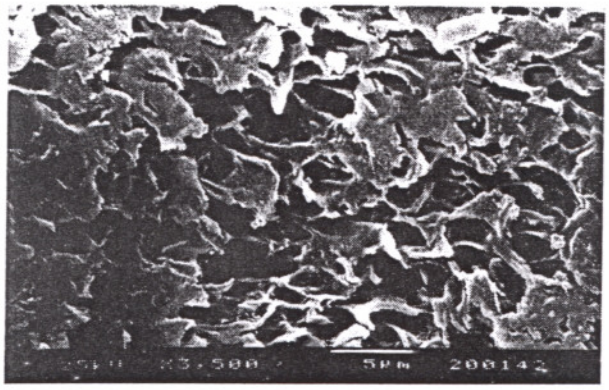

Figure 6.37. SEM picture of cross section of a membrane. Initial composition: %17 Water, %76 Acetone, % 7 Cellulose Acetate. Magnification×3500.

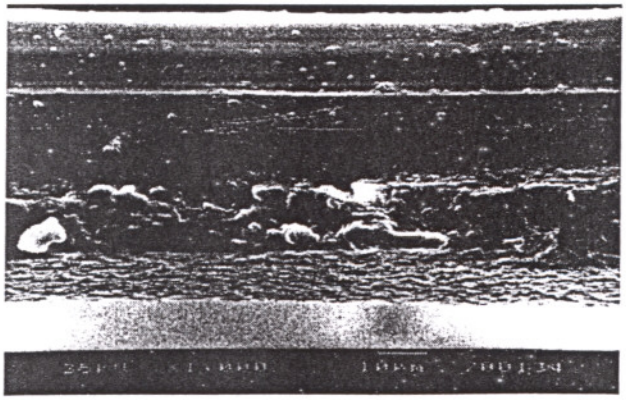

Figure 6.38. SEM picture of cross section of a membrane. Initial composition: %10 Water, %80 Acetone, % 10 Cellulose Acetate. Magnification×1000.

CHAPTER 7

MEASUREMENT OF WATER VAPOR PERMEABILITY OF CELLULOSE ACETATE MEMBRANES

The permeability and selectivity values of water vapor and other gases through cellulose acetate membranes have industrial importance, especially for the gas separation applications. The gases are transported through membranes by several mechanisms such as solution diffusion, Knudsen flow and convective flow depending on the pore dimension and distribution. In addition to the morphology, the rate of mass transfer of species in membranes is altered by the molecular interaction of the permeating gas and the membrane. For polymeric membranes, additional factors such as molecular weight, crystallinity and orientation of the polymer also influence the permeability and selectivity characteristics. Therefore, due to the differences in membrane preparation routes different values were reported in the literature.

The permeability of several atmospheric and industrial gases and water vapor through CA membranes are summarized in Table 7.1.

Table 7.1. Permeability coefficient data of various gases and water vapor given in the literature

PERMEABILITY (cm^3 (STP) × cm) / (cm^2 × s × atm)						
He	H_2	N_2	O_2	H_2O	CO_2	CH_4
1.03×10^{-7} (1)	2.66×10^{-8} (1)	2.13×10^{-9} (1)	5.93×10^{-9} (1)	4.18×10^{-5} (1)	1.75×10^{-7} (1)	1.42×10^{-9} (4)
9.30×10^{-8} (4)	7.59×10^{-8} (4)	1.19×10^{-9} (4)	6.79×10^{-9} (4)	3.04×10^{-5} (2)	3.04×10^{-8} (3)	
					4.09×10^{-8} (4)	

1 (Pauly 1999)
2 (Feng et al. 1997)
3 (Sada et al. 1988)
4 (Hao and Wang 1998)

In this chapter the permeability of water vapor through cellulose acetate membranes prepared from different initial casting compositions was calculated using

steady state measurements. The differences in the values were discussed considering the model results.

7.1. Permeation methods

The permeability of diffusants through films and membranes can be measured, mainly, by steady state diffusion and time lag technique (Crank and Park 1968). The first method requires to measure diffusion rates under steady state conditions and it is preferred if the time to reach steady state conditions is short. Using time lag technique, it is possible to determine both diffusivity and permeability with one set of experimental data. However, this method is limited to systems having low enough permeability values such that it takes some time for the diffusant to pass through the sheet. In this study; steady state diffusion measurements were used. Therefore, in the following section, this method is discussed in detail.

Under unsteady state conditions diffusion through a plane sheet or membrane of thickness L is described by Fick's second law:

$$\frac{\partial C}{\partial x} = \frac{\partial}{\partial x}\left(D\frac{\partial C}{\partial x}\right) \tag{7.1}$$

After a time, steady state is reached in which the concentration remains constant at all positions of the sheet. If diffusion coefficient, D, remains constant, then equation 7.1 reduces to.

$$\frac{d^2C}{dx^2} = 0 \tag{7.2}$$

If concentrations of diffusant at surface x=0 and x=L are maintained constant at C_1, C_2 respectively and if equation 7.2 is integrated twice between x=0 and x=L, then following concentration profile is obtained.

$$\frac{C - C_1}{C_2 - C_1} = \frac{x}{L} \tag{7.3}$$

Using equation 7.3 the rate of mass transfer of diffusing substance is calculated as follows:

$$F = -D\frac{dC}{dx} = \frac{D(C_1 - C_2)}{L} \tag{7.4}$$

If the thickness, L, and the surface concentrations C_1 and C_2 are known, then D can be calculated from a single measurement of the flow rate, F. In some systems, in

which a gas or vapor diffuses through a membrane, the surface concentrations may not be known but only gas or vapor pressures on the two sides of the sheet are known. If a linear relationship between the external vapor pressure and the corresponding concentration within the surface of the sheet is assumed, i.e, if Henry's law is used,

$$C = p\,S \tag{7.5}$$

then equation 7.4 becomes

$$F = \frac{DS(p_1 - p_2)}{L} \tag{7.6}$$

In this equation, the product of diffusivity and solubility is defined as permeability coefficient P.

$$P = DS \tag{7.7}$$

Therefore, if the quantity of permeant, F, p_1 and p_2 are measured at steady state conditions, then the permeability coefficient can be calculated.

7.2. Experimental

Cellulose acetate with a molecular weight of 50000 and an acetyl content of 39.7 % was purchased from Aldrich. 99 % pure acetone obtained from Merck was used as the solvent and distilled and deionized water used as nonsolvent.

Binary and ternary solutions were prepared with compositions given in Table 7.2.

Table 7.2. The volume fractions of the components in the casting solution.

	F1	F2	F3
Water	0.00	0.10	0.18
Acetone	0.90	0.80	0.76
Cellulose Acetate	0.10	0.10	0.06

Due to the fast evaporation of solvent the solution was prepared in a closed glass container. To prevent the precipitation of the polymer, water was added after a homogeneous acetone cellulose acetate solution was obtained. The solutions were cast on a glass support with a 300 μm opening cast plate at 20 ^{0}C and 60 % relative humidity. The thickness and the density of the membranes were measured by

micrometer and picnometer respectively. The volume fraction of the porous layer was calculated using densities of membrane, polymer and pores respectively.

The water vapor permeability of the membranes was measured with the experimental setup given in Figure 7.1. The experiments were performed at 20^0C. The lower side of the membrane is in thermodynamic equilibrium with water vapor having 100 % relative humidity, while the upper side faces the open atmosphere with 60 % relative humidity. The mass loss of water in the cell was recorded for 2 hours using an analytical balance with 10^{-4} g accuracy. From the slope of the linear plot of mass loss of water with respect to time, the amount of water permeated per unit area, F, was calculated. Partial pressures of water vapor on the lower and upper sides were calculated by assuming both phases are ideal. Finally, permeability of water vapor through cellulose acetate membranes was calculated from equation 7.6.

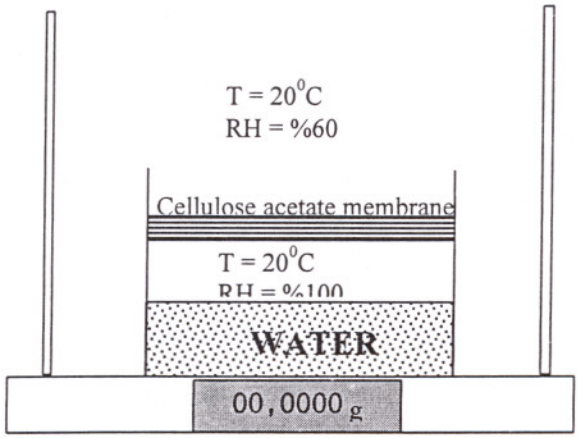

Figure 7.1. Schematic of experimental setup used in measuring water vapor permeability coefficients.

7.3. Results and discussion

The physical properties and water vapor permeability values of the prepared membranes are given in Table 7.3.

The results in Table 7.3 indicate that with increasing water concentration in the initial casting solution, both pore volume fraction and water vapor permeabilities increased. The former results is an agreement with model predictions discussed in Chapter 6. When the volume fraction of water was increased from 0.1 to 0.15, the difference in polymer compositions of the two interfaces was predicted to be smaller, as shown in Figure 6.7 and 6.14, respectively. The implication of this prediction is that

increasing water concentration in the casting solution causes a final membrane structure with thinner skin layer. When the volume fraction of water was increased from 10 % to 18%, the fraction of skin layer decreased from 0.53 to 0.29 respectively. Consequently, the measurement of densities, and water vapor permeability of prepared membranes allowed to verify the model predictions qualitatively.

The membranes prepared from water containing solutions were white in color and can be named as opaque, while the membrane prepared from acetone and cellulose acetate (F1) was colorless and transparent.

Table 7.3. The thickness, density, pore volume fraction and water vapor permeability values of the obtained membranes.

	F1	F2	F3
Thickness (μm)	24	27	41
Density (gr/cm^3)	1.1	0.7	0.4
Pore volume fraction	0.16	0.47	0.71
Water vapor permeability (cm^3 (cm^3 (STP).cm)/(cm^2.s.atm)	$2.26\ 10^{-4}$	$4.94\ 10^{-4}$	$9.90\ 10^{-4}$

There is no doubt that, differences in densities, pore volume fractions, permeability coefficients and optical properties of membranes arise due to the volume fraction of water in the casting solution.

CONCLUSIONS

In this study, mathematical model was used to describe the formation of asymmetric membranes by dry casting method. The model is fully predictive, i.e., does not utilize any adjustable parameters. It is based on fundamental conservation laws, so can be applied to any membrane forming system. The predictive ability of the model was evaluated by comparing experimentally measured total weight loss data and model predictions. The comparison has shown excellent agreement between the predictions and the experimental data for two sets of data and slight deviation for the case in which the solution was dilute in polymer. Once the model was verified, simulations have been performed to investigate the effects of gas phase conditions, initial film thickness and composition on the final structure of the membrane. Using SEM pictures, morphological studies were performed and in addition, water vapor permeability coefficients of the prepared membranes were measured.

The water concentration in the initial casting solution was found to be one of the key factors controlling the final structure of the membrane. It was seen that, as the water concentration in the initial cast solution increased, the onset of phase separation was delayed and greater asymmetric structure was obtained. Also the model predictions indicated that when the water concentration is low enough, dense, nonporous and symmetric structures can be formed. These results were verified with the SEM pictures and water vapor permeability measurements. Membrane cast from a solution including higher water concentration has higher porosity and shown higher permeability to water vapor.

The decrease in the thickness of the initial casting solution resulted in a decrease in the precipitation time and less asymmetry in structure. The predictions indicated that, thicker solution should lead to membrane structure with denser top layer, i.e., thicker skin layer.

The evaporation conditions, i.e., velocity of air, were found to have a significant effect on the structure formation. The results have shown that, with increasing velocity of air, dense and nonporous membranes should be obtained. Therefore, the predictions imply that to obtain an asymmetric structure with dense top layer over a porous sublayer, membranes should be prepared under free convection conditions.

The model predictions are quite sensitive to diffusion formalism and parameters used in self diffusion calculations. The results have clearly shown that multicomponent diffusion effects have strong impact on the prediction of membrane formation, therefore, should be included in the model. Otherwise, it was seen that results can be very misleading.

Finally, all the results suggest that the model can be utilized as a tool to optimize membrane formation, since slight changes in the membrane fabrication recipes can greatly influence the final structure. This is a very important advantage since modeling of this process avoids extensive trial and error experimentation and so reduces the cost of fabrication.

FUTURE WORK

Future researches following this study may include both experimental and modeling studies.

The results presented in this work have shown that the model predictions are quite sensitive to diffusion formalism and associated thermodynamic to diffusion formalism and associated thermodynamic and transport properties. In this respect, multicomponent diffusivities were found to have significant effect on the predictions of structure formation. Experimental part of the future work should involve measurements of multicomponent diffusivities in membrane forming systems. This is a very challenging area in which no one has succeeded yet to measure diffusivities in multicomponent polymer solutions. Even if it is not possible, diffusion and thermodynamics of the binary pairs of the membrane system should be measured. These measurements will allow to determine required transport and thermodynamic properties accurately. The validity of the model was confirmed using only total weight loss data. In addition to weight loss, temperature of the solution can be measured and onset of phase separation can be determined by noninvasive real-time measurement techniques. Experimental measurements can be carried in a more controlled environment in which temperature and relative humidity can be varied. Membranes prepared under different conditions from different recipes should be investigated through scanning electron microscopy and resulting structures should be compared with the model predictions. This task can be accomplished much more easily once SEM is installed in the laboratory.

Asymmetric membranes prepared by dry casting method can have many different applications ranging from gas separations to ultrafiltration. The key parameter which determines the solubility of a membrane for a specific application is the permeability. So, to determine possible applications of prepared membranes, their permeability to atmospheric gases, such as H_2, O_2, N_2, CO_2 and industrial gases such as CH_4, He, CO, Ar as well as to the compounds involved in the application can be determined. These measurements will allow to investigate the effect of preparation conditions on the selectivity and permeability of membranes.

The model presented here describes the kinetic of membrane formation process until the solution cross the binodal. The model does not provide any information of the microstructure of the membrane. Currently, no modeling studies exist to describe microstructure formation in dry casting method. Therefore, following this thesis, future modeling studies should involve the kinetics in the spinodal line in which two phases are present. These approaches will significantly contribute to the literature.

REFERENCES

1. Alsoy S., "Modeling of polymer drying and devolatilization processes," PhD Thesis, The Pennsylvania State University, University Park (1998).
2. Alsoy S. and Duda J.L., "Modeling of multicomponent drying of polymer films," *AIChE Journal*, **45**, (1999), 896.
3. Altena F., "Phase separation phenomena in cellulose acetate solutions in relation to asymmetric membrane formation," PhD Thesis, University of Twente, 1982.
4. Anderson J.E., Ullman R., "Mathematical analysis of factors influencing the skin thickness of asymmetric reverse osmosis membranes," *Journal of Applied Physics*, **44**, (1973), 4303.
5. Ataka M., Sasaki K., "Gravimetric analysis of membrane casting. I. Cellulose acetate-acetone binary casting solutions," *Journal of Membrane Science*, **11**, (1982), 11.
6. Bearman R.J., "on the molecular basis of some current theories of diffusion," *Journal of Physical Chemistry*, **65**, (1961), 1961
7. Beltsios K., Athanasiou E., Aıdinis C., Kanellopoulos N., "Microstructure formation phenomena in phase inversion membranes," *Journal of Macromolecular Science-Physics*, **B38**, (1999), 1.
8. Brandrup J., Immergut E.H., Grulke E.A., *Polymer Handbook* (John Wiley & Sons Inc., 1999).
9. Bristow G.M. and Watson W.F., "Cohesive energy densities of polymers. Part 1. Cohesive energy densities of rubbers by swelling measurements," *Trans. Faraday Soc.*, **54**, (1958), 1721.
10. Caneba G.T. and Soong D.S., "Polymer membrane formation through the thermal-inversion process. 2. Mathematical modeling of membrane structure formation," *Macromolecules*, **18**, (1985), 2545.
11. Castellari C, Ottani S., "Preparation of reverse osmosis membranes. A numerical analysis of asymmetric membrane formation by solvent evaporation from cellulose acetate casting solutions," *Journal of Membrane Science*, **9**, (1981), 29.
12. Cheng L.P., Soh Y.S., Dwan A.H., Gryte C.C., "An improved model for mass transfer during the formation of polymeric membranes by the immersion-

precipitation process," *Journal of Polymer Science: Part B: Polymer Physics*, **32**, (1994), 1413.

13. Cohen C., Tanny G.B., Prager S., "Diffusion controlled formation of porous structures in ternary polymer systems," *Journal of Polymer Science. Polymer Physics Edition*, **17**, (1979), 477.
14. Dabral M., Franers L.F., Scriven L.E., "Structure evolution in asymmetric polymer coatings," in *International Society of Coating Science and Technology. 9th International Coating Science and Technology Symposium Final Program and Extended Abstracts* (Newark, Delaware, 1998).
15. Doolittle A.K., "Studies in Newtonian flow. II: The dependence of the viscosity of liquids on free space", *Journal of Applied Physics*, **22**, (1951), 1471.
16. Duda J.L., Vrentas S.T., Liu H.T., "Prediction of diffusion coefficients for polymer solvent systems," *AIChE Journal*, **28**, (1982), 285.
17. Ferguson J.D., Meerwal E.V., "Free volume interpretation of self diffusion in ternary solutions: n-Paraffin-Hexafluorobenzene-cis-4-Polybutadiene," *Journal of Polymer Science. Part B: Polymer Physics*, **18**, (1980), 1285.
18. Ferry J.D., *Viscoelastic properties of polymers* (Wiley, New York, 1970).
19. Fujita H., "Interpretation of diffusion coefficient data," in *Diffusion in Polymers*, edited by Crank J., Park G.S., (Academic, New York, 1968).
20. Greenberg A.R., Shojaie S.S., Krantz W.B., Tantekin-Ersolmaz S.B., "Use of infrared thermography for temperature measurement during evaporative casting of thin polymeric films," *Journal of Membrane Science*, **107**, (1995), 249.
21. Grulke E.A., "Solubility parameter values" in ., *Polymer Handbook* edited by Brandrup J., Immergut E.H., Grulke E.A. (John Wiley & Sons Inc., 1999).
22. Hong, S., "Prediction of polymer/solvent solution behavior using frevolume theory," *Ind. Eng. Chem. Res.*, **34**, (1995), 2536.
23. Incropera F.P., Dewitt D.P. , *Fundamentals of heat and mass transfer*, (John Wiley and Sons, 1990).
24. Kools W.F.C., "Membrane formation by phase inversion in multicomponent polymer systems," PhD Thesis, University of Twente (1998).
25. Krantz W.B., Ray R.J., Sani R.L., Gleason K.J., "Theoretical study of the transport processes occurring during the evaporation step in asymmetric membrane casting," *Journal of Membrane Science*, **29**, (1986), 11.

26. Kumins C.A. and Kwei T.K., "Free volume and other theories" in *Diffusion in Polymers*, edited by Crank J., Park G.S. (Academic Press London and New York, 1968).
27. Laxminarayan A., McGuire K.S., Kim S.S., Lloyd D.R., "Effect of initial composition, phase separation temperature and polymer crystallization on the formation of microcellular structures via thermally induced phase separation," *Polymer*, **35**, (1994), 3060.
28. Matsuyama H., Teramoto M., Nakatani R., Maki T., "Membrane formation via phase separation induced by penetration of nonsolvent from vapor phase. II. Membrane morphology," *Journal of Applied Polymer Science*, **74**, (1999), 171.
29. Matsuyama H., Teramoto M., Uesaka T., "Membrane formation and structure development by dry cast process," *Journal of Membrane Science*, **135**, (1997), 271.
30. Park H.C., Kim Y.P., Kim H.Y., Kang Y.S., "Membrane formation by water induced phase inversion," *Journal of Membrane Science*, **156**, (1999), 169.
31. Perry R.H. and Chilton C., Chemical engineer's handbook, (McGraw Hill, 1973).
32. Pinnau I. and Koros W.J., "Structures and gas separation properties of asymmetric polysulfone membranes made by dry, wet, and dry/wet phase inversion," *Journal of Applied Polymer Science*, **43**, (1991), 1491.
33. Pinnau I. and Koros W.J., "A qualitative skin layer formation mechanism for membranes made by dry/wet phase inversion," *Journal of Polymer Science: Part B: Polymer Physics*, **31**, (1993), 419.
34. Rautenbach R., and Albrecht R., "Membranes structure, materials and performance", in *Membrane Processes* (John Wiley & Sons, 1989).
35. Reuvers A.J. and Smolders C.A., "Formation of membranes by means of immersion precipitation Part 2. The mechanism of formation of membranes prepared from the system cellulose acetate-acetone-water," *Journal of Membrane Science*, **34**, (1987), 67.
36. Reid R.C., Prausnitz J.M., Sherwood T.K., *The properties of gases and liquids*, (McGraw Hill, New York, 1977).
37. Reuvers A.J., Smolders C.A. "Formation of membranes by means of immersion precipitation. Part II. The mechanisms of formation of membranes prepared from the system cellulose acetate-acetone-water," *Journal of Membrane Science*, **34**, (1987), 67.

38. Shojaie S.S., Krantz W.B., Greenberg A.R., "Dense polymer film and membrane formation via the dry cast process. Part I. Model development," *Journal of Membrane Science*, **94**, 1994a , 255.

39. Shojaie S.S., Krantz W.B., Greenberg A.R., "Dense polymer film and membrane formation via the dry-cast process. Part II. Model validation and morphological studies," *Journal of Membrane Science*, **94**, 1994b, 281.

40. Strathmann H., "Synthetic membranes and their preparation", in *Synthetic Membranes: Science, Engineering and Applications*, edited by P.M. Bungay, H.K. Lonsdale and M.N. Pinho (NATO ASI Series, 1986).

41. Tompa H., "Phase Relationships," in *Polymer Solutions*, (New York, Academic Press Inc. Publishers, London, Butterworths Scientific Publications, 1956).

42. Tsay C.S., McHugh A.J., "Mass transfer dynamics of the evaporation step in membrane formation by phase inversion," *Journal of Membrane Science*, **64**, (1991), 81.

43. Tsay C.S., McHugh A.J., "Mass transfer modeling of asymmetric membrane formation by phase inversion," *Journal of Polymer Science: Part B: Polymer Physics*, **28**, (1990), 1327.

44. Tsay C.S., McHugh A.J., "A rationale for structure formation during phase inversion," *Journal of Polymer Science: Part B: Polymer Physics*, **29**, (1991), 1261.

45. Vrentas J.S., Duda J.L., Ling H.C., "Self diffusion in polymer solvent systems," *Journal of Polymer Science*, **22**, (1984), 459

46. Vrentas J.S., Vrentas C.M. "Drying of solvent coated polymer films," *Journal of Polymer Science: Part B: Polymer Physics*, **32**, (1994), 187.

47. Wienk I.M., Boom R.M., Beerlage M.A.M., Bulte A.M.W., Smolders C.A., Strathmann H., "Recent advances in the formation of phase inversion membranes made from amorphous and semicrystalline polymers," *Journal of Membrane Science*, **113**, (1996), 361.

48. Wijmans J.G. and Smolders C.A., "Preparation of asymmetric membranes by the phase inversion process", in *Synthetic Membranes: Science, Engineering and Applications*, edited by P.M. Bungay, H.K. Lonsdale and M.N. Pinho, (NATO ASI Series, 1986).

49. Witte P., Dijkstra P.J., Berg J.W.A., Feijen J., "Phase separation processes in relation to membrane formation," *Journal of Membrane Science*, **117**, (1996), 1.

50. Yamasaki A., Tyagi R.K., Fouda A.E., Matsuura T., Jonasson K., "Effect of solvent evaporation conditions on gas separation performance for asymmetric polysulfone membranes," *Journal of Applied Polymer Science*, **71**, (1999), 1367.

51. Yilmaz L., A.J. McHugh, "Analysis of nonsolvent-solvent-polymer phase diagrams and their relevance to membrane formation modeling," *Journal of Applied Polymer Science*, **31**, (1986), 997.

52. Yilmaz L., A.J. McHugh, "Modelling of asymmetric membrane formation. I. Critique of evaporation models and development of a diffusion equation formalism for the quench period," *Journal of Membrane Science*, **28**, (1986b), 287.

53. Zeman L., Fraser T., "Formation of air-cast cellulose acetate membranes. Part I. Study of macrovoid formation," *Journal of Membrane Science*, **84**, (1993), 93.

54. Zielinski J.M. and Duda J.L., "Predicting polymer/solvent diffusion coefficients using free-volume theory," *AIChE Journal*, **38**, 1992, 405.

55. Zolandz R.R. and Fleming G.K. "Definitions" in *Membrane Handbook* edited by Winston Ho W.S. and Sirkar K.K. (Von Nostrand Reinhold New York, 1992).

APPENDIX

Program (written in FORTRAN and using DNEQNF subroutine from IMSL) for calculating the volume fractions of the component in the film, and, temperature and thickness of film during dry casting for a ternary solution.

```
C "Modeling of Asymmetric Membrane Formation by
C Dry-Casting Method."
C
C PROGRAM FOR
C CALCULATING THE VOLUME FRACTIONS IN THE FILM
C TEMPERATURE AND THICKNESS OF FILM
C
C 1:nonsolvent 2: solvent 3: polymer
C
C N: Number of grid points
C NEQ: Number of equations
C VMi: molar volume of comp. i
C SVi: specific volume of comp. i
C CVi: critical volume of comp. i
C DENSi: pure density of comp. i
C DENSS: density of substrate
C HVAPi: heat of vapor. of comp. i
C THINS: Thickness of support
C TSA:Temperature of  air (support side)
C TFA:Temperature of  air (film side)
C PBULi: Bulk pressure comp. i
C PIi: interphase pressure of comp i
C HTCS: Heat transfer coeff. of substrate side
C HTCF: Heat transfer coeff. of film side
C CMTi: Mass transfer coeff. of comp. i
C HCAPF,HCAPS: heat capacity of film and substrate
C VINIi: Initial volume fraction of comp. i (dimensional)
C TINI: Initial temperature of film and substrate
C THINF: Initial thickness of film (dimensional)
C Free volume parameters:
C  CD01(D01) D02(D02) K11/?(FK11) K12/?(FK12) K13/?(FK13)
C  K21-Tg1(FK21) K22-Tg2(FK22) K23-Tg3(FK23) JUMP13(FJU13),VFH
C CV31: crit. vol. of CA/crit. vol. of water
C CV32: crit. vol. of CA/crit. vol. of acetone
C Flory Huggins Interaction parameters: FH12,FH13,FH23
C H(i): distance between grid points as a function of GRIC1,GRIC2 and H(0)
C PO(i): the distance of grid points w.r.t. origin (film-substarate)
C DELT: derivative time
C DDELT: dimensionless of time increments
C ENDTIME: stopage time of calculation
C VFi: Volume fraction of comp. i
C VOLi: Volume fraction of comp. i
```

```
C WFi: Weight fraction of comp. i
C DMi: Mass density of comp. i
C TOTDM: Total mass density of film
C Di: self diffusion coeff.
C Dii: Mutual diffusion coeff.
C DCPii: derivative of chemical potential.
C THJ1: thickness of film at current time (dimensionless)
C THJ: thickness of film at previous time (dimensionless)
C TJ1: temperature of film at current time (dimensionless)
C TJ: temperature of film at previous time (dimensionless)
C XJ1: concentrations and temperature at current time.
C XJ:  concentrations and temperature at previous time.
C TEMPER, TEM: temperature of film
C T: dimensionless temperature
C A,B,E,G: constants defining the dimensionless temperature.
C SUMiJ: summation of volume fractions at the grid points of i in film
C AVENSO,AVESOL,AVEPOL: average volume fractions of nonsolvent,solvent and
polymer
C VSi: volume fraction of i at the substrate side
C VAi,VIi: volume fraction of i at the air side
C XGUESS :volume fractions and temperature guess vector
C AS,BS,CS,DS,ES antoine constant for solvent
C AN,BN,CN,DN,EN antoine constant for nonsolvent
C ERRREL: error criteria
      USE MSIMSLMD
      IMPLICIT DOUBLE PRECISION(A-H,O-Z)
      LOGICAL TPRINT
      PARAMETER (NMAX=800, NEQMAX=800)
      EXTERNAL FCN
C DATA TYPE AND DIMENSION DECLERATION
      DIMENSION XJ1(NEQMAX),XJ(NEQMAX),XGUESS(NEQMAX)
      DIMENSION H(0:NMAX),PO(NMAX)
      DIMENSION VOL1(NEQMAX),VOL2(NEQMAX),VOL3(NEQMAX)
      COMMON /SPMOVO/SV1,SV2,SV3,VM1,VM2,VM3
      COMMON /FREVO1/FK11,FK12,FK13,FK21,FK22,FK23
      COMMON /FREVO2/D01,D02,CV1,CV2,CV31,CV32
      COMMON /INICON/VINI1,VINI2,VINI3,THINF,THINS
      COMMON /THERCO/FH12,FH13,FH23,FH21
      COMMON /GRIDSI/H,PO
      COMMON /ANTOIN/AS,BS,CS,DS,TCS,PCS,AN,BN,CN,DN,TCN,PCN
      COMMON /PARA1/HTCF,HTCS,CMT1,CMT2
      COMMON /PARA2/HCAPF,HCAPS,TSA,DENSS
      COMMON /PARA3/PBUL1,PBUL2,D110,HVAP1,HVAP2
      COMMON /PRETIM/XJ,THJ,TJ
      COMMON /RESULT/THJ1, SUM1J1,SUM2J1,SUM3J1, DENSF, VJ1C10,
     1       VJ1C20
      COMMON /TEMPER/TFA,TINI
      COMMON /DELT/DDELT
      COMMON /SUM/SUM1J,SUM2J
      COMMON /TIME/TIME
```

```
      COMMON /DIFA/D11TA,D12TA,D21TA,D22TA
      COMMON /DIFS/D11TS,D12TS,D21TS,D22TS
      COMMON /PRESS/PI1,PI2
C DATA INPUT FROM FILE "INPCA"
      OPEN (UNIT=1, FILE='INPCA.TXT')
 1    FORMAT (////,8(T50,D10.5,/),T50,D10.5)
      WRITE (*,*) 'B'
      READ (1,1) THINS,TSA,TFA,PBUL1,PBUL2,HTCS,HTCF,CMT1,CMT2
      WRITE (*,*) 'C'
 2    FORMAT (///,12(T50,D10.5,/),////,6(T50,D10.5,/))
      READ (1,2) AN,BN,CN,DN,TCN,PCN,AS,BS,CS,DS,TCS,PCS,VM1,
     +SV1,CV1,DENS1,HVAP1
 3    FORMAT (/,5(T50,D10.5,/))
      READ (1,3) VM2,SV2,CV2,DENS2,HVAP2
 4    FORMAT (/,5(T50,D10.5,/),/,3(T50,D10.5,/))
      READ (1,4) VM3,SV3,CV31,CV32,DENS3,HCAPF,HCAPS,DENSS
 5    FORMAT (//,5(T50,D10.5,/),///,4(T50,D10.5,/),T50,D10.5)
      READ (1,5) VINI1,VINI2,VINI3,TINI,THINF,D01,D02,FK11,FK12,FK13
 6    FORMAT (3(T50,D10.3,/),///,3(T50,D10.5,/))
      READ (1,6) FK21,FK22,FK23,FH12,FH13,FH23
 7    FORMAT (//,3(T45,D15.7,/),////,3(T45,D15.7,/))
      READ (1,7) GRIC1,GRIC2,H(0),DELT,ENDT,ERRREL
      CLOSE (1)
C End of input file
C Output files
      OPEN (UNIT=2, FILE='OUTU1.TXT')
      OPEN (UNIT=3, FILE='OUTU2.TXT')
      OPEN (UNIT=12, FILE='SUBST.TXT')
      OPEN (UNIT=13, FILE='SURFA.TXT')
      OPEN (UNIT=27, FILE='SURFA2.TXT')
      OPEN (UNIT=16, FILE='ERROR.TXT')
      OPEN (UNIT=25, FILE='DIFFUS.TXT')
      OPEN (UNIT=26, FILE='PRESS.TXT')
C     END OF INPUT DATA CONTROL
C FORMAT OF OUTPUT FILES OUTU1.TXT AND OUTU2.TXT
 8  FORMAT (30X, 'VOLUME FRACTIONS', /,'POSITION', 10X,
    + 'NONSOLVENT', 8X, 'SOLVENT',5X, 'POLYMER')
      WRITE (2,8)
 9    FORMAT ('AVERAGE VOLUME FRACTIONS, THICKNESS AND
TEMPERATURE', /,
    + 'TIME sec', 5X, 'NONSOLVENT', 3X, 'SOLVENT', 3X, 'POLYMER', 3X,
    + 'THICKNESS cm' , 'TEMPERATURE (C)')
      WRITE (3,9)
22    FORMAT ('VOLUME FRACT. ON SUBSTRATE'/,5X,'V1',15X,'V2',15X,'V3')
      WRITE (12,22)
23    FORMAT ('VOLUME FRACT. ON SURFACE'/,5X,'V1',15X,'V2',15X,'V3')
      WRITE (13,23)
C NUMBER OF GRID LINES AND NUMBER OF EQUATIONS
      N=100
      NEQ=2*N-1
```

```
C Maximum number of iterations
      ITMAX=500
C Calculation of fh21
      FH21=FH12*VM2/VM1
C  Calculation of grid intervals
      POST=0.0
            DO 50 I=1,N-2
            POST=POST+H(I-1)
            PO(I)=POST
            H(I)=H(I-1)*(1+GRIC1*((1-PO(I))**GRIC2)*H(I-1))
 50         CONTINUE
C
C Calculation of D110
C     VF1: Volume fraction of comp. 1
C     WF1: Weight fraction of comp. 1
C     DM1: Mass density of comp. 1
C     TOTDM: Total mass density
      VF1=VINI1
      VF2=VINI2
      VF3=VINI3
      DM1=VINI1/SV1
      DM2=VINI2/SV2
      DM3=VINI3/SV3
      TOTDM=DM1+DM2+DM3
      WF1=DM1/TOTDM
      WF2=DM2/TOTDM
      WF3=DM3/TOTDM
C Calculation of a free volume parameter
      VFH=(FK11*(FK21+TINI)*WF1)+(FK12*(FK22+TINI)*WF2)+(FK13*
      +(FK23+TINI)*WF3)
C Calculation of self diffusion coefficient of water and acetone at t=0
      D1=D01*DEXP(-(WF1*CV1+WF2*CV2*CV31/CV32+WF3
      +*CV31)/VFH)
      D2=D02*DEXP(-(WF1*CV1*CV32/CV31+WF2*CV2+
      +WF3*CV32)/VFH)
C Calculation of derivative of chemical potentials
      DCP11=SV1*(1/VF1-1+VM1/VM3+VF2*(VM1/VM2*FH23-FH12)-
      +(VF2+2*VF3)*FH13)
      DCP21=SV1*(-VM2/VM1+VM2/VM3+(VF1+VF3)*(FH21-
FH23)+VM2/VM1*
      +(VF1-VF3)*FH13)
C Calculation of D11 (main diff. coeff.) at t=0
      D110=DM1*(1.0-DM1*SV1)*D1*DCP11-DM1*DM2*SV2*D2*DCP21
C Initial volume fractions, temperature and thickness
      DO 60 I=1,N-1
      XJ(I)=1.0
      XJ(I+N-1)=1.0
 60   CONTINUE
C temperature
      XJ(2*N-1)=0.0
```

```
C dimensionless temperature
      TJ=0.0
C dimensionless thickness
      THJ=1.0
C initial integral of dimensionless volume fractions
      SUM1J=1.0
      SUM2J=1.0
C********** TIME LOOP  FROM DELT TO ENDT*********************
C dimensionless del time
      INGTIM=ENDT/DELT
      write (*,*) 'ingtim=',ingtim
      TIME=0.0
      DO 1000 J=1,INGTIM
      TIME=TIME+DELT
C Calculation of dimensionless of time increment
      ddelt=delt*d110/thinf**2
      WRITE (*,*) 'TIME=' ,TIME, 'SEC'
            DO 100 I=1,N-1
            XGUESS(I)=XJ(I)
            XGUESS(I+N-1)=XJ(I+N-1)
100         CONTINUE
C
      XGUESS(2*N-1)=XJ(2*N-1)
C IMSL DNEQNF SUBROUTINE TO FIND THE ROOTS OF 2*N-1 EQUATIONS
C     CALL ERSET (0,1,0)
      CALL DNEQNF (FCN, ERRREL, NEQ, ITMAX, XGUESS, XJ1, FNORM)
            DO 80 M=1,N-1
            XJ(M)=XJ1(M)
            XJ(M+N-1)=XJ1(M+N-1)
80          CONTINUE
            XJ(2*N-1)=XJ1(2*N-1)
            TJ=XJ1(2*N-1)
            THJ=THJ1
            SUM1J=SUM1J1
            SUM2J=SUM2J1
C RESULTS
C Dimensional results
            AVENSO=SUM1J*VINI1
            AVESOL=SUM2J*VINI2
            AVEPOL=1.0-AVENSO-AVESOL
            THICKN=THJ*THINF
            TEMPER=TJ*(TFA-TINI)+TINI
      WRITE(3,10) TIME,AVENSO,AVESOL,AVEPOL,THICKN,TEMPER
10    FORMAT(6(F10.5, 3X))
      TPRINT=(TIME.EQ.5.0).OR.(TIME.EQ.10.0).OR.(TIME.EQ.15.0).OR.
     +(TIME.EQ.20.0).OR.(TIME.EQ.30.0).OR.(TIME.EQ.40.0).OR.
     +(TIME.EQ.50.0).OR.(TIME.EQ.60.0).OR.(TIME.EQ.70.0).OR.
     +(TIME.EQ.80.0).OR.(TIME.EQ.90.0).OR.(TIME.EQ.100.0).OR.
     +(TIME.EQ.105.0).OR.(TIME.EQ.110.0).OR.(TIME.EQ.115.0).OR.
```

```
     +(TIME.EQ.120.0).OR.(TIME.EQ.125.0).OR.(TIME.EQ.130.0).OR.
     +(TIME.EQ.135.0).OR.(TIME.EQ.140.0).OR.(TIME.EQ.145.0).OR.
     +(TIME.EQ.150.0).OR.(TIME.EQ.155.0).OR.(TIME.EQ.160.0).OR.
     +(TIME.EQ.165.0).OR.(TIME.EQ.170.0).OR.(TIME.EQ.175.0).OR.
     +(TIME.EQ.180.0).OR.(TIME.EQ.190.0).OR.(TIME.EQ.200.0).OR.
     +(TIME.EQ.250.0).OR.(TIME.EQ.300.0).OR.(TIME.EQ.350.0).OR.
     +(TIME.EQ.400.0).OR.(TIME.EQ.450.0).OR.(TIME.EQ.500.0).OR.
     +(TIME.EQ.550.0).OR.(TIME.EQ.600.0).OR.(TIME.EQ.800.0).OR.
     +(TIME.EQ.1000.0)
     IF (TPRINT) THEN
     write (2,*) 'TIME=', TIME
           DO 2500 I=1,N-1
     VOL1(I)=XJ(I)*VINI1
     VOL2(I)=XJ(I+N-1)*VINI2
     VOL3(I)=1.0-VOL1(I)-VOL2(I)
     WRITE (2,21) PO(I),VOL1(I),VOL2(I),VOL3(I)
21   FORMAT (4(E15.4))
2500       CONTINUE
     ELSE
     END IF
27  FORMAT(3(E15.6))
     VS1=XJ(1)*VINI1
     VS2=XJ(N)*VINI2
     VS3=1-VS1-VS2
     VA1=XJ(N-1)*VINI1
     VA2=XJ(2*N-2)*VINI2
     VA3=1-VA1-VA2
     VNA1=XJ(N-2)*VINI1
     VNA2=XJ(2*N-3)*VINI2
     VNA3=1-VNA1-VNA2
     WRITE (12,27) VS1,VS2,VS3
     WRITE (13,27) VA1,VA2,VA3
     WRITE (27,27) VNA1,VNA2,VNA3
     WRITE (*,*) FNORM
     WRITE (16,*) TIME, FNORM
55   FORMAT (4(E15.6))
     WRITE (25,*) 'TIME=',TIME
     WRITE (25,55) D11TA, D12TA, D21TA, D22TA
     WRITE (25,55) D11TS, D12TS, D21TS, D22TS
     WRITE (26,*) TIME, PI1, PI2
1000 CONTINUE
C END OF TIME LOOP
     CLOSE (2)
     CLOSE (3)
     CLOSE (12)
     CLOSE (13)
     CLOSE (16)
     CLOSE (55)
     CLOSE (26)
     CLOSE (27)
```

```
      END
C.....
C
C IMSL REQUIRED SUBROUTINE FCN.....
      SUBROUTINE FCN (XJ1, F, NEQ)
      IMPLICIT DOUBLE PRECISION (A-H,O-Z)
      PARAMETER (NMAX=800, NEQMAX=800)
      DIMENSION XJ1(NEQ), XJ(NEQMAX), F(NEQ)
      DIMENSION H(0:NMAX),PO(NMAX)
      DIMENSION D11PI(NMAX),D12PI(NMAX),D21PI(NMAX),D22PI(NMAX)
      DIMENSION D11MI(NMAX),D12MI(NMAX),D21MI(NMAX),
     1          D22MI(NMAX)
      COMMON /GRIDSI/H,PO
      COMMON /THERCO/FH12,FH13,FH23,FH21
      COMMON /SPMOVO/SV1,SV2,SV3,VM1,VM2,VM3
      COMMON /INICON/VINI1,VINI2,VINI3,THINF,THINS
      COMMON /ANTOIN/AS,BS,CS,DS,TCS,PCS,AN,BN,CN,DN,TCN,PCN
      COMMON /PARA1/HTCF,HTCS,CMT1,CMT2
      COMMON /PARA2/HCAPF,HCAPS,TSA,DENSS
      COMMON /PARA3/PBUL1,PBUL2,D110,HVAP1,HVAP2
      COMMON /PRETIM/XJ,THJ,TJ
      COMMON /RESULT/THJ1,SUM1J1,SUM2J1,SUM3J1,DENSF,VJ1C10,
     1          VJ1C20
      COMMON /TEMPER/TFA,TINI
      COMMON /DELT/DDELT
      COMMON /SUM/SUM1J,SUM2J
      COMMON /TIME/TIME
      COMMON /PRESS/PI1,PI2
C     number of gridlines
      N=(NEQ+1)/2
C Calculation of surface concentrations at the substrate side
      VJ1C10=(XJ1(1)*((H(0)+H(1))**2)-XJ1(2)*H(0)**2)/
     +((H(0)+H(1))**2-H(0)**2)
      VJ1C20=(XJ1(N)*((H(0)+H(1))**2)-XJ1(N+1)*H(0)**2)/
     +((H(0)+H(1))**2-H(0)**2)
C
C Integration of volume fractions(dimensionless)
      SUM1J1=H(0)*(VJ1C10+XJ1(1))/2
      SUM2J1=H(0)*(VJ1C20+XJ1(N))/2
      DO 500  L=2,N-1
      SUM1J1=SUM1J1+H(L-1)*(XJ1(L)+XJ1(L-1))/2
      SUM2J1=SUM2J1+H(L-1)*(XJ1(L+N-1)+XJ1(L+N-2))/2
500   CONTINUE
      SUM3J1=(1-(SUM1J1*VINI1)-(SUM2J1*VINI2))/VINI3
C
C Thickness of film
      THJ1=VINI3/(1-((VINI1*SUM1J1)+(VINI2*SUM2J1)))
C
C Density of the film
```

```
      DENSF=(SUM1J1*VINI1/SV1)+(SUM2J1*VINI2/SV2)+(SUM3J1*VINI3/SV
3)
C Calculation of saturated vapor pressures
      TEM=(XJ1(2*N-1)*(TFA-TINI))+TINI
      TN=1-TEM/TCN
      PSAT1=1.0E6*PCN*DEXP((1/(1-TN))*(AN*TN+BN*TN**1.5+
      +CN*TN**3+DN*TN**6))
      TS=1-TEM/TCS
      PSAT2=1.0E6*PCS*DEXP((1/(1-TS))*(AS*TS+BS*TS**1.5+
      +CS*TS**3+DS*TS**6))
C Calculation of interphase pressure
      VI1=XJ1(N-1)*VINI1
      VI2=XJ1(2*N-2)*VINI2
      VI3=1-VI1-VI2
      PI1=PSAT1*DEXP(DLOG(VI1)+1-VI1-VM1/VM2*VI2-VM1/VM3*VI3+
      +(FH12*VI2+FH13*VI3)*(VI2+VI3)-FH23*VM1/VM2*VI2*VI3)
      PI2=PSAT2*DEXP(DLOG(VI2)+1-VI2-VM2/VM1*VI1-VM2/VM3*VI3+
      +(FH12*VM2/VM1*VI1+FH23*VI3)*(VI1+VI3)-FH13*VM2/VM1*VI1*VI3)
C Calculation of temperature constants
      A=THINF*(HTCF+HTCS)/(D110*DENSF*HCAPF)
      B=-THINF*(CMT1*HVAP1*(PI1-PBUL1)+CMT2*HVAP2*(PI2-PBUL2))/
      +(DENSF*HCAPF*D110*(TFA-TINI))
      E=THINF*HTCS*(TSA-TFA)/(D110*DENSF*HCAPF*(TFA-TINI))
      G=(DENSS*HCAPS*THINS)/(DENSF*HCAPF*THINF)
      CALL DIFFUS(N,VJ1C10,VJ1C20,XJ1,D11PI,D12PI,D21PI,D22PI
      +,D11MI,D12MI,D21MI,D22MI)
C
C time derivative of thickness
      DRTH=(THJ1-THJ)/DDELT
C
      DO 300 I=1,N-2
      IF (I.EQ.1) THEN
            VJ1C1B=VJ1C10
            VJ1C2B=VJ1C20
      ELSE
            VJ1C1B=XJ1(I-1)
            VJ1C2B=XJ1(I+N-2)
      END IF
            VJ1C1N=XJ1(I)
            VJ1C2N=XJ1(I+N-1)
            VJ1C1F=XJ1(I+1)
            VJ1C2F=XJ1(I+N)
C Previous time results
            VJC1N=XJ(I)
            VJC2N=XJ(I+N-1)
C Time and position derivatives
C time derivative of concentrations of comp. 1 and 2
      DRT1=(VJ1C1N-VJC1N)/DDELT
      DRT2=(VJ1C2N-VJC2N)/DDELT
C first derivative of  dimensionless conc. of comp. 1 and 2 w.r.t. position
```

```
          DRX11=((VJ1C1F)-(((H(I)/H(I-1))**2)*VJ1C1B)-
          +((1-(H(I)/H(I-1))**2)*VJ1C1N))/(H(I)*(1+H(I)/H(I-1)))
          DRX12=((VJ1C2F)-(((H(I)/H(I-1))**2)*VJ1C2B)-
          +((1-(H(I)/H(I-1))**2)*VJ1C2N))/(H(I)*(1+H(I)/H(I-1)))
 C Equations (continuity)
          F(I)=DRT1-(PO(I)/THJ1*DRTH*DRX11)-(2/((THJ1**2)*D110*(H(I)+H(I-1)
          +)))*(D11PI(I)*(VJ1C1F-VJ1C1N)/H(I)-D11MI(I)*(VJ1C1N-VJ1C1B)
     +/H(I-1)+(VINI2*SV1/VINI1/SV2)*(D12PI(I)*(VJ1C2F-VJ1C2N)
     +/H(I)-D12MI(I)*(VJ1C2N-VJ1C2B)/H(I-1)))
      F(I+N-1)=DRT2-(PO(I)/THJ1*DRTH*DRX12)-(2/((THJ1**2)*D110*
 C
          +(H(I)+H(I-1))))*(D22PI(I)*(VJ1C2F-VJ1C2N)/H(I)-D22MI(I)*
     +(VJ1C2N-VJ1C2B)/H(I-1)+
     +(VINI1*SV2/VINI2/SV1)*(D21PI(I)*(VJ1C1F-VJ1C1N)/H(I)-D21MI(I)
     +*(VJ1C1N-VJ1C1B)/H(I-1)))
 C
 300   CONTINUE
 C Equations from boundary condition
          F(N-1)=(((THJ1*SUM1J1)-(THJ*SUM1J))/DDELT)+(CMT1*(PI1-PBUL1)
          +*THINF)/(VINI1/SV1*D110)
 C
          F(2*N-2)=(((THJ1*SUM2J1)-(THJ*SUM2J))/DDELT)+(CMT2*(PI2-PBUL2)
          +*THINF)/(VINI2/SV2*D110)
 C Heat transfer equation
          TJ1=XJ1(2*N-1)
          F(2*N-1)=(TJ1-TJ)/DDELT-(A*(1-TJ1)+E+B)/(G+THJ1)
 C
          open (unit=10, file='fnorm.txt')
          write (10,*) 'time',time
          DO K=1,2*N-1
           WRITE(10,*) K, F(K)
          END DO
          close (10)

          RETURN
          END
C.....
C DIFFUSION SUBROUTINE.....
          SUBROUTINE DIFFUS(N,VJ1C10,VJ1C20,XJ1,D11PI,D12PI,D21PI,D22PI
          +,D11MI,D12MI,D21MI,D22MI)
           IMPLICIT DOUBLE PRECISION(A-H,O-Z)
          PARAMETER (NMAX=800, NEQMAX=800)
          DIMENSION XJ1(NEQMAX),V1(0:NEQMAX),V2(0:NEQMAX)
          DIMENSION D11PI(NMAX),D12PI(NMAX),D21PI(NMAX),D22PI(NMAX)
          DIMENSION
D11MI(NMAX),D12MI(NMAX),D21MI(NMAX),D22MI(NMAX)
           COMMON /FREVO1/FK11,FK12,FK13,FK21,FK22,FK23
          COMMON /FREVO2/D01,D02,CV1,CV2,CV31,CV32
          COMMON /SPMOVO/SV1,SV2,SV3,VM1,VM2,VM3
          COMMON /THERCO/FH12,FH13,FH23,FH21
```

```
      COMMON /INICON/VINI1,VINI2,VINI3,THINF,THINS
      COMMON /TEMPER/TFA,TINI
      COMMON /DIFA/D11TA,D12TA,D21TA,D22TA
      COMMON /DIFS/D11TS,D12TS,D21TS,D22TS
C Dimensional temperature
      T=(XJ1(2*N-1)*(TFA-TINI))+TINI
C Volume and mass freaction and mass density conversion
      DO 750 K=0,N-1
       IF (K.EQ.0) THEN
      V1(K)=VJ1C10*VINI1
      V2(K)=VJ1C20*VINI2
      ELSE
      V1(K)=XJ1(K)*VINI1
      V2(K)=XJ1(K+N-1)*VINI2
      ENDIF
750   CONTINUE
C     DİJ i+1/2 AND DİJ i-1/2 calculation
      DO 780 M=1,2
      DO 760 K=1,N-2
            IF (M.EQ.1) THEN
      VF1=(V1(K)+V1(K+1))/2
      VF2=(V2(K)+V2(K+1))/2
            ELSE
      VF1=(V1(K)+V1(K-1))/2
      VF2=(V2(K)+V2(K-1))/2
            END IF
      VF3=1-VF1-VF2
      DM1=VF1/SV1
      DM2=VF2/SV2
      DM3=VF3/SV3
      TOTDM=DM1+DM2+DM3
      WF1=DM1/TOTDM
      WF2=DM2/TOTDM
      WF3=DM3/TOTDM
C  Calculation of self diffusion coefficients
      VFH=(FK11*(FK21+T)*WF1)+(FK12*(FK22+T)*WF2)+
      +(FK13*(FK23+T)*WF3)
      D1=D01*DEXP(-(WF1*CV1+WF2*CV2*CV31/CV32+
      +WF3*CV31)/VFH)
      D2=D02*DEXP(-(WF1*CV1*CV32/CV31+WF2*CV2+
      +WF3*CV32)/VFH)
C Calculation of derivative of chemical potentials w.r.t.
      DCP11=SV1*(1/VF1-1+VM1/VM3+VF2*(VM1/VM2*FH23-FH12)-
      +(VF2+2*VF3)*FH13)
      DCP12=SV2*(-(VM1/VM2)+VM1/VM3+(VF2+VF3)*(FH12-
FH13)+VM1/VM2*
      +(VF2-VF3)*FH23)
      DCP21=SV1*(-VM2/VM1+VM2/VM3+(VF1+VF3)*(FH21-
FH23)+VM2/VM1*
      +(VF1-VF3)*FH13)
```

```
      DCP22=SV2*(1/VF2-1+VM2/VM3+VM2/VM1*VF1*(FH13-FH12)-
      +(VF1+2*VF3)*FH23)
C Calculation of diffusion constants
            IF (M.EQ.1) THEN
      D11PI(K)=DM1*(1-DM1*SV1)*D1*DCP11-DM1*DM2*SV2*D2*DCP21
      D12PI(K)=DM1*(1-DM1*SV1)*D1*DCP12-DM1*DM2*SV2*D2*DCP22
      D21PI(K)=DM2*(1-DM2*SV2)*D2*DCP21-DM1*DM2*SV1*D1*DCP11
      D22PI(K)=DM2*(1-DM2*SV2)*D2*DCP22-DM1*DM2*SV1*D1*DCP12
C
            ELSE
      D11MI(K)=DM1*(1-DM1*SV1)*D1*DCP11-DM1*DM2*SV2*D2*DCP21
      D12MI(K)=DM1*(1-DM1*SV1)*D1*DCP12-DM1*DM2*SV2*D2*DCP22
      D21MI(K)=DM2*(1-DM2*SV2)*D2*DCP21-DM1*DM2*SV1*D1*DCP11
      D22MI(K)=DM2*(1-DM2*SV2)*D2*DCP22-DM1*DM2*SV1*D1*DCP12
            END IF
760   CONTINUE
780   CONTINUE
C
      D11TA=(D11PI(N-2)+D11MI(N-2))/2
      D12TA=(D12PI(N-2)+D12MI(N-2))/2
      D21TA=(D21PI(N-2)+D21MI(N-2))/2
      D22TA=(D22PI(N-2)+D22MI(N-2))/2
c
      D11TS=(D11PI(1)+D11MI(1))/2
      D12TS=(D12PI(1)+D12MI(1))/2
      D21TS=(D21PI(1)+D21MI(1))/2
      D22TS=(D22PI(1)+D22MI(1))/2

      RETURN
      END
```

Program (written in FORTRAN and using DNEQNF subroutine from IMSL) for plotting the binodal curve for the cellulose acetate-acetone-water ternary solution

```
c
c   BINODAL CURVE
c   nonsolvent: 1
c   solvent: 2
c   polymer: 3
c   k: interaction parameter
c
      USE MSIMSLMD
       Parameter (n=5)
      double precision v(n),k12,k23,k13,m1,m2,m3, fnorm, errrel
      double precision xguess(n), x(n), v11,v12,v13,v21,v22,v23,c
      external fcn
      common /const/v13,k12,k23,k13,m1,m2,m3,c
      Data k12,k23,k13,m1,m2,m3/1.3,0.5,1.4,18.0,73.92,30532.0/
      ERRREL=1.0E-8
      ITMAX=3000
      open (unit=2, file='Binodal.txt')
      open (unit=3, file='fnorm.txt')
20    format (e12.6, e12.6, e12.6, e12.6, e15.9, e12.6)
      write (*,*) 'Enter initial estimates of  v11, v12, v21, v22, v23'
      read (*,*) v11, v12, v21, v22, v23
10    write (*,*) 'enter v13'
      read (*,*) v13
      v(1)=v11
      v(2)=v12
      v(3)=v21
      v(4)=v22
      v(5)=v23
      DO I=1,5
        XGUESS(I)=V(I)
      END DO
      CALL DNEQNF (FCN, ERRREL, N, ITMAX, XGUESS, X,  FNORM)
      v11=X(1)
      v12=X(2)
      v21=X(3)
      v22=x(4)
      v23=x(5)
      write (2,20) v11,v12,v13,v21,v22,v23
      goto 10
       end
      Subroutine fcn (x, f, n)
      double precision   f1, f2,f3,f4,f5,k12,k23,k13,m1,m2,m3,c
      double precision  x(n), f(n), v11,v12,v13,v21,v22,v23
      common /const/v13,k12,k23,k13,m1,m2,m3,c
```

```
      v11=x(1)
      v12=x(2)
      v21=x(3)
      v22=x(4)
      v23=x(5)
      f(1)=(DLOG(v11)+1-v11-m1/m2*v12-m1/m3*v13+(k12*v12+k13*v13)*
     .(v12+v13)-k23*m1/m2*v12*v13)-(DLOG(v21)+1-v21-m1/m2*v22-
     m1/m3*v23+
     .(k12*v22+k13*v23)*(v22+v23)-k23*m1/m2*v22*v23)
      f(2)=(DLOG(v12)+1-v12-m2/m1*v11-
     m2/m3*v13+(k12*m2/m1*v11+k23*v13)
     .*(v11+v13)-k13*m2/m1*v11*v13)-(DLOG(v22)+1-v22-m2/m1*v21-m2/m3*
     .v23+(k12*m2/m1*v21+k23*v23)*(v21+v23)-k13*m2/m1*v21*v23)
      f(3)=(dlog(v13)+1-v13-m3/m1*v11-m3/m2*v12+(k13*m3/m1*v11+k23*
     .m3/m2*v12)*(v11+v12)-k12*m3/m1*v11*v12)-(dLOG(v23)+1-v23-m3/m1*
     .v21-m3/m2*v22+(k13*m3/m1*v21+k23*m3/m2*v22)*(v21+v22)
     .-k12*m3/m1*v21*v22)
      f(4)=1.0-(v11+v12+v13)
      f(5)=1.0-(v21+v22+v23)
    Return
    End
```

Program (written in FORTRAN and using DNEQNF subroutine from IMSL) for plotting the spinodal curve for the cellulose acetate-acetone-water ternary solution

```
      USE MSIMSLMD
      EXTERNAL FCN
      Double precision v1,v2,v3,k12,k23,k13,MV1,MV2,MV3
      Double precision x,xguess,fnorm,errrel,v
      Dimension x(1),xguess(1),v(1)
      Common /const/ k12,k23,k13,MV1,MV2,MV3,v3
      Data k12,k23,k13,MV1,MV2,MV3/0.9,0.5,1.11,18.0,127.8,30532.0/
      ERRREL=1E-10
      ITMAX=300
      N=1
c
      open (unit=1, file='spin1.txt')
2   format (20x,16HVolume Fractions,//,12x,2Hv1,25x,2Hv2,22x,2Hv3)
      write (1,2)
      V(1)=0.4
C Initial guess
10    write (*,*) 'enter v3'
      read (*,*) v3
      xguess(1)=v(1)
      CALL DNEQNF (FCN,ERRREL,N,ITMAX,XGUESS,X,FNORM)
      v(1)=x(1)
      v2=1-v(1)-v3
      write (1,*) v(1),v2,V3
```

```
      GOTO 10
      close (unit=1)
      end
C IMSL required subroutine FCN
      Subroutine fcn (x,f,n)
      Double precision v1,v2,v3,k12,k23,k13,MV1,MV2,MV3
      Double precision f,x,G22,G23,G33
      Dimension f(n),x(n)
      common /const/k12,k23,k13,MV1,MV2,MV3,v3
      v1=x(1)
      v2=1-v1-v3
      G22=1/V1+MV1/(MV2*V2)-2*K12
      G23=1/V1-(K12+K13)+MV1/MV2*K23
      G33=1/V1+MV1/(MV3*V3)-2*K13
      f(1)=G22*G33-G23**2
      return
      end
```

Program (written in FORTRAN and using DNEQNF subroutine from IMSL) for plotting the critical point for the cellulose acetate-acetone-water ternary solution

```
c
c    PLAIT POINT
c    S: solvent : 2
c    P: polymer   :3
c    N: non-solvent :1
c    m: molar ratio
c    K: interaction parameter
c    V: volume fraction
      USE MSIMSLMD
      PARAMETER (N=2)
      IMPLICIT DOUBLE PRECISION (A-M,O-Z)
      INTEGER ITMAX
      EXTERNAL FCN
      DIMENSION  XGUESS(N), X(N)
      COMMON /CONST/K12,K23,K13,M1,M2,M3
      ITMAX=300
      ERRREL=1E-10
c    Data
      k12=1.3
      k23=0.5
      k13=1.4
      mv1=18.0
      mv2=73.9242
      mv3=30532.0
      m1=mv1/mv1
      m2=mv2/mv1
```

```
      m3=mv3/mv1
c     Inital guesses
      write (*,*) 'enter initial guesses v1,v2'
      read (*,*) v1,v2
          X(1)=V1
          X(2)=V2
          XGUESS(1)=X(1)
          XGUESS(2)=X(2)
          CALL DNEQNF (FCN, ERRREL, N, ITMAX, XGUESS, X, FNORM)
          V1=X(1)
          V2=X(2)
          V3=1-V1-V2
          WRITE (*,*) V1,V2,V3
          WRITE (*,*) FNORM
              end
          SUBROUTINE FCN (X,F,N)
          IMPLICIT DOUBLE PRECISION (A-M,O-Z)
          DIMENSION F(N), X(N)
          COMMON /CONST/K12,K23,K13,M1,M2,M3
          V1=X(1)
          V2=X(2)
          v3=1.0-v1-v2
          G22=1/V1+M1/(M2*V2)-2*K12
          G23=1/V1-(K12+K13)+M1/M2*K23
          G33=1/V1+M1/(m3*v3)-2*K13
          G222=(1/V1**2-M1/M2/V2**2)
          G223=(1/V1**2)
          G233=G223
          G333=(1/V1**2-M1/M3/V3**2)
          f(1)=(g23**2)-g22*g33
          f(2)=G222*G33**2-3*G223*G23*G33+3*G233*G23**2-G22*G23*G333
           write (*,*) f(1), f(2),v3
           RETURN
           END
```